AD-A138 269 EVALUATION OF A DIGITAL FLIGHT CONTROLLER FOR A FLEXIBLE-FIGHTER AIRCRAFT(U) AIR FORCE INST OF TECH WRIGHT-PATTERSON AFB OH SCHOOL OF ENGINEERING 1/2

UNCLASSIFIED M L HOFFMAN DEC 82 AFIT/GE/EE/83D-30 F/G 1/4 NL

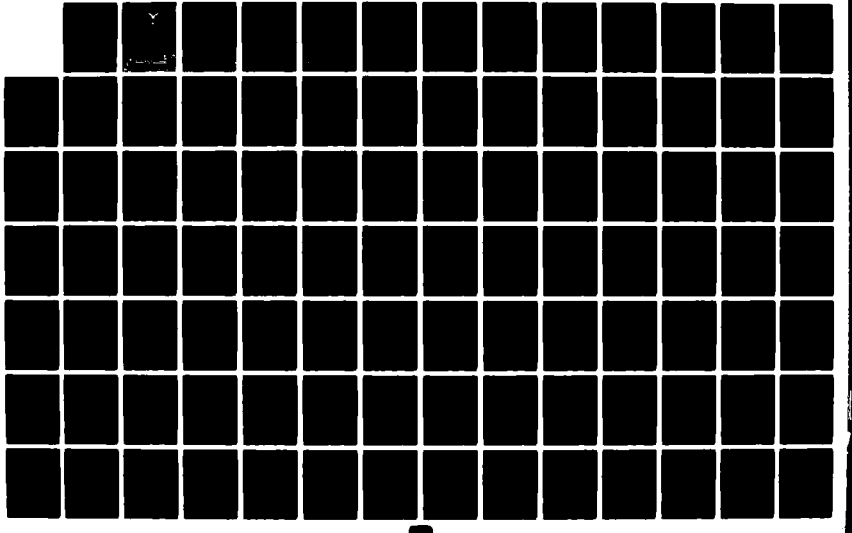

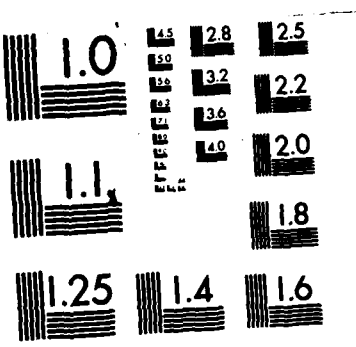

AFIT/GE/EE/83D-30

EVALUATION OF A DIGITAL FLIGHT CONTROLLER FOR A FLEXIBLE-FIGHTER AIRCRAFT

THESIS

Marc L. Hoffman
First Lieutenant, USAF

AFIT/GE/EE/83D-30

Approved for public release; distribution unlimited

AFIT/GE/EE/83D-30

EVALUATION OF A DIGITAL FLIGHT CONTROLLER FOR A FLEXIBLE-FIGHTER AIRCRAFT

THESIS

Presented to the Faculty of the School of Engineering
of the Air Force Institute of Technology
Air University
In Partial Fulfillment of the
Requirements for the Degree of
Master of Science in Electrical Engineering

Marc L. Hoffman, B.S.E.E.
First Lieutenant, USAF

December 1982

Preface

Theses in the past developed flight controllers for rigid body aircraft. In this thesis one digital flight controller is developed for both a rigid body and flexible-fighter aircraft. That is a bending mode is combined with the dynamic of the rigid body aircraft to form the flexible-fighter.

I would like to thank both Dr Robert Schwanz and Mr Finley Barfield of the Flight Dynamics Laboratory for their assistance and guidance in the development of the bending mode equation for the flexible-fighter aircraft. Without their help and suggestions, the development of the flexible-fighter aircraft would not have been possible.

The technique used in the design of the flight controller is based on the theory developed by Professor Brian Porter from the University of Salford, England. I would like to express my appreciation to my thesis advisor Dr John J. D'Azzo and to my reader, Dr Constantine H. Houpis, both of whom are Professors of the Department of Electrical Engineering at the Air Force Institute of Technology.

This thesis was accomplished in parallel with four fellow students. I would especially like to thank Capt. William Locken who also helped in the development of the flexible-fighter aircraft model. Also, my sincere thanks to Lt. Jeff Simmers, Lt. Brian Mayhew, and Lt. Scott Feldmann

who, along with Capt. Locken, comprised the discussion group which aided in accomplishing my objectives.

Finally, but most of all, I want to express my love and appreciation to my parents and the rest of the family who supported me during my stay at AFIT.

Lt Marc L. Hoffman

Table of Contents

List of Figures

List of Tables

List of Symbols

$\underline{A}$	Continuous-time plant matrix
A_n	Longitudinal acceleration (positive upward along the negative z body axis)
$A_{n_{cg}}$	Longitudinal acceleration at the center of gravity
A_{n_p}	Longitudinal acceleration at the pilot's station
α	Angle of attack, perturbation angle of attack in perturbation equations
α_T	Trim angle of attack
$\bar{\alpha}$	Ratio of proportional to integral feedback
$\underline{B}$	Continuous-time plant matrix
b	Wing span
BW	Bandwidth
$\underline{C}$	Continuous-time Output Matrix
c	Mean Aerodynamic Cord
cg	Center of gravity
C_D	Nondimensional coefficient of drag (along velocity vector)
C_{D_α}	Nondimensional variation of drag with angle of attack
C_{D_δ}	Nondimensional variation of drag with elevator (δ_e) of flaperon (δ_f)
C_{D_u}	Nondimensional variation of drag with forward velocity perturbations from trim velocity
C_L	Nondimensional coefficient of lift (normal to velocity vector)
C_{L_α}	Nondimensional variation of lift with angle of attack

$C_{L_{\dot{\alpha}}}$	Nondimensional variation of lift with the rate of change of angle of attack
$C_{L_{\delta}}$	Nondimensional variation of lift with elevator (δ_e) of flaperon (δ_f)
C_{L_q}	Nondimensional variation of lift with pitch rate
C_m	Nondimensional coefficient of pitching moment
$C_{m_{\alpha}}$	Nondimensional variation of pitching moment with angle of attack
$C_{m_{\delta}}$	Nondimensional variation of pitching moment with elevator (δ_e) or flaperon (δ_f)
C_{m_q}	Nondimensional variation of pitching moment with pitch rate
C_{m_u}	Nondimensional variation of pitching moment with forward velocity perturbations
CMD	Command
cos	Cosine
C_x	Nondimensional x-force coefficient
$C_{x_{\alpha}}$	Nondimensional variation of x-force with angle of attack
$C_{x_{\delta}}$	Nondimensional variation of x-force with elevator (δ_e) or flaperon (δ_f)
C_{x_q}	Nondimensional variation of x-force with pitch rate
C_{x_u}	Nondimensional variation of x-force with forward velocity perturbation
C_z	Nondimensional z-force coefficient
$C_{z_{\alpha}}$	Nondimensional variation of z-force with angle of attack
$C_{z_{\dot{\alpha}}}$	Nondimensional variation of z-force with the rate of change of angle of attack
$C_{z_{\delta}}$	Nondimensional variation of z-force with elevator (δ_e) or flaperon (δ_f)

C_{z_q}	Nondimensional variation of z-force with pitch rate
C_{z_u}	Nondimensional variation of z-force with forward velocity perturbation
deg	Degree
δ_e	Elevator or horizontal tail deflection
δ_f	Flap deflection
$\underline{e}(t), \underline{e}$	Error vector
$\underline{e}(kT)$	Discrete error vector
ϵ	Epsilon scalar multiplier
F_s	Stick input
ft	Feet
f	Sampling frequency
g	Gravity, type of pilot command, gain constant
$\underline{G}(s)$	Transfer function matrix
I_{xx}	Moment of inertia about x-axis
I_{yy}	Moment of inertia about y-axis
I_{zz}	Moment of inertia about z-axis
I_{xz}	Product of inertia about xz-axes
$\underline{I}$	Identity matrix
$\underline{K}_0$	Proportional control law feedback matrix
$\underline{K}_1$	Integral control law feedback matrix
K_p	Gain constant in pilot model
l_x	Distance from CG to sensor location along x-axis
l_y	Distance from CG to sensor location along y-axis
l_z	Distance from CG to sensor location along z-axis
$\underline{M}$	Measurement matrix

m	Aircraft mass, number of inputs
M_α	Dimensional variation of pitching moment with angle of attack
$M_{\dot{\alpha}}$	Dimensional variation of pitching moment with the rate of change of angle of attack
M_q	Dimensional variation of pitching moment with pitch rate
M_θ	Dimensional variation of pitching moment with pitch angle
M_x	Moment about the x-axis
M_y	Moment about the y-axis
M_z	Moment about the z-axis
n	Number of states
p	Number of outputs, Roll rate
PR	Pilot Rating
q	Pitch rate
$\bar{q}$	Dynamic pressure
rad	Radians
S	Surface area
s	Laplace operator, seconds
sec	Seconds
sin	Sine
σ	Elements of the Sigma (Σ) matrix
Σ	Sigma Gain Weighting matrix
T	Sampling period, Thrust
U	Velocity along x-axis
$\Delta u, u$	Perturbation velocity along x-axis

$\underline{u}$	Input vector
V	Velocity along y-axis
Ve	Velocity relative to earth
$\underline{v}$	Command input vector
V_T	Forward Velocity
W	Velocity along z-axis, Aircraft wright
w	Perturbation velocity along z-axis
$\underline{w}$	Controller output vector
$\underline{x}$	State vector
X_α	Dimensional variation of x-force with angle of attack
$X_{\dot{\alpha}}$	Dimensional variation of x-force with the rate of change of angle of attack
X_δ	Dimensional variation of x-force with elevator (δe) or flaperon (δf)
X_q	Dimensional variation of x-force with pitch rate
X_u	Dimensional variation of x-force with forward velcoity
$\underline{y}$	Output vector
$\underline{z}(t), \underline{z}$	Integral of error vector
$\underline{z}(kT)$	Discrete Integral of error vector
Z_α	Dimensional variation of z-force with angle of attack
$Z_{\dot{\alpha}}$	Dimensional variation of z-force with the rate of change of angle of attack
Z_δ	Dimensional variation of z-force with elevator (δe) or flaperon (δa)
Z_q	Dimensional variation of z-force with pitch rate
Z_u	Dimensional variation of z-force with forward velocity perturbation

Z_t	Transmission zeros
$\underline{Z}_{1,2}$	Finite system roots
$\underline{Z}_3$	Infinite system roots
θ	Pitch angle
θ_c	Pitch angle command
θ_e	Pitch angle error
$\Gamma(\lambda)$	Asymptotic transfer function matrix

Abstract

This thesis evaluates the effect of a digital flight controller on a flexible-fighter aircraft (FFA) at the flight condition of 0.8 Mach at 30,000 feet. The two maneuvers incorporated in this flight controller are the g-command pull-up maneuver and the pitch-pointing maneuvers. Using a control law that is based on the control system theory developed by Professor Brian Porter, at the University of Salford, England, a digital flight controller is first designed for a rigid body aircraft, and the same design is then used on a flexible-fighter aircraft, FFA. This thesis evaluates the effect of the controller for the rigid body design when used on the flexible-fighter. The results showed excellent performance by the flexible-fighter aircraft FFA.

The flexible-fighter model is based on the rigid body dynamics of the AFTI/F-16 combined with the first bending mode of a flexible aircraft. The bending mode of the FFA flexible aircraft was selected to correspond to the expected characteristics in a typical fighter aircraft.

Incorporating a time delay in the controller to represent the expected microprocessor computational time delay did not significantly affect the simulation time

response of either the rigid body or the flexible-fighter aircraft.

To determine the acceptance of the design by a pilot, the Neal-Smith Criterion is used. The results of applying this criterion showed that the pilot would accept the design for both the rigid body and the flexible-fighter aircraft.

EVALUATION OF A DIGITAL FLIGHT CONTROLLER FOR A FLEXIBLE-FIGHTER AIRCRAFT

I. Introduction

Background

Modern flight controller designs involve strongly coupled Multiple Input-Multiple Output (MIMO) non linear plants with large parameter variations due to a wide range of Mach numbers and altitudes. Many controllers in the past have been designed on the basis of Single Input-Single Output (SISO) system design using conventional techniques such as root-locus and frequency response analysis (Ref. 1). The state and output equations for a SISO system have the form

$$\dot{\underline{x}} = \underline{A}\underline{x} + \underline{b}u \tag{1.1}$$

$$\underline{y} = \underline{C}\underline{x} \tag{1.2}$$

where

$\dot{\underline{x}}$ is an n x 1 column vector,

$\underline{A}$ is an n x n plant coefficient matrix,

$\underline{x}$ is an n x 1 state vector,

$\underline{b}$ is an n x 1 control matrix,

u is a one dimensional control vector,

$\underline{y}$ is a one dimensional output vector,

$\underline{C}$ is an 1 x n output matrix,

and

$\underline{n}$ is the set of first-order differential equations with n independent states.

The SISO system design methods have been around for sometime and many examples and short cuts have been developed for the different design techniques. It can, therefore, be used by a control designer by replacing the MIMO system with a number of separate SISO systems (Ref. 2). Because the SISO systems are intercoupled, this approach requires an iterative approach which can make the design process tedious.

Because of the advancement in computational technology, design procedures for MIMO systems can be more readily applied. For this reason, staying with a MIMO system design approach offers a greater amount of control and greater precision for the design of Digital Flight Control Systems (DFCS). Many different methods and theories have been developed for multi-variable control designs. One recent method has been developed by a Professor Porter at the University of Salford, England, exploiting high-gain error actuated flight control systems.

Professor Porter's method shows promise in enabling the design of exceptionally good performing systems without many of the drawbacks that occur in other modern control methods. This method leads to decoupling of the outputs and therefore, decoupled maneuvers are readily achievable. The theory behind Professor Porter's work is presented in Chapter III

and can also be found in Reference 3.

The longitudinal and lateral-directional dynamics are frequently considered separately in order to reduce the size of the design problem. That procedure is used in this thesis.

Problem

Much of the work on fighter-type aircraft deals with designing flight control systems considering the aircraft as a rigid body vehicle. These studies examine the response of the aircraft when performing various maneuvers. It is now desired to include the flexible characteristics of a fighter-type aircraft and to examine the performance compared to the rigid body response when performing constant acceleration, and pitch-pointing maneuvers.

The evaluation of the flight controller is defined in this thesis as the way the flexible-fighter aircraft deviates from the rigid body response. The constant acceleration maneuver allows the pilot to command a constant "g" pull-up. The pitch-pointing maneuver allows the pilot to command an angle of attack without developing a normal acceleration. What this means is that the pilot can point the nose of the aircraft up or down without changing its flight path.

Assumptions

In order to simplify the computations and analysis the following assumptions are made:

(1) The earth is flat and non-rotating.

(2) The atmosphere is fixed to the earth. (no wind)

(3) The acceleration due to gravity is constant.

(4) The aircraft has a constant mass.

(5) The aircraft is a rigid body except for one bending mode for the longitudinal axis.

(6) The aircraft performs maneuvers while flying straight with wings level, unless otherwise stated.

(7) The motion of the aircraft about a straight and level trim condition can be adequately modeled by a linear dynamical system of equations.

(8) The dynamics of the elevator and flaperon actuators can be adequately modeled by first-order differential equations.

These are the basic assumptions that are made when developing flight dynamics equations for a flexible fighter-type aircraft (FFA).

Summary of Current Knowledge

The aircraft's aerodynamic coefficients of the rigid body are known. Also, the bending mode equation of the flexible aircraft is known. Pitch-rate and normal acceleration (A_n) are employed as command parameters for the two maneuvers specified in the problem statement. When the pilot demands a specific "g" level it has a corresponding

pitch rate which can be determined from the following relationship (Ref 4):

$$q = [1845/U]\,(A_n) \qquad (1.3)$$

Standards

In order to have a successful flight control design, certain criteria must be established; therefore, some design requirements are established. First, the design must provide control and stability augmentation. Second, the responses are to be fast and well behaved. Third, surface deflections and rates are not commanded beyond preset limits. Fourth, the aircraft rates and accelerations must be controllable. Fifth, the feedback signals can be reliably obtained with sensors. Last, the maneuvers described previously are capable and available for the flexible aircraft.

Approach Sequence

The first step is to determine the bending mode equation and to combine it with the rigid body equations of the fighter. This process is described in Chapter II. Chapter III contains a summary of the multivariable control design method developed by Professor Brian Porter of the University of Salford, England. Using this method, a control design is first developed for the rigid body aircraft. Then, the same controller developed for the rigid body is applied to the flexible-fighter aircraft (FFA), and the time simulation response results are compared.

The rigid body and the flexible-fighter aircraft responses to the design are examined in Chapter IV. The evaluations and conclusions are discussed in Chapter V and VI, respectively.

There are three appendices in this thesis that deal with improvements which have been incorporated into the design program called MULTI. The changes given in Appendix A are intended to make the program user friendly by making it easy to input corrections into the input data. This is accomplished by the Subroutine Fix. Appendix B helps the user to form combinations of states. For instance, to look at the flight path angle γ the equation $\theta - \alpha$ must be formed. This is accomplished by using a new routine that forms different combinations of states. Appendix C deals with forming the measurment matrix $\underline{M}$ without recalculating the $\underline{K}_0$ and $\underline{K}_1$ matrices that may already exist. Also, this improvement to MULTI allows the user to change either or both the $\underline{K}_0$ and $\underline{K}_1$ matrices. The purpose of this change is to study the possibility of achieving the desired tracking command with a reduced number of non-zero elements in the controller gain matrices.

II. Aircraft Modeling

Aircraft Description

The vehicle that is described in this chapter is a flexible-fighter-type aircraft. It is basically modeled as a modified AFTI/F-16 rigid body aircraft and is expanded to include a longitudinal bending mode taken from a flexible aircraft. This has been accomplished by matching the flexible aircrafts dynamic pressure ($\bar{q}$), forward velocity (V_T), and its speed relative to the earth (V_e) with that of the AFTI/F-16. Table 1 shows three different flight conditions of the AFTI/F-16 and the one for the flexible aircraft.

Table 1

Matching Flight Characteristics

AIRCRAFT	FLEXIBLE	AFTI/F-16		
MACH/ALT.	0.60/21K	0.6/20K	0.8/10K	0.8/30K
ρ_o	0.001225	0.001267	0.001267	0.00089
V_T	712.33	622.15	829.54	795.88
V_e	303.1	269.15	358.8	288.66
$\bar{q}$	311.03	245.27	436.03	282.09

After examining Table 1, the flight condition that most closely matches the flexible aircraft occurs at 0.8

mach at 30,000 feet. The next sections in this chapter deal with forming of the state model for the rigid body AFTI/F-16 and the steps taken to combine the flexible aircraft with that of the AFTI/F-16. Reference 4 is the primary source used in the next section.

Aerodynamic Model

For the purpose of designing a digital flight controller, the equations of motion must be written as state equations in the form $\dot{\underline{x}} = \underline{A}\underline{x} + \underline{B}\underline{u}$. The rigid body space state aircraft model has the form

$$\begin{bmatrix} \dot{\theta} \\ \dot{U} \\ \dot{\alpha} \\ \dot{q} \end{bmatrix} = \begin{bmatrix} 0 & 0 & 0 & 1 \\ X'_\theta & X'_u & X'_\alpha & X'_q \\ Z'_\theta & Z'_u & Z'_d & Z'_q \\ M'_\theta & M'_u & M'_\alpha & M'_q \end{bmatrix} \begin{bmatrix} \theta \\ U \\ \alpha \\ q \end{bmatrix} + \begin{bmatrix} 0 & 0 \\ X'_{\delta_e} & X'_{\delta_f} \\ Z'_{\delta_e} & Z'_{\delta_f} \\ M'_{\delta_e} & M'_{\delta_f} \end{bmatrix} \begin{bmatrix} \delta_e \\ \delta_f \end{bmatrix} \tag{2.1}$$

where $X'_\theta = X_\theta = -g\cos\theta_T$ (2.2)

$$X'_u = X_u = \frac{\bar{q}S}{mU} C_{x_u} \tag{2.3}$$

$$X'_\alpha = X_\alpha = \frac{\bar{q}S}{m} C_{x_\alpha} \tag{2.4}$$

$$X'_q = X_q - U\alpha_T = \frac{\bar{q}Sc}{m2U} C_{x_q} - U\alpha_T \tag{2.5}$$

$$X'_{\delta_e} = X_{\delta_e} = \frac{\bar{q}S}{m} C_{x_{\delta_e}} \tag{2.6}$$

$$X'_{\delta_f} = X_{\delta_f} = \frac{\bar{q}S}{m} C_{x_{\delta_f}} \tag{2.7}$$

$$Z'_\theta = \frac{Z_\theta}{U} = \frac{-g}{U} \sin\theta_T \tag{2.8}$$

$$Z'_u = \frac{Z_u}{U} = \frac{\bar{q}S}{mU^2} C_{Z_u} \tag{2.9}$$

$$Z'_\alpha = \frac{Z_\alpha}{U} = \frac{\bar{q}S}{mU} C_{Z_\alpha} \tag{2.10}$$

$$Z'_q = 1 + \frac{Z_q}{U} = 1 + \frac{\bar{q}Sc}{m2U^2} C_{Z_q} \tag{2.11}$$

$$Z'_{\delta_e} = \frac{Z_{\delta e}}{U} = \frac{\bar{q}S}{mU} C_{Z_{\delta_e}} \tag{2.12}$$

$$Z'_{\delta_f} = \frac{Z_{\delta f}}{U} = \frac{\bar{q}S}{mU} C_{Z_{\delta_f}} \tag{2.13}$$

$$M'_\theta = \frac{\bar{q}Sc^2}{2UI_{yy}} (C_{m_{\dot{\alpha}}})_b Z'_\theta \tag{2.14}$$

$$M'_u = \frac{\bar{q}Sc}{UI_{yy}} (C_{m_u})_b + \frac{\bar{q}Sc^2}{2UI_{yy}} (C_{m_{\dot{\alpha}}})_b Z'_u \tag{2.15}$$

$$M'_\alpha = \frac{\bar{q}Sc}{I_{yy}} (C_{m_\alpha})_b + \frac{\bar{q}Sc^2}{2UI_{yy}} (C_{m_{\dot{\alpha}}})_b Z'_\alpha \tag{2.16}$$

$$M'_q = \frac{\bar{q}Sc^2}{2UI_{yy}} (C_{m_q})_b + (C_{m_\alpha})_b Z'_q \tag{2.17}$$

$$M'_{\delta_e} = \frac{\bar{q}Sc}{I_{yy}} \left[(C_{m_{\delta_e}})_b + \frac{\bar{q}Sc^2}{2UI_{yy}} (C_{m_{\dot{\alpha}}})_b \right] Z'_{\delta_e} \tag{2.18}$$

$$M'_{\delta_f} = \frac{\bar{q}Sc}{I_{yy}} (C_{m_{\delta_e}})_b + \frac{\bar{q}Sc^2}{2UI_{yy}} (C_{m_{\dot{\alpha}}})_b Z'_{\delta_f} \tag{2.19}$$

Note: $(\ )_b$ denotes that the coefficients are expressed in terms of the body axis reference frame.

Most aerodynamic data taken from wind tunnel and flight tests by convention, are not in the same reference frame or in the same units. For instance, by convention, static derivatives (C_{m_α}, C_{L_α}, etc.) are listed in units of per

degree (1/deg) while the dynamic derivatives (C_{L_q}, $C_{L_{\dot{\alpha}}}$, etc.) are listed in units of per radian. It should also be mentioned that the aerodynamic derivatives are in the stability axis reference frame while the mass properties (moments and products of inertia, and positions of sensors) are referenced in terms of the body axis. Figure 1 illustrates the differences in the body and stability axes. Therefore, in order for an analysis to be accomplished the data must be converted to a consistent reference frame (Ref. 4).

The body axis reference frame is chosen for this design. The two main reasons for choosing the body axis are as follows:

1. The sensors providing feedback signals are actually measuring body accelerations and rates;

2. The pilot desires to control variables that he actually feels, which are body accelerations and rates.

Because the pilot desires to control body accelerations and rates, the output equation takes the form

$$\begin{bmatrix} A_{Z_{cg}} \\ q \end{bmatrix} = \begin{bmatrix} 0 & Z_u & Z_\alpha & Z_q \\ 0 & 0 & 0 & 1 \end{bmatrix} \begin{bmatrix} \theta \\ u \\ \alpha \\ q \end{bmatrix} + \begin{bmatrix} Z_{\delta_e} & Z_{\delta_f} \\ 0 & 0 \end{bmatrix} \begin{bmatrix} \delta_e \\ \delta_f \end{bmatrix} \qquad (2.20)$$

The design method used in this report does not provide for a $\underline{D}$ matrix. Therefore, the aircraft model must be reformulated so that there is no $\underline{D}$ matrix. This is done by augmenting the aircraft state vector with the actuator states.

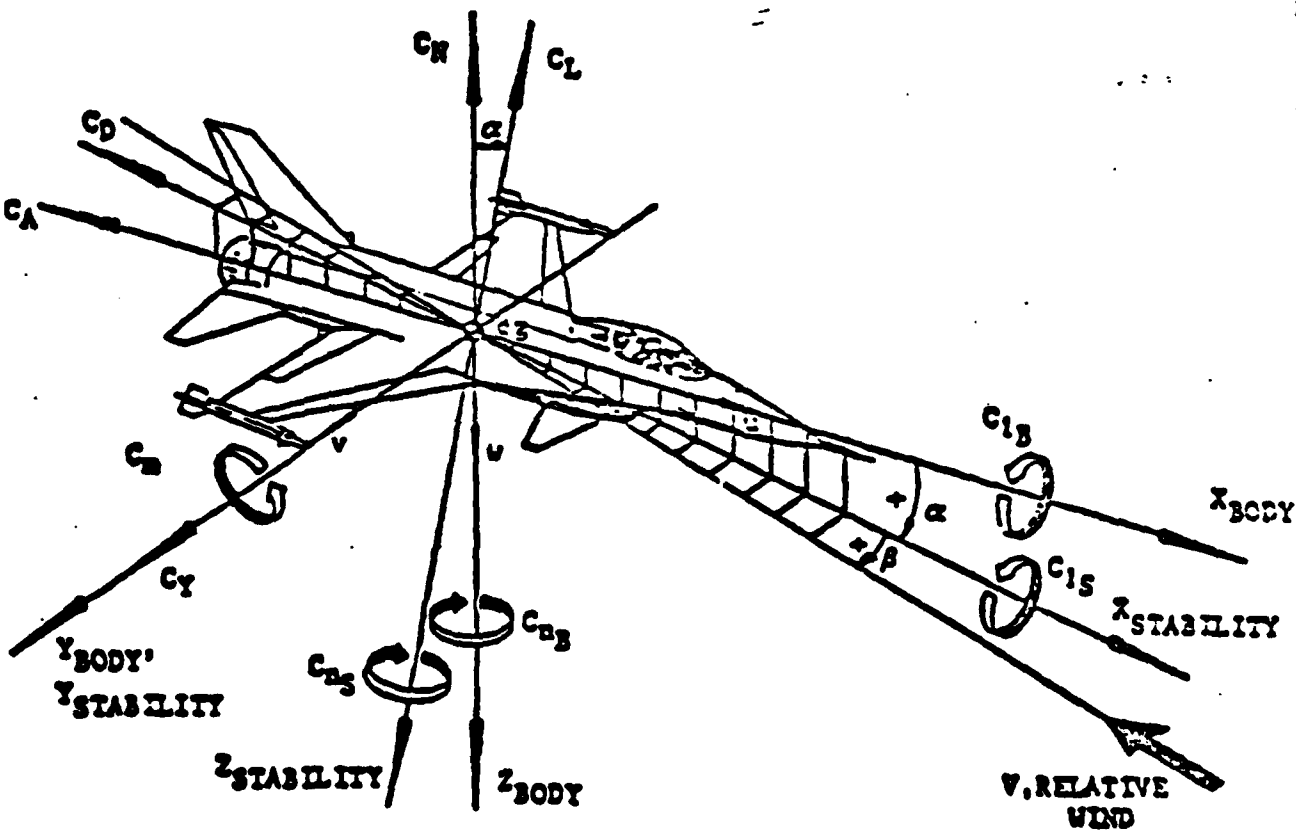

Figure 1. Stability and Body Axis Differences

Using a first-order actuator transfer function model of 20/(s+20) for both the elevator and flaperon surfaces of the AFTI/F-16 results in the following state and output equations that do not contain a $\underline{D}$ matrix:

$$\begin{bmatrix} \dot{\theta} \\ \dot{U} \\ \dot{\alpha} \\ \dot{q} \\ \dot{\delta}_e \\ \dot{\delta}_f \end{bmatrix} = \left[\begin{array}{cccc|cc} 0 & 0 & 0 & 1 & 0 & 0 \\ X'_\theta & X'_u & X' & X'_q & X'_{\delta_e} & X'_{\delta_f} \\ Z'_\theta & Z'_u & Z'_\alpha & Z'_q & Z'_{\delta_e} & Z'_{\delta_f} \\ M'_\theta & M'_u & M'_\alpha & M'_q & M'_{\delta_e} & M'_{\delta_f} \\ \hline 0 & 0 & 0 & 0 & -20 & 0 \\ 0 & 0 & 0 & 0 & 0 & -20 \end{array}\right] \begin{bmatrix} \theta \\ U \\ \alpha \\ q \\ \delta_e \\ \delta_f \end{bmatrix} + \left[\begin{array}{cc} 0 & 0 \\ 0 & 0 \\ 0 & 0 \\ 0 & 0 \\ \hline 20 & 0 \\ 0 & 20 \end{array}\right] \begin{bmatrix} \delta_{e_{CMD}} \\ \delta_{f_{CMD}} \end{bmatrix} \tag{2.21}$$

$$\begin{bmatrix} A_{z_{cg}} \\ q \end{bmatrix} = \left[\begin{array}{cccc|cc} 0 & Z_u & Z_\alpha & Z_q & Z_{\delta_e} & Z_{\delta_f} \\ \hline 0 & 0 & 0 & 1 & 0 & 0 \end{array}\right] \begin{bmatrix} \theta & u & \alpha & q & \delta e & \delta f \end{bmatrix}^T \tag{2.22}$$

This form, where $\underline{B}$ is in the "zero-B_2" form is also helpful in the design. One use of this format is that it can be used for the direct evaluation of the transmission zeros. A relatively simple means of calculating transmission zeros is available for systems in the "zero-B_2" form (Ref. 3).

The output Equation (2.22) $A_{z_{cg}}$ is the longitudinal acceleration in the z-direction at the center of gravity. A desirable output is the acceleration at the pilot station (A_{n_p}). This is accomplished by the following steps: (Ref. 4)

Note: $A_{n_p} = -A_z$ (2.23)

$$A_{n_p} = A_{n_{cg}} - (l_x)(pr-\dot{g}) - (l_y)(rq+\dot{q}) + (l_z)(p^2+q^2) \quad (2.24)$$

where lx, ly, and l_z are distances in the body from the pilot station to the center of gravity.

Since l_y and l_z are much smaller than l_x for the AFTI/F-16 aircraft and since the assumption is made that the longitudinal and lateral-directional motions can be decoupled, Equation (2.24) reduces to the approximate form

$$A_{n_p} = A_{n_{cg}} + (l_x)\dot{q} \quad (2.25)$$

where $l_x = 13.95$.

Combining $\dot{q}$ as given in Equation (2.21), and l_x with $A_{n_{cg}}$ yields the following equation

$$A_{n_p} = (l_x M'_\theta)\,\theta + (l_x M'_u - Z_u)\,u + (l_x M'_\alpha - Z_\alpha)\,\alpha + (l_x M'_q - Z_q)\,q + (l_x M'_{\delta_e} - Z_{\delta_e})\,\delta_e + (l_x M_{\delta_f} - Z_{\delta_f})\,\delta_f \quad (2.26)$$

Therefore, the new output equation has the form

$$\begin{bmatrix} A_{n_p} \\ q \end{bmatrix} = \begin{bmatrix} (l_x M'_\theta) & (l_x M'_u - Z_o) & (l_x M'_\alpha - Z_\alpha) & (l_x M'_q - Z_q) & (l_x M'_{\delta_e} - Z_{\delta_e}) & (l_x M'_{\delta_f} - Z_{\delta_f}) \\ 0 & 0 & 0 & 1 & 0 & 0 \end{bmatrix} \begin{bmatrix} \theta & u & \alpha & q & \delta_e & \delta_f \end{bmatrix}^T \quad (2.27)$$

The Flexible-Fighter Aircraft Model

The first step in forming the flexible aircraft model is calculating the $\underline{A}$ and $\underline{B}$ matrix in Equation (2.21) for the rigid body aircraft. The aerodynamic data for the AFTI/F-16 found in Table 2 was developed by General Dynamic Corporation of Fort Worth, Texas (Ref. 5). Instead of taking this data and calculating the matrices by hand, a computer program called Conversion and Transformation (CAT) is used (Ref. 3). The data from the program CAT shown in Table 3 is put into the state and output Equations (2.21 & 2.27)

$$\begin{bmatrix} \dot{\theta} \\ \dot{u} \\ \dot{\alpha} \\ \dot{q} \\ \dot{\delta}_e \\ \dot{\delta}_f \end{bmatrix} = \underline{A} \begin{bmatrix} \theta \\ u \\ \alpha \\ q \\ \delta_e \\ \delta_f \end{bmatrix} + \begin{bmatrix} 0 & 0 \\ 0 & 0 \\ 0 & 0 \\ 0 & 0 \\ 20 & 0 \\ 0 & 20 \end{bmatrix} \begin{bmatrix} \delta_{e_{CMD}} \\ \delta_{f_{CMD}} \end{bmatrix}$$

where

$$\underline{A} = \begin{bmatrix} 0 & 0 & 0 & 1 & 0 & 0 \\ -32.15 & -0.006647 & 29.75 & -42.38 & 3.131 & -1.131 \\ -0.002161 & -0.00004481 & -0.8488 & 0.9968 & -0.08824 & -0.151 \\ 0.0002948 & 0.0008292 & 2.064 & -0.4555 & -11.71 & -2.702 \\ 0 & 0 & 0 & 0 & -20 & 0 \\ 0 & 0 & 0 & 0 & 0 & -20 \end{bmatrix} \quad (2.28)$$

Table 2

Aircraft Data for the 0.8 Mach and 30,000 Feet Flight Condition

Aircraft Parameters

$\bar{q}$ (dynamic pressure - lbs/ft^2) = 282.33

S (wing reference area - ft^2) = 300.0

c (wing mean aerodynamic cord - ft) = 11.32

b (wing span - ft) = 30.0

V_T (trim velocity - ft/sec) = 795.88

W (weight - lbs) = 21,018.0

Inertias: I_{xx} (slug - ft^2) = 10,033.4

I_{yy} (slug - ft^2) - 53,876.3

I_{zz} (slug - ft^2) - 61,278.5

I_{xz} (slug - ft^2) - 282.132

Aircraft Aerodynamic Coefficients in the Stability Axis System

α (deg) = 3.0615

C_L = 0.24704	C_m = 0.014623	C_D = 0.02746
$C_{L_\alpha}(\frac{1}{deg})$ = 0.09014	$C_{m_\alpha}(\frac{1}{deg})$ = 0.001886	$C_{D_\alpha}(\frac{1}{deg})$ = 0.005118
$C_{L_{\delta_e}}(\frac{1}{deg})$ = 0.00946	$C_{m_{\delta_e}}(\frac{1}{deg})$ = -0.011496	$C_{D_{\delta_e}}(\frac{1}{deg})$ = 0.000084
$C_{L_{\delta_f}}(\frac{1}{deg})$ = 0.01613	$C_{m_{\delta_f}}(\frac{1}{deg})$ = -0.00267	$C_{D_{\delta_f}}(\frac{1}{deg})$ = 0.001015

Table 2 (continued)

$C_{L_q}(\frac{1}{rad})$	= 3.0042	$C_{m_q}(\frac{1}{rad})$	= -2.5245		
$C_{L_\dot{}}(\frac{1}{rad})$	= -1.3146	$C_{m_\dot{}}(\frac{1}{rad})$	= -1.0796		
$C_{L_u}(\frac{1}{ft/sec})$	= 0.000166	$C_{m_u}(\frac{1}{ft/sec})$	= -0.00004	$C_{D_u}(\frac{1}{ft/sec})$	= 0.000013

Table 3

0.8 Mach 20,000 Feet Flight Condition

Longitudinal Body Axis

Dimensional Derivatives

$Z = -21018.0$	$M = 14020.4$	$X = -1205.28$
$Z_\alpha = -675.528$	$M_\alpha = 1.94806$	$X_\alpha = 29.753$
$Z_{\delta_e} = -70.228$	$M_{\delta_e} = -11.722$	$X_{\delta_e} = 3.1306$
$Z_{\delta_e} = -120.153$	$M_{\delta_f} = -2.7224$	$X_{\delta_f} = -1.13077$
$Z_q = -2.7683$	$M_q = -0.3195$	$X_q = 0.14806$
$Z_{\dot{\alpha}} = 1.20961$	$M_{\dot{\alpha}} = -0.13644$	$X_{\dot{\alpha}} = -0.064694$
$Z_u = -0.035664$	$M_u = 0.0005231$	$X_u = -0.006647$

Primed Dimensional Derivatives

$Z'_\alpha = -0.8488$	$M'_\alpha = 2.064$	$X'_\alpha = 29.75$
$Z'_{\delta e} = -0.08824$	$M'_{\delta e} = -11.71$	$X'_{\delta e} = 3.131$
$Z'_{\delta f} = -0.151$	$M'_{\delta f} = -2.702$	$X'_{\delta f} = -1.131$
$Z'_q = 0.9965$	$M'_q = -.4555$	$X'_q = -42.38$
$Z'_u = -0.00004481$	$M'_u = 0.0005292$	$X'_u = -0.006647$
$Z'_\theta = -0.002161$	$M'_\theta = 0.0002948$	$X'_\theta = -32.15$

$$\begin{bmatrix} A_{n_p} \\ q \end{bmatrix} = \begin{bmatrix} 0.004113 & 0.04305 & 704.3 & -3.585 & -93.12 & 82.5 \\ 0 & 0 & 0 & 1 & 0 & 0 \end{bmatrix}$$

$$X \quad [\theta \; u \; \alpha \; q \; \delta_e \; \delta_f]^T \qquad (2.29)$$

The state vector has the following units

$$\begin{bmatrix} \theta & \text{(rad.)} \\ u & \text{(ft/s)} \\ \alpha & \text{(rad.)} \\ q & \text{(rad/sec)} \\ \delta_e & \text{(rad.)} \\ \delta_f & \text{(rad.)} \end{bmatrix}$$

The state space model of a flexible aircraft was obtained from Dr. Robert Schwanz of the Flight Dynamics Laboratory at Wright-Patterson AFB, Ohio. The following state quation is a short period approximation of the flexible aircraft.

$$\begin{bmatrix} \dot{\theta} \\ \dot{w} \\ \dot{q} \\ \dot{\chi}_1 \\ \dot{\chi}_2 \end{bmatrix} = \underline{A} \begin{bmatrix} \theta \\ w \\ q \\ \chi_1 \\ \chi_2 \end{bmatrix} + \begin{bmatrix} 0 \\ -349.87 \\ -0.4937 \\ 0 \\ -7328 \end{bmatrix} \begin{bmatrix} \delta_e \end{bmatrix}$$

where

$$\underline{A} = \begin{bmatrix} 0 & 0 & 1 & 0 & 0 \\ -14.3629 & -1.08346 & 8425.84 & -0.705394 & -0.0242707 \\ -0.0006129 & -0.000050184 & -1.6585 & -0.0001167 & -0.0007194 \\ 0 & 0 & 0 & 0 & 1 \\ 16.76 & -13.96 & 7272 & -47.41 & -2.469 \end{bmatrix} \qquad (2.30)$$

where χ_1, and χ_2 represent the bending mode state variables.

Before a comparison can be made between the rigid body of the AFTI/F-16 with that of the flexible aircraft, w must be changed to α. This is done by using the equation $\alpha = w/u$ where u = 713.068 ft/s and w is in inches per second. When w is changed to α and the aircraft model is augmented with the actuator dynamics, the following space state model is obtained:

$$\begin{bmatrix} \dot{\theta} \\ \dot{\alpha} \\ \dot{q} \\ \dot{\delta}_e \\ \dot{\chi}_1 \\ \dot{\chi}_2 \end{bmatrix} = \underline{A} \begin{bmatrix} \theta \\ \alpha \\ q \\ \delta_e \\ \chi_1 \\ \chi_2 \end{bmatrix} + \begin{bmatrix} 0 \\ 0 \\ 0 \\ 20 \\ 0 \\ 0 \end{bmatrix} \begin{bmatrix} \delta_{e_{CMD}} \end{bmatrix}$$

where

$$\underline{A} = \begin{bmatrix} 0 & 0 & 1 & 0 & 0 & 0 \\ 0.001679 & -1.08346 & .9846 & -0.04088 & -0.000002836 & -0.00008243 \\ -0.0008129 & -4.294 & -1.6585 & -0.49375 & -0.0001168 & -0.00007194 \\ 0 & 0 & 0 & -20 & 0 & 0 \\ 0 & 0 & 0 & 0 & 1 & 1 \\ 16.76 & 119400 & 7272 & -7328 & -47.41 & -2.469 \end{bmatrix}$$

(2.31)

Comparing the $\dot{\alpha}$ and $\dot{q}$ equations for both the rigid body aircraft and the flexible aircraft, the following table is formed:

Table 4

Comparison Between the F-16 & Flexible Aircraft

AFIT/F-16 (Rigid Body)		Flexible A/C		
$\dot{\alpha}$	$\dot{q}$	$\dot{\alpha}$	$\dot{q}$	
-0.002161	0.0002948	0.001679	-0.0008129	θ
-0.8488	2.064	-1.08346	-4.294	α
0.9965	-0.4555	.9846	-1.6585	q
-0.08824	-11.71	-0.04088	-0.49375	δ_e

The magnitudes of the equations are nearly equal to each other. As far as modeling goes they are close enough, because only the bending mode equations of the flexible aircraft are used.

Combining the rigid body of the AFTI/F-16 and the bending mode of the flexible aircraft, Equation (2.32) is formed. The term that is missing from Equation (2.32) must be approximated. To do this, the following ratio is used:

$$\frac{Z'_{\delta_e}}{Z'_{\delta_f}} = \frac{-0.08824}{-0.151} = \frac{-7328}{*} \qquad (2.33)$$

This yields * = -12540, where Z'_{δ} represents the z-force with either the elevator or flaperon.

To determine if the flexible aircraft in Equation (2.32) represents a flexible fighter-type vehicle, the following steps are taken:

$$\begin{bmatrix} \dot{\theta} \\ \dot{u} \\ \dot{\alpha} \\ \dot{q} \\ \dot{\delta}_e \\ \dot{\delta}_f \\ \dot{\chi}_1 \\ \dot{\chi}_2 \end{bmatrix} = \underline{A} \begin{bmatrix} \theta \ (\text{rad}) \\ u \ (\text{ft/s}) \\ \alpha \ (\text{rad}) \\ q \ (\text{rad/s}) \\ \delta_e \ (\text{deg}) \\ \delta_f \ (\text{deg}) \\ \chi_1 \ (\text{in}) \\ \chi_2 \ (\text{in/s}) \end{bmatrix} + \begin{bmatrix} 0 & 0 \\ 0 & 0 \\ 0 & 0 \\ 0 & 0 \\ 20 & 0 \\ 0 & 20 \\ 0 & 0 \\ 0 & 0 \end{bmatrix} \begin{bmatrix} \delta_{e_{CMD}} \ (\text{deg}) \\ \delta_{f_{CMD}} \ (\text{deg}) \end{bmatrix}$$

where

$$\underline{A} = \begin{bmatrix} 0 & 0 & 0 & 1 & 0 & 0 & 0 & 0 \\ -32.15 & -0.006647 & 29.75 & -42.38 & 3.131 & -1.131 & 0 & 0 \\ -0.002161 & -0.00004481 & -0.8488 & 0.9965 & -0.08824 & -0.151 & -0.000002836 & -0.00008243 \\ 0.0002948 & 0.0005292 & 2.064 & -0.4555 & -11.71 & -2.702 & -0.0001168 & -0.00007194 \\ 0 & 0 & 0 & 0 & -20 & 0 & 0 & 0 \\ 0 & 0 & 0 & 0 & 0 & -20 & 0 & 0 \\ 0 & 0 & 0 & 0 & 0 & 0 & 0 & 1 \\ 16.76 & 0 & -119400 & 7272 & -7328 & * & -47.41 & -2.469 \end{bmatrix}$$

(2.32)

Note- *represents the term that is missing from the flexible aircraft.

$$M\ddot{\chi} + B\dot{\chi} + K\chi = F\ (\theta,\alpha,q,\delta_e,\&\ \delta_f) \tag{2.34}$$

where Equation (2.34) represents a standard second-order bending for the mass, spring, and damper system. Dividing by M, Equation (3.34) becomes

$$\ddot{\chi} + \frac{B}{M}\dot{\chi} + \frac{K}{M}\chi = \frac{F}{M}\ (\theta,\alpha,q,\delta_e,\&\delta_f) \tag{2.35}$$

$$\ddot{\chi} + 2\zeta\omega_n\dot{\chi} + \omega_n^2\chi = F'(\theta,\alpha,q,\delta_e,\&\delta_f) \tag{2.36}$$

where ζ is the damping ratio, ω_n is the undamped natural frequency and $F'(\theta,\alpha,q,\delta_e\ \&\ \delta_f) = 16.76\ \theta - 119400\ \alpha + 7272\ q - 7328\ \delta_e - 12540\ \delta_f$ as incorporated in Equation (2.32). For a fighter-type aircraft typical values for the first bending mode are $\zeta = 0.025$ and $\omega_n = 21.0$. Substituting these values for ζ and ω_n of the fighter into Equation (3.36) yields the following equations:

$$\ddot{\chi} + 1.05\ \dot{\chi} + 441\ \chi = F'(\theta,\alpha,q,\delta_e\ \&\ \delta_f) \tag{2.37}$$

Let $\chi_1 = \chi$ (2.38)

$$\chi_2 = \dot{\chi}_1 = \dot{\chi} \tag{2.39}$$

$$\dot{\chi}_2 = -1.05\ \chi_2 - 441\chi_1 + F'(\theta,\alpha,q,\delta_e\ \&\ \delta_f) \tag{2.40}$$

Substituting Equation (2.40) into the place of the $\dot{\chi}_2$ equation found in (2.32), Equation (2.41) is formed.

To determine if Equation (2.41) actually represents a

$$\begin{bmatrix} \theta \\ u \\ \alpha \\ q \\ \delta_e \\ \delta_f \\ \chi_1 \\ \chi_2 \end{bmatrix} = \underline{A} \begin{bmatrix} \theta \\ u \\ \alpha \\ q \\ \delta_e \\ \delta_f \\ \chi_1 \\ \chi_2 \end{bmatrix} + \begin{bmatrix} 0 & 0 \\ 0 & 0 \\ 0 & 0 \\ 0 & 0 \\ 20 & 0 \\ 0 & 20 \\ 0 & 0 \\ 0 & 0 \end{bmatrix} \begin{bmatrix} \delta_{e_{CMD}} \\ \delta_{f_{CMD}} \end{bmatrix}$$

where

$$\underline{A} = \begin{bmatrix} 0 & 0 & 0 & 0 & 1 & 0 & 0 & 0 \\ -32.15 & -0.006647 & 29.75 & -42.38 & 3.131 & -1.131 & 0 & 0 \\ -0.002161 & -0.00004481 & -0.8488 & 0.9965 & -0.08824 & -0.151 & -0.0008243 & -0.000002836 \\ 0.0002948 & 0.0005292 & 2.064 & -0.4555 & -11.71 & -2.702 & -0.0001167 & -0.00007194 \\ 0 & 0 & 0 & 0 & -20 & 0 & 0 & 0 \\ 0 & 0 & 0 & 0 & 0 & -20 & 0 & 0 \\ 0 & 0 & 0 & 0 & 0 & 0 & 0 & 1 \\ 16.76 & 0 & -119400 & 7272 & -7328 & -12540 & -441 & -1.05 \end{bmatrix} \quad (2.41)$$

flexible fighter, its bending mode is examined while performing two different maneuvers. The maneuvers performed are the g-command pull-up and pitch-pointing which are described in Chapter I. Before the effects of structural bending on the aircraft performance are looked at, columns 7 and 8 of the $\dot{\alpha}$ and $\dot{q}$ equations are initially set to zero. Figures 2 and 3 represents the structural bending while performing the two maneuvers. Examining the two figures, the aircraft's bending is larger than what would normally be expected. Therefore, the bending due to the elevator and flaperon is reduced by a factor of 10. Performing the two maneuvers again, the structural bending is illustrated in Figures 4 and 5. Still, the aircraft bends more than a fighter is expected to. For instance, the g-command of 2g's probably bends the aircraft no more than a ½" to 1". Accordingly, another value in the $\dot{\chi}_2$ equation must be reduced. Knowing the bending equation of a KC-135, its values are nearly of the same magnitudes as the flexible fighter, except for the bending due to α (Ref. 6). Therefore, reducing the influence on bending mode due to α by a factor of 10 and keeping δ_e and δ_f at the reduced values, the structural bending while performing the maneuvers resembles reasonable values. Figures 6 and 7 illustrate the bending taking place as the aircraft performs the maneuvers.

Before a comparison is made between the rigid body and the flexible fighter an output equation must be computed for

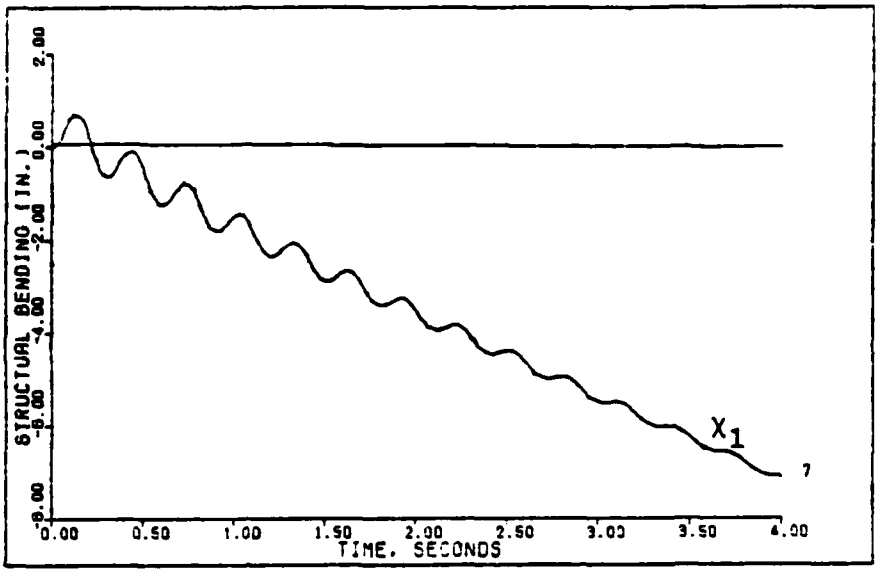

Figure 2. Structural Bending while performing the G-Command Pull-Up Maneuver. (From Eq. (2.41)

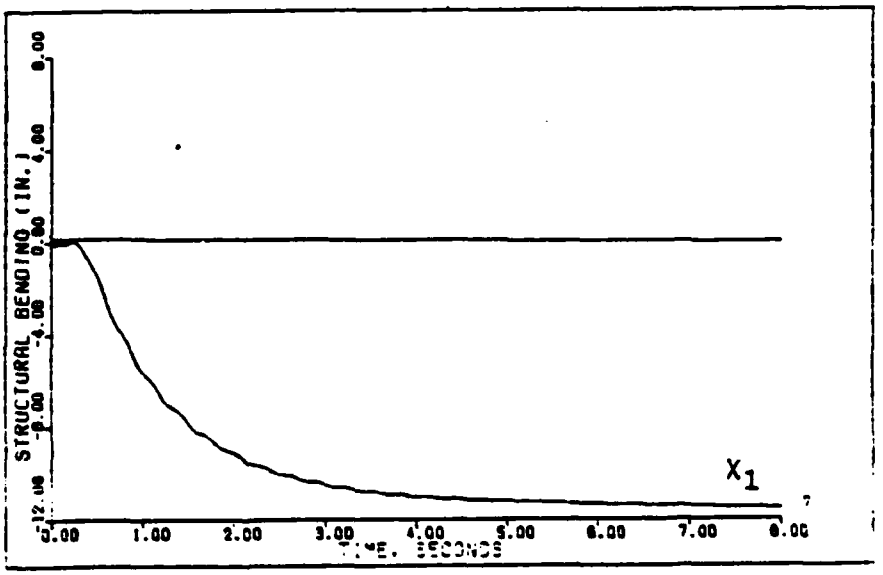

Figure 3. Structural Bending while performing the Pitch-Pointing Maneuver. (From Eq. (2.41)

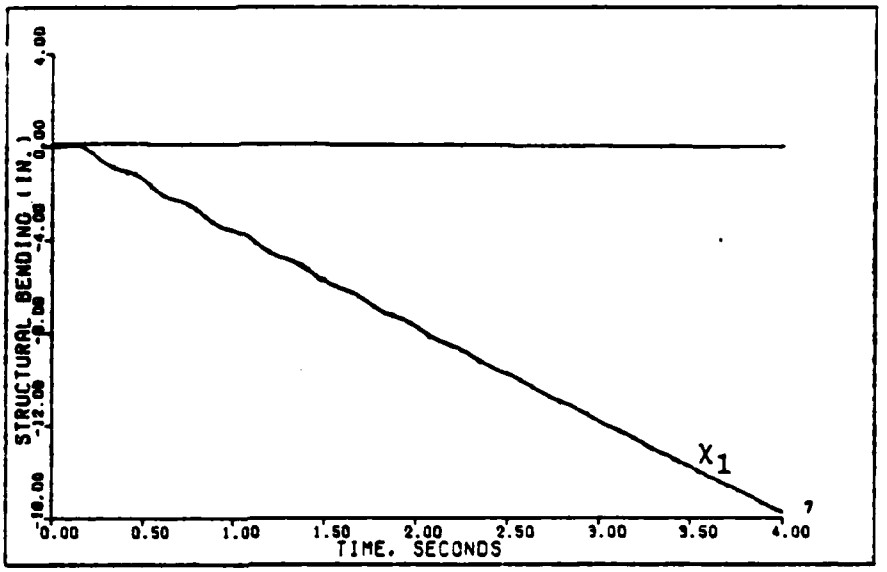

Figure 4. Structural Bending while performing the Pitch-Pointing Maneuver. (From Eq. (2.41) with δ_e and δ_f reduced).

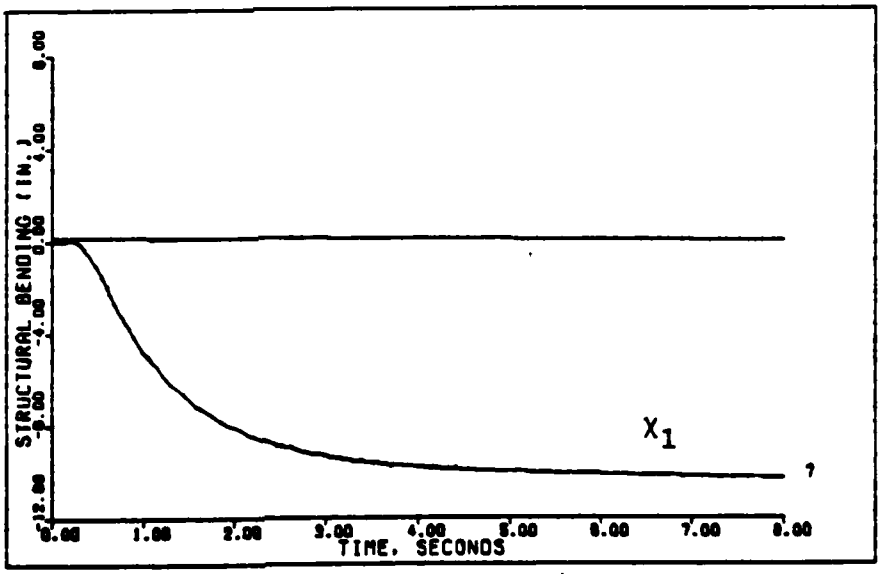

Figure 5. Structural Bending while the G-Command Pull Up Maneuver. (From Eq. (2.41) with δ_e and δ_f reduced)

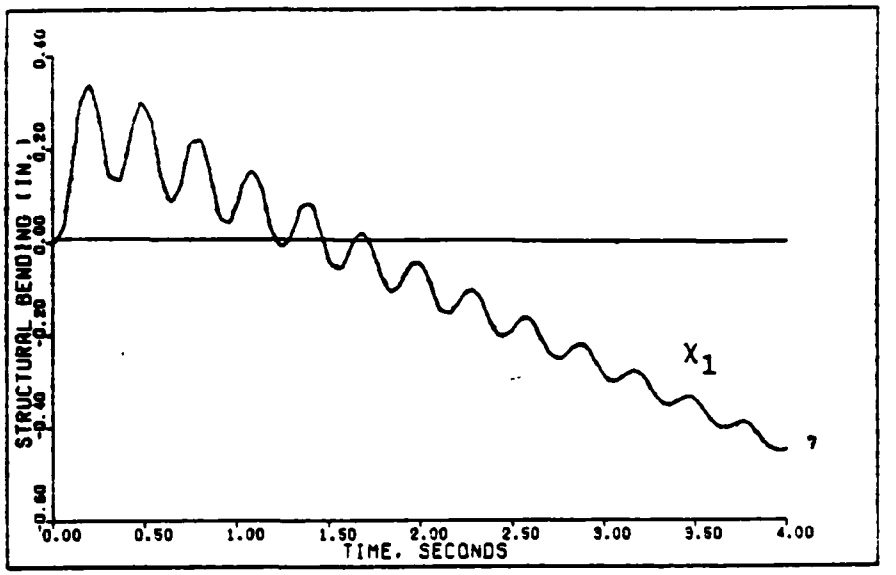

Figure 6. Structural Bending while performing the Pitch-Pointing Maneuver. (From Eq. (2.41) with δ_e, δ_f, and α reduced)

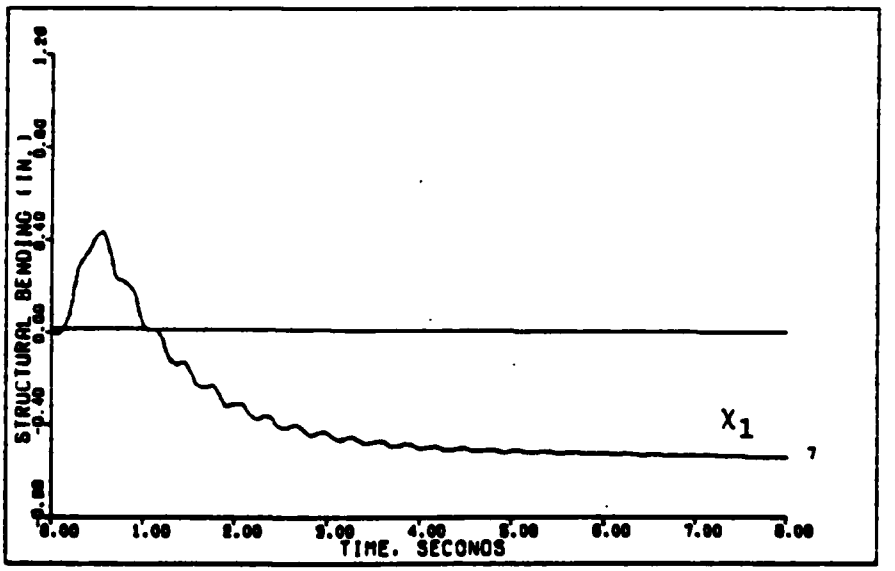

Figure 7. Structural Bending while performing the G-Command Pull Up Maneuver. (From Eq. (2.41) with δ_e, δ_f, and α reduced)

the flexible aircraft. Since the output equation for the rigid body has A_{n_p} as an output, the A_{n_p} equation for the flexible-fighter aircraft must also be developed. This is accomplished by using equations (2.25), (2.26), and $\dot{q}$ in Equation (2.41). The following equation is the result:

$$A_{n_p} = ({}_{1_x}M'_{\theta})\theta + ({}_{1_x}M'_{u}-Z_u)u + ({}_{1_x}M'_{\alpha}-Z_{\alpha})\alpha + ({}_{1_x}M'_{q}-Z_q)q + ({}_{1_x}M'_{\delta_e}-Z_{\delta_e})\delta_e + ({}_{1_x}M'_{\delta_f}-Z_{\delta_f})\delta_f + ({}_{1_x}M'_{\chi_1}-Z_{\chi_1})\chi_1 + ({}_{1_x}M'_{\chi_2}-Z_{\chi_2})\chi_2 \quad (2.42)$$

where $Z_{\chi_1} = Z_{\chi_2} = 0$. Therefore,

$$A_{n_p} = \begin{bmatrix} 0.004113 & 0.04305 & 704.3 & -3.585 & -92.12 & 82.5 & -0.001628 & -0.001004 \end{bmatrix} \begin{bmatrix} \theta \\ u \\ \alpha \\ q \\ \delta_e \\ \delta_f \\ \chi_1 \\ \chi_2 \end{bmatrix} \quad (2.43)$$

Designing the DFSC for the rigid body aircraft and comparing it with the flexible-fighter aircraft (FFA), the units of the state equation is changed to the following:

$$\begin{bmatrix} \theta & \text{(deg)} \\ u & \text{(ft/s)} \\ \alpha & \text{(deg)} \\ q & \text{(deg/s)} \\ \delta_e & \text{(deg)} \\ \delta_f & \text{(deg)} \\ \chi_1 & \text{(in)} \\ \chi_2 & \text{(in/s)} \end{bmatrix}$$

For the output equation the units are

$$\begin{bmatrix} A_{n_p} & \text{(g)} \\ q & \text{(deg)} \end{bmatrix}$$

Tables 5 and 6 are the values for the rigid body and the flexible-fighter aircraft, respectively, that are used in the designing of the DCFS. The flexible-fighter aircraft has 5 different bending mode set ups that are explained in Chapter IV.

TABLE 5

Rigid Body (R.B.)

A MATRIX

$$\begin{bmatrix} 0 & 0 & 0 & 0 & 0 & 0 \\ -.5611 & -.006647 & .5192 & -.7396 & .05464 & -.01974 \\ -.002161 & -.002568 & -.8488 & .9965 & -.08824 & -.151 \\ .0002948 & .03032 & 2.064 & -.4555 & -11.71 & -2.702 \\ 0 & 0 & 0 & 0 & -20 & 0 \\ 0 & 0 & 0 & 0 & 0 & -20 \end{bmatrix}$$

X VECTOR

$$\begin{bmatrix} \theta & \text{(deg)} \\ u & \text{(ft/s)} \\ \alpha & \text{(deg)} \\ q & \text{(deg/s)} \\ \delta_e & \text{(deg)} \\ \delta_f & \text{(deg)} \end{bmatrix}$$

B MATRIX

$$\begin{bmatrix} 0 & 0 \\ 0 & 0 \\ 0 & 0 \\ 0 & 0 \\ 20 & 0 \\ 0 & 20 \end{bmatrix} \begin{bmatrix} \delta_{e_{CDM}} & \text{(deg)} \\ \delta_{f_{CDM}} & \text{(deg)} \end{bmatrix}$$

C MATRIX

$$\begin{bmatrix} .2229E\text{-}5 & .001337 & .3817 & -.001943 & -.0547 & .04469 \\ 0 & 0 & 0 & 1 & 0 & 0 \end{bmatrix}$$

OUTPUT

$$\begin{bmatrix} A_{n_p} & \text{(g)} \\ q & \text{(deg/s)} \end{bmatrix}$$

TABLE 6

Flexible-Fighter Aircraft (FFA)

"A" MATRIX

$$\begin{bmatrix}
0 & 0 & 0 & 1 & 0 & 0 & 0 & 0 \\
-0.5611 & -0.006647 & 0.5192 & -0.7396 & 0.05464 & -0.01974 & 0 & 0 \\
-0.002161 & -0.002568 & -0.8488 & 0.9965 & -0.08824 & -0.151 & -0.004723 & -0.0001625 \\
0.0002948 & 0.0302 & 2.064 & -0.4555 & -11.71 & -2.702 & -0.006687 & -0.004122 \\
0 & 0 & 0 & 0 & -20 & 0 & 0 & 0 \\
0 & 0 & 0 & 0 & 0 & -20 & 0 & 0 \\
0 & 0 & 0 & 0 & 0 & 0 & 0 & 1 \\
0.2925 & 0 & -208.4 & 126.9 & -12.79 & -21.88 & -441 & -1.05
\end{bmatrix}$$

X VECTOR

$$\begin{bmatrix}
\theta \quad \text{(deg)} \\
u \quad \text{(ft/s)} \\
\alpha \quad \text{(deg)} \\
q \quad \text{(deg/s)} \\
\delta_e \quad \text{(deg)} \\
\delta_f \quad \text{(deg)} \\
\chi_1 \quad \text{(in)} \\
\chi_2 \quad \text{(in/s)}
\end{bmatrix}$$

B MATRIX

$$\begin{bmatrix}
0 & 0 \\
0 & 0 \\
0 & 0 \\
0 & 0 \\
20 & 0 \\
0 & 20 \\
0 & 0 \\
0 & 0
\end{bmatrix}
\begin{bmatrix}
\delta_{e_{CMD}} \quad \text{(deg)} \\
\delta_{f_{CMD}} \quad \text{(deg)}
\end{bmatrix}$$

C MATRIX

$$\begin{bmatrix}
0.000002229 & 0.001337 & 0.3817 & -0.001943 & -0.0547 & 0.04469 & -0.00005056 & -0.00003118 \\
0 & 0 & 0 & 1 & 0 & 0 & 0 & 0
\end{bmatrix}$$

OUTPUT

$$\begin{bmatrix}
A_{n_p} \quad \text{(g)} \\
q \quad \text{(deg/s)}
\end{bmatrix}$$

III. Multivariable Control Law Development

Introduction

Of all the digital control design methods available today, this thesis uses the method developed by Professor Brian Porter of the University of Salford, England. A summary of the techniques presented in Reference 3 is given in this chapter. The design techniques described in the references are both conceptually and computationally simple. In addition to the techniques utilizing singular perturbation methods, these are also applicable to the design of both analogue and digital controllers. The digital controller developed in this thesis produces a proportional plus integral control signal that is held piece-wise constant for each sampling period.

Output decoupling is essential in the design of many Multiple Input-Multiple Output (MIMO) control systems. The system can be represented by either a continuous-time plant model or a discrete-time plant model. For the continuous-time representation the state and output equations are:

$$\dot{\underline{x}}(t) = \underline{A}\,\underline{x}(t) + \underline{B}\,\underline{u}(t) + \underline{D}\,\underline{d}(t) \tag{3.1}$$

$$\underline{y}(t) = \underline{C}\,\underline{x}(t) \tag{3.2}$$

where

$\underline{A}$ = continuous - time plant matrix

$\underline{B}$ = continuous - time control matrix

$\underline{D}$ = continuous - time disturbance matrix

$\underline{C}$ = continuous - time output matrix

The discrete-time state and output equations of the plant follow the form:

$$\underline{x}(kT+T) = \phi\underline{x}(kT) = \Psi\underline{u}(kT) + \Delta\underline{d}(kT) \tag{3.3}$$

$$\underline{y}(kT) = \Gamma\underline{x}(kT) \tag{3.4}$$

where

ϕ = sampled-data plant matrix

Ψ = sampled-data control matrix

Δ = sampled-data disturbance matrix

Γ = sampled-data output matrix

and

$$\phi = \exp(\underline{A}T) \tag{3.5}$$

$$\Psi = \int_0^T \exp(\underline{A}T)\ \underline{B}\ dt \tag{3.6}$$

$$\Delta = \int_0^T \exp(\underline{A}T)\ \underline{D}\ dt \tag{3.7}$$

$$\Gamma = \underline{C} \tag{3.8}$$

The dimensions n, m, and p represent the number of states, inputs, and outputs, respectively.

The plant in state space form has the following format:

$$\begin{bmatrix} \dot{\underline{x}}_1 \\ \dot{\underline{x}}_2 \end{bmatrix} = \left[\begin{array}{c|c} \underline{A}_{11} & \underline{A}_{12} \\ \hline \underline{A}_{22} & \underline{A}_{22} \end{array}\right] \begin{bmatrix} \underline{x}_1 \\ \underline{x}_2 \end{bmatrix} + \begin{bmatrix} \underline{B}_1 \\ -- \\ \underline{B}_2 \end{bmatrix} \underline{u} \tag{3.9}$$

$$\begin{bmatrix} \underline{y} \end{bmatrix} = \begin{bmatrix} \underline{C}_1 & C_2 \end{bmatrix} \begin{bmatrix} \underline{x}_1 \\ \underline{x}_2 \end{bmatrix} \tag{3.10}$$

where $\underline{B}_2$ is a square matrix with a row and column size equal to the number of inputs in the vector $\underline{u}$; and $\underline{C}_2$ is a square matrix with the number of rows and columns equal to the number of outputs. Also, $\underline{A}_{22}$ has the same dimensions as $\underline{B}_2$ and $\underline{C}_2$. Knowing these dimensions allows the system matrices to be easily partitioned as shown above. It is preferable, but not necessary, if $\underline{B}_1 = 0$. This may occur as in a kinematic equation or may be achieved by a transformation of variables.

Requirements to have a successful design using Porter's techniques are as follows:

(1) The system must be controllable and observable.

(2) The number of inputs must equal the number of outputs.

Two design methods discussed in this chapter are the regular and the irregular designs for the case where the state and output equations are known. The choice between the two design methods is determined by the type of plant being considered, and the outputs which are to be controlled.

Regular Plants

To be considered as a "regular" plant, the rank of

the first Markov parameter, [$\underline{CB}$], must have full rank. Because [$\underline{CB}$] is of full rank, the gain matrix for feedback control is found using the inverse of [$\underline{CB}$].

The control law is a proportional plus integral output feedback law expressed in the descrete case, shown in Figure 8 (for the regular plant the $\underline{M}$ matrix is not utilized), as:

$$u(kT) = (\frac{1}{T}) \ [\underline{K}_0\underline{e}(kT) + \underline{K}_1\underline{z}(kT)] \qquad (3.11)$$

where

$\frac{1}{T}$ = is a scalar gain which is equal to the sampling frequency

$\underline{K}_0$ = is the proportional gain matrix for the error signal $\underline{e}(kT)$

$\underline{K}_1$ = is the gain matrix for the backward difference of the error signal, which is designated as $\underline{z}(kT)$

Although a continuous integrator is shown in Figure 8, the digital implementation represents the discrete state equation

$$\underline{e}(kT) = \underline{r}(kT) - \underline{y}(kT)$$

$$\underline{z}[\ (k+1)T\ ] = \underline{z}(kT) + T\underline{e}(kT)$$

For the continuous case, shown in Figure 9, the law is expressed as

$$\underline{u}(t) = g(\underline{K}_0\underline{e}(t) + \underline{K}_1\int\underline{e}(t))dt \qquad (3.12)$$

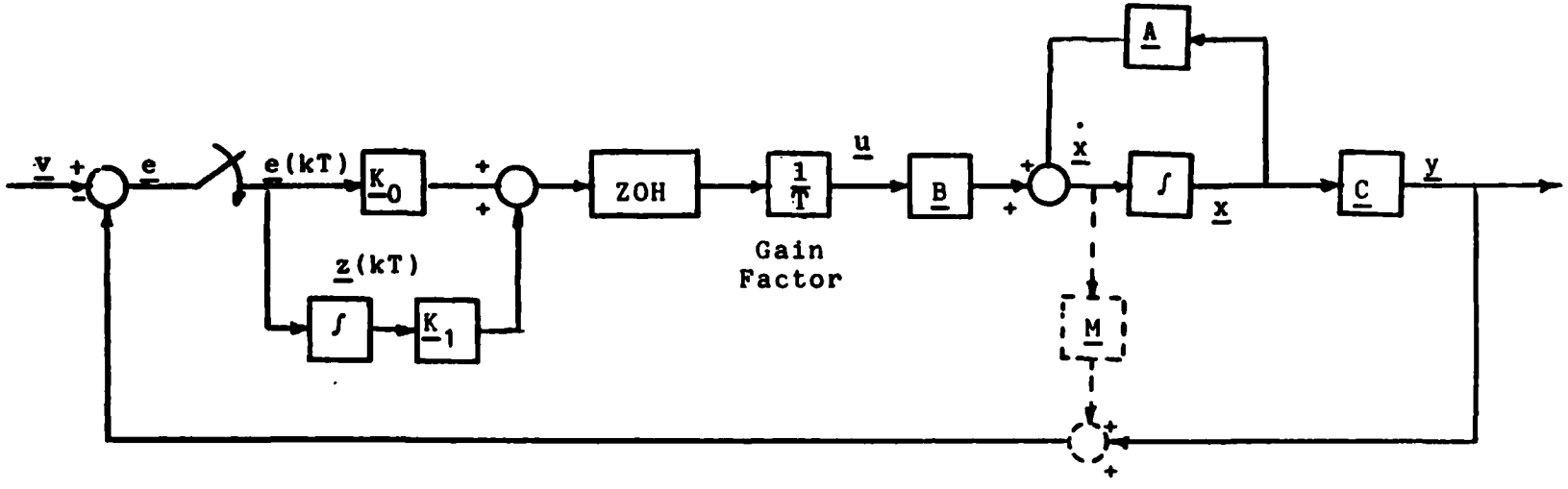

Figure 8. System Block Diagram - Discrete Design

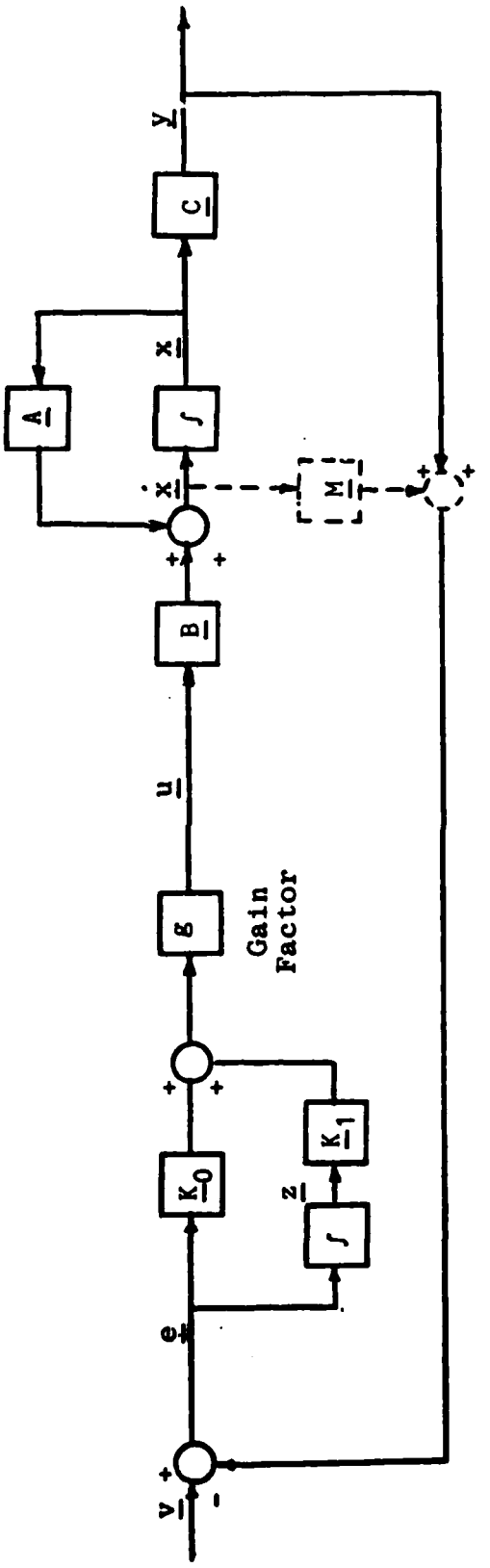

Figure 9. System Block Diagram - Continuous Design

where

g is the forward path gain

$\underline{K}_0$ is the proportional gain for the error signal

$\underline{K}_1$ is the gain for the integral of the error signal

The $\underline{K}_0$ and the $\underline{K}_1$ matrices are determined using the following equations:

$$\underline{K}_0 = (\underline{CB})^{-1}\underline{\Sigma} \tag{3.13}$$

$$\underline{K}_1 = \bar{\alpha}(\underline{CB})^{-1}\underline{\Sigma} \tag{3.14}$$

where

$\bar{\alpha}$ is the ratio of the error $\underline{e}$ to the integral of error $\underline{z}$

$\underline{\Sigma}$ is the diagonal weighting matrix whose scalar elements, σ_i, are chosen by the designer. These values determine the respective gains or weighting of each error signal on the control surface.

The error vector $\underline{e}$ is expressed as $\underline{e} = \underline{v}-\underline{y}$. Each command in the $\underline{v}$ vector is compared with its corresponding output element in the $\underline{y}$ vector and is the input for the proportional plus integral controller. Since the complete system includes a vector integrator, the steady-state value of the error vector is zero for a constant command vector input, and tracking is achieved. Therefore, because the error vector is driven to zero, the resulting output equals the command input.

Irregular Plant

Plants in which the First Markov parameter, $[\underline{CB}]$, is rank deficient are designated as "irregular". For the

irregular plant the $\underline{M}$ matrix in Figure 8 is utilized to allow the design to be accomplished. An $\underline{F}$ matrix is formed, as shown, and used in place of the $\underline{C}$ matrix:

$$\underline{F} = [\underline{F}_1 \mid \underline{F}_2] \tag{3.15}$$

where

$$\underline{F}_1 = [\underline{C}_1 + \underline{MA}_{11}] \tag{3.16}$$

$$\underline{F}_2 = [\underline{C}_2 + \underline{MA}_{12}] \tag{3.17}$$

The elements of the measurement matrix $\underline{M}$ are selected to obtain a matrix $[\underline{FB}]$ having full rank and thus being invertible. $\underline{M}$ is slected to be as sparse as possible (Ref. 7).

The control law for the discrete case in Equation (3.11) and for the continuous case in Equation (3.12) are the same as the regular plant, except that the $\underline{K}_0$ and the $\underline{K}_1$ matrices are determined by the following equations:

$$\underline{K}_0 = (\underline{FB})^{-1}\underline{\Sigma} \tag{3.18}$$

$$\underline{K}_1 = \bar{\alpha}(\underline{FB})^{-1}\underline{\Sigma} \tag{3.19}$$

In the irregular design the $\underline{e}$ vector is defined by

$$\underline{e} = \underline{v}-\underline{w} \tag{3.20}$$

where

$$\underline{w} = \underline{y} + \dot{\underline{M}}\underline{x}_1 \tag{3.21}$$

These outputs $\underline{w}$ are developed with the measurement matrix $\underline{M}$ and the derivatives $\underline{\dot{x}}_1$ of the system states. The error vector, $\underline{e}$, for the irregular design becomes the same as the regular design when the states reach their steady-state value. This can be seen as follows: With a constant command vector $\underline{v}$ the states reach constant steady-state values and therefore:

$$\underline{\dot{x}}_1 = 0 \text{ (when } \underline{x}_1 \text{ reaches steady-state)}$$

so that

$$\underline{w}_{ss} = \underline{y}_{ss} \tag{3.22}$$

Substituting Equation (3.22) into Equation (3.20) the steady-state error vector again becomes $\underline{e} = \underline{v}-\underline{y}$. Therefore, since the error $\underline{e} = 0$, as before, the output equals the command input, that is $\underline{y} = \underline{v}$.

Asymptotic Characteristics

The system transfer function $\underline{G}(\lambda) = \underline{C}(\lambda\underline{I}-\underline{A})^{-1}\underline{B}$ assumes the asymptotic form

$$\underline{\Gamma}(\lambda) = \tilde{\underline{\Gamma}}(\lambda) + \hat{\underline{\Gamma}}(\lambda) \tag{3.23}$$

where

$\tilde{\underline{\Gamma}}(\lambda)$ is the "slow" transfer function matrix,

and

$\hat{\underline{\Gamma}}(\lambda)$ is the "fast" transfer function matrix.

The system reaches these asymptotic values as the gain factor $g \to \infty$ for the continuous design or as the gain factor $\frac{1}{T} \to \infty$ for the discrete case. The poles of $\underline{\tilde{\Gamma}}(\lambda)$ consist of two sets of roots that are designated as $\underline{Z}_1$ and $\underline{Z}_2$. The poles of the fast transfer function $\underline{\hat{\Gamma}}(\lambda)$ are designated as $\underline{Z}_3$. For a regular design the slow modes associated with the set of roots $\underline{Z}_1$ become uncontrollable while modes associated with the set of roots $\underline{Z}_2$ (composed of the transmission zeroes) become unobservable as the gain factor increases toward infinity. As this happens, the system response is increasingly dominated by the fast modes which are associated with the set of roots $\underline{Z}_3$. Thus, the slow modes contained in $\underline{\tilde{\Gamma}}(\lambda)$ disappear from the overall transfer function $\underline{\Gamma}(\lambda)$, and only the fast modes in $\underline{\hat{\Gamma}}(\lambda)$ remain for a regular design. The expressions for the asymptotic modes are given in Table 7.

The system transfer function $\underline{G}(\lambda)$ approaches a diagonal asymptotic form of increasingly non-interacting control. Therefore, as a result, the output responses become decoupled as the gain increases. The asymptotic closed-loop transfer function of the discrete system has the form:

$$\underline{\Gamma}(\lambda) = \text{diag}\ \{\frac{\sigma_1}{\lambda-1+\sigma_1}, \frac{\sigma_2}{\lambda-1+\sigma_2}, \ \ldots\ldots, \frac{\sigma_i}{\lambda-1+\sigma_i}\} \qquad (3.24)$$

For the continuous system, the asymptotic transfer function has the form

Table 7

Asymptotic Equations for Zero-$\underline{B}_2$ Form

System is represented by:

$$\begin{bmatrix} \dot{\underline{x}}_1 \\ \dot{\underline{x}}_2 \end{bmatrix} = \left[\begin{array}{c|c} \hat{\underline{A}}_{11} & \hat{\underline{A}}_{12} \\ \hline \hat{\underline{A}}_{21} & \hat{\underline{A}}_{22} \end{array}\right] \begin{bmatrix} \underline{x}_1 \\ \underline{x}_2 \end{bmatrix} + \left[\begin{array}{c} 0 \\ \hline \hat{\underline{B}}_2 \end{array}\right] \underline{u} \qquad \text{and} \qquad \underline{y} = [\, \hat{\underline{C}}_1 \;\; \hat{\underline{C}}_2 \,] \begin{bmatrix} \underline{x}_1 \\ \underline{x}_2 \end{bmatrix}$$

Continuous Case	Discrete Case
Gain Factor = g	Gain Factor = 1/T
(Poles are in the s-plane)	(Poles are in the z-plane)
$\tilde{\Gamma}(\lambda) = \underline{C}_o(\lambda \underline{I}_n - \underline{A}_o)^{-1}\underline{B}_o = 0$	$\tilde{\Gamma}(\lambda) = \underline{C}_o(\lambda \underline{I}_n - \underline{A}_o)^{-1}\underline{B}_o$
$\hat{\Gamma}(\lambda) = (\lambda \underline{I}_m + g\, \hat{\underline{C}}_2\hat{\underline{B}}_2\, K_o)^{-1} g\, \hat{\underline{C}}_2\hat{\underline{B}}_2\, \underline{K}_0$	$\tilde{\Gamma}(\lambda) = (\lambda \underline{I}_m - \underline{I}_m + \hat{\underline{C}}_2\hat{\underline{B}}_2\, \underline{K}_0)^{-1}\hat{\underline{C}}_2\hat{\underline{B}}_2\, \underline{K}_0$
Finite roots	
$\underline{Z}_1 = \{\lvert \lambda\, \underline{K}_0 + \underline{K}_1 \rvert\} = 0$	$\underline{Z}_1 = \{\lvert \lambda \underline{I}_m - \underline{I}_m + T\, \underline{K}_0^{-1}\underline{K}_1 \rvert = 0\}$
$\underline{Z}_2 = \{\lvert \lambda\, \underline{I}_{n-m} - \hat{\underline{A}}_{11} + \hat{\underline{A}}_{12}\, \hat{\underline{C}}_{12}^{-1}\hat{\underline{C}}_1 \rvert = 0\}$	$\underline{Z}_2 = \{\lvert \lambda \underline{I}_{n-m} - T\, \hat{\underline{A}}_{11} + \hat{\underline{A}}_{12}\, \hat{\underline{C}}_2^{-1}\hat{\underline{C}}_1 \rvert\} = 0$

Table 7 (continued)

Infinite roots

$$\underline{Z}_3 = \{|\lambda \underline{I}_m + g\, \hat{\underline{C}}_2 \hat{\underline{B}}_2\, \underline{K}_0| = 0\} \qquad \underline{Z}_3 = \{|\lambda \underline{I}_m - \underline{I}_m + \hat{\underline{C}}_2 \hat{\underline{B}}_2\, \underline{K}_0| = 0\}$$

where:

$$\underline{A}_o = \left[\begin{array}{c|c} -\underline{K}_0^{-1}\underline{K}_1 & 0 \\ \hline \underline{A}_{12}\underline{C}_2^{-1}\underline{K}_0^{-1}\underline{K}_1 & \underline{A}_{11}-\underline{A}_{12}\underline{C}_2^{-1}\underline{C}_1 \end{array}\right]$$

$$\underline{B}_o = \left[\begin{array}{c} 0 \\ \hline \underline{A}_{12}\underline{C}_2^{-1} \end{array}\right]$$

Regular Design

$$\underline{C}_o = [\underline{K}_0^{-1}\underline{K}_1 \,|\, 0]$$

Irregular Design

$$\underline{C}_o = [\underline{C}_2\underline{F}_2^{-1}\underline{K}_0^{-1}\underline{K}_1 \,|\, \underline{C}_1 - \underline{C}_2\underline{F}_2^{-1}\underline{F}_1]$$

$$\underline{\Gamma}(\lambda) = \text{diag} \quad \frac{g\sigma_1}{\lambda+g\sigma_1}, \frac{g\sigma_2}{\lambda+g\sigma_2}, \ldots, \frac{g\sigma_i}{\lambda+g\sigma_i} \tag{3.25}$$

where the σ's come from the weighting matrix $\underline{\Sigma}$.

For the irregular plant, the previous equations can be applied. The equations in Table 5 are the same for the irregular design after replacing the $\underline{C}$ matrix with the $\underline{F}$ matrix. The component $\underline{C}_1$ is replaced by $\underline{F}_1$ and $\underline{C}_2$ is replaced by $\underline{F}_2$ as calculated in Equations (3.16) and (3.17). It should be noted for the irregular case the $\underline{C}_o$ is different as indicated in the table. Also, for the irregular design, as the slow modes associated with the set of roots $\underline{Z}_1$ become uncontrollable the modes associated with the set of roots $\underline{Z}_2$ remain observable as the gain factor increases toward infinity.

The asymptotic closed-loop system roots can be calculated from the equations in Table 5 and are composed of the sets $\underline{Z}_1$, $\underline{Z}_2$, and $\underline{Z}_3$. The following rules can be used to estimate root locations in the s-plane as $g \to \infty$.

The set of roots $\underline{Z}_1$ are m in number and are all equal to $\bar{\alpha}$, the ratio of integral to proportional gain values, if $\underline{K}_1 = \bar{\alpha}\underline{K}_0$. The set of roots $\underline{Z}_2$ are n-m in number and located at the transmission zero locations. Thus, the transmission zeros (Z_t) can be calculated from the $\underline{Z}_2$ equation in Table 7 if the $\underline{B}$ matrix has the "zero-$\underline{B}_2$" form shown.

The set of roots $\underline{Z}_3$ are m in number and for the continuous case they are located at $-g\sigma_i$ on the real axis where g is the

gain factor and σ_i is the respective weighting element in the $\underline{\Sigma}$ matrix. For the discrete case the roots are located at $1-\sigma_i$.

IV. Responses for the Rigid Body and the Flexible-Fighter Aircraft

Frequency Responses

The effect of a bending mode on the frequency response of the longitudinal acceleration at the pilot's station (A_{n_p}) with either an elevator or flaperon input is examined in this section. Figures 10 and 11 show the frequency responses A_{n_p}/δ_e and A_{n_p}/δ_f, respectively, for the rigid body aircraft. Figures 12 and 13, correspond to the flexible-fighter aircraft (FFA) as modeled in Table 6, Chapter II.

A series of five representations of the bending mode and its coupling into the aircraft motion variables is studied. This permits a study of the effects of a wide range of aircraft structural bending characteristics on the aircraft tracking performance. Examining the effect that the bending mode has an A_{n_p}, the factors dealing with the bending mode states χ_1 and χ_2 are increased by a factor of 10 which yields the following output equation:

$$A_{n_p} = [0.000002229 \quad 0.001337 \quad 0.3817 \quad -0.001943 \quad -0.0547 \quad 0.04469 \quad -0.0005056 \quad -0.0003118]\ \underline{x} \tag{4-1}$$

where $\underline{x} = [\theta \ u \ \alpha \ q \ \delta_e \ \delta_f \ \chi_1 \ \chi_2]^T$

Figures 14 and 15 show the frequency responses of A_{n_p}/δ_e

FIGURE 10. AN/DELTA ELV. FOR THE RIGID BODY (R.B.)

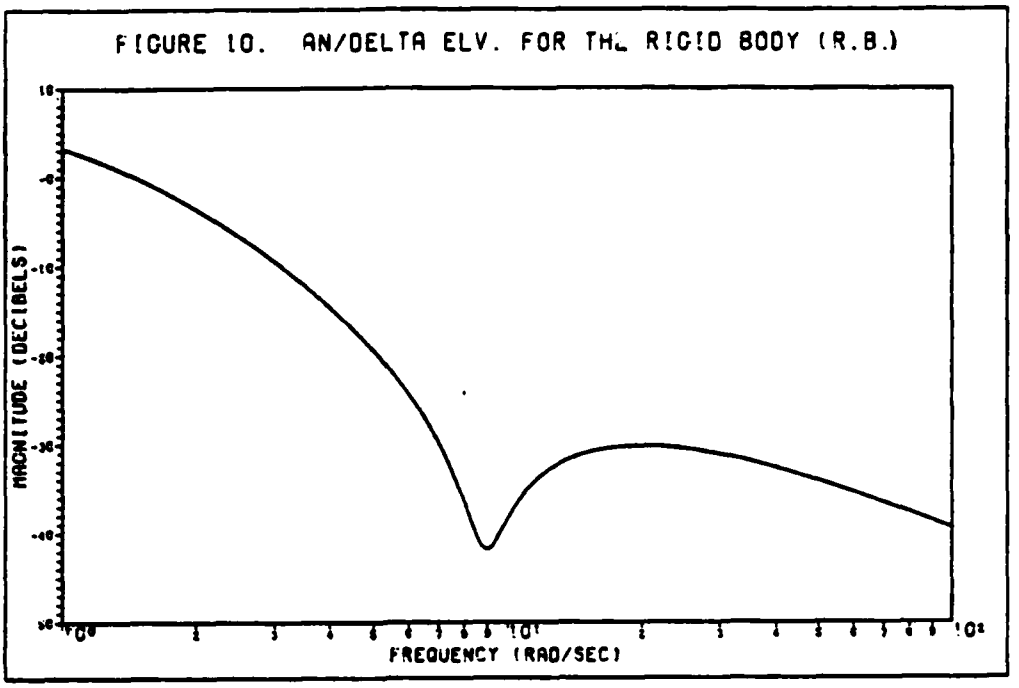

FIGURE 11. AN/DELTA FPN. FOR THE R.B.

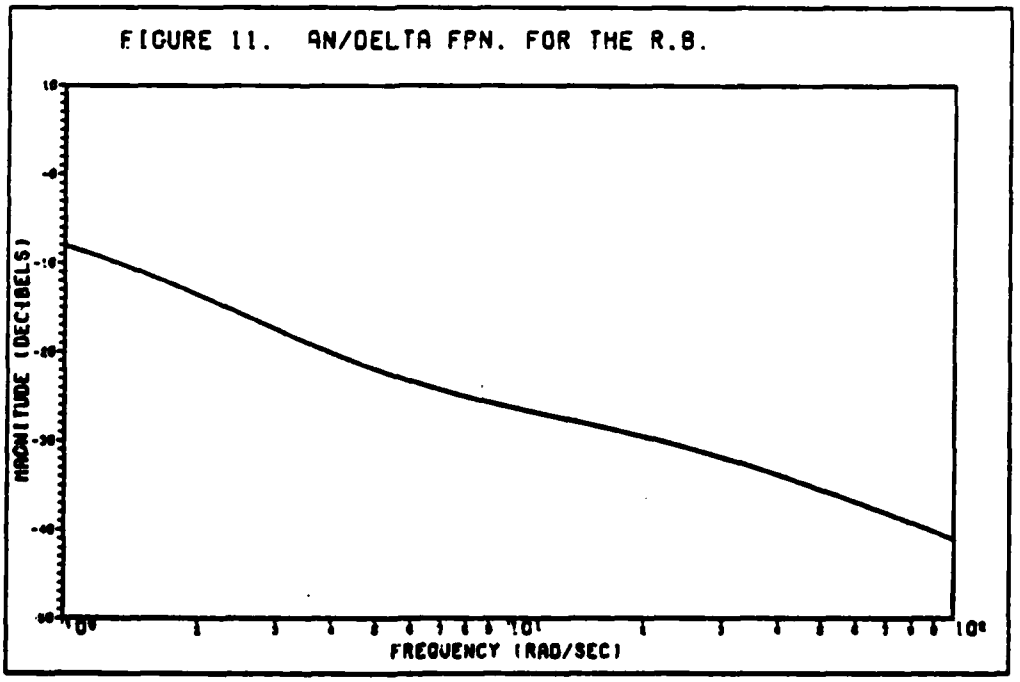

FIGURE 12. AN/DELTA ELV. FOR THE FFA.

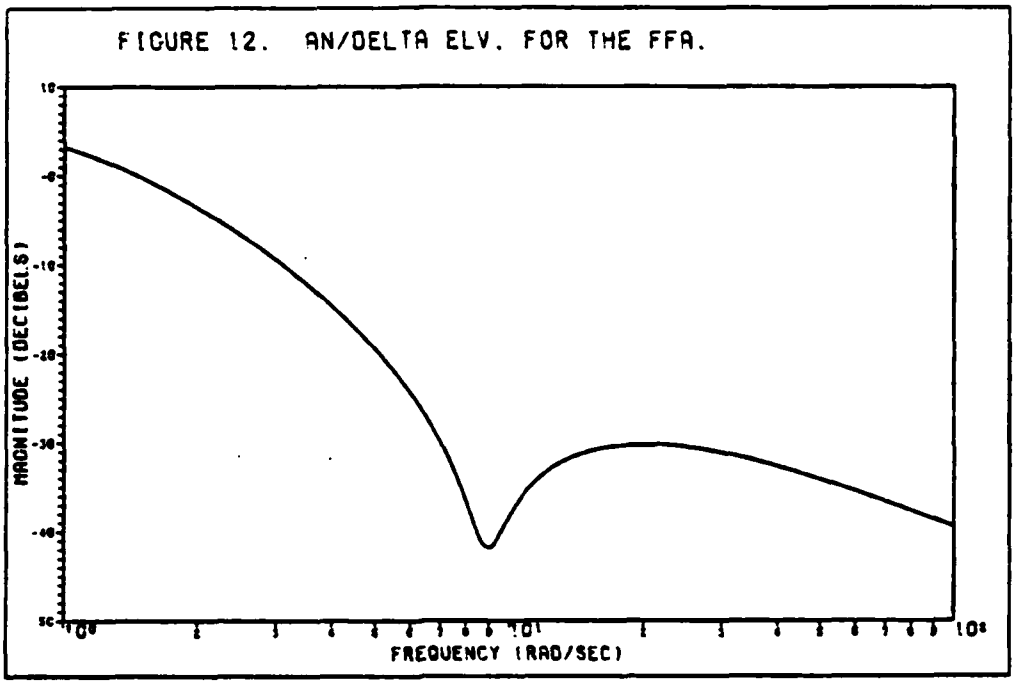

FIGURE 13. AN/DELTA FPN. FOR THE FFA.

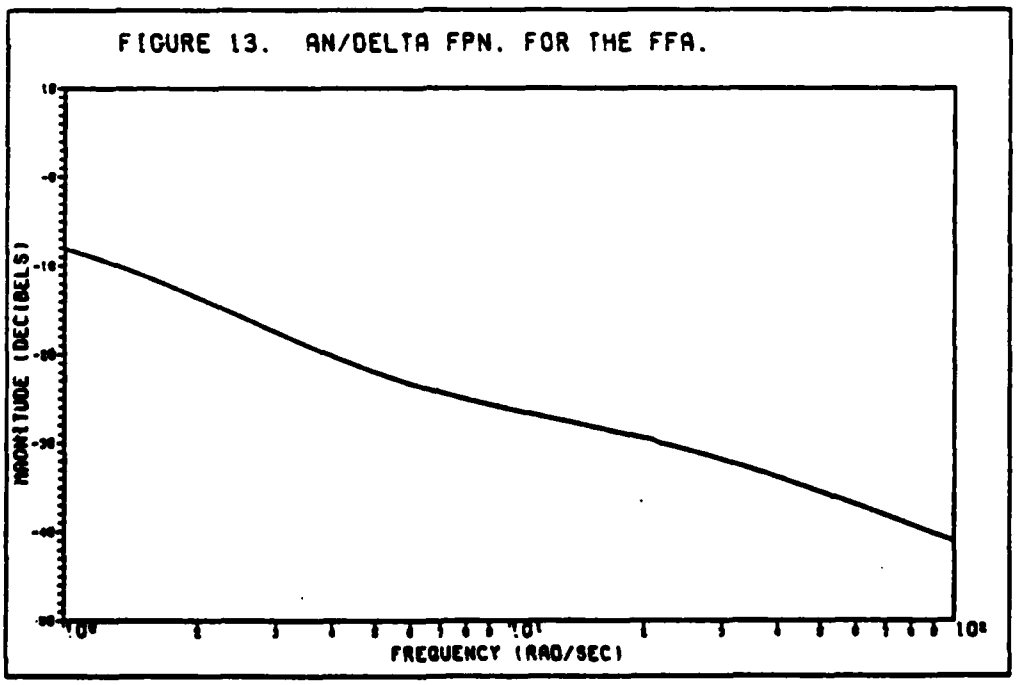

FIGURE 14. AN/DELTA ELV. FOR THE FFA1C.

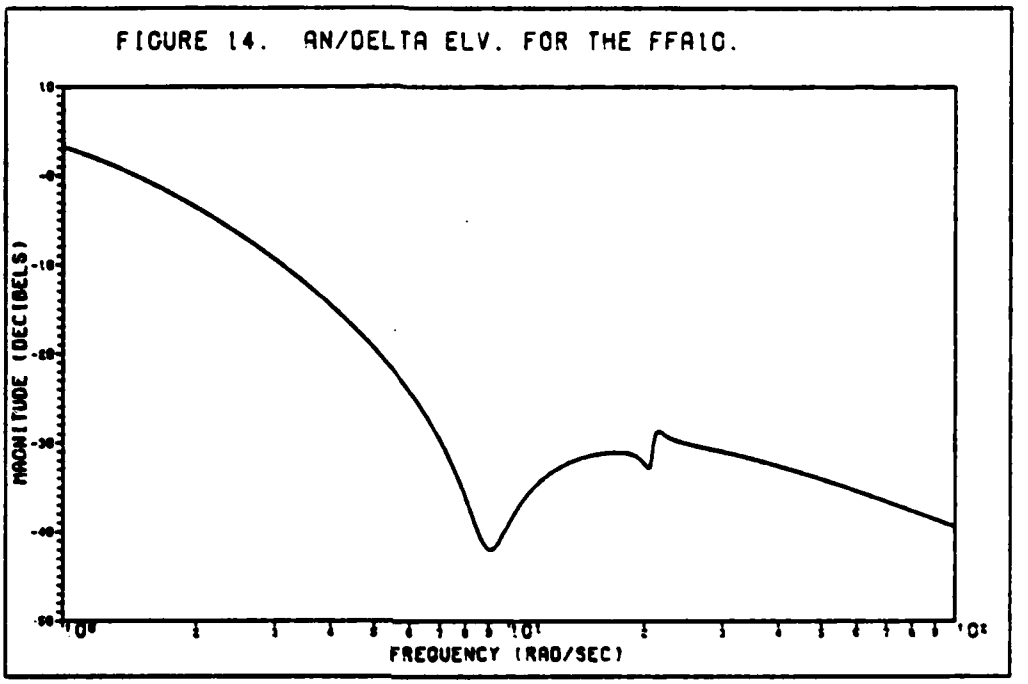

FIGURE 15. AN/DELTA FPN. FOR THE FFA1C.

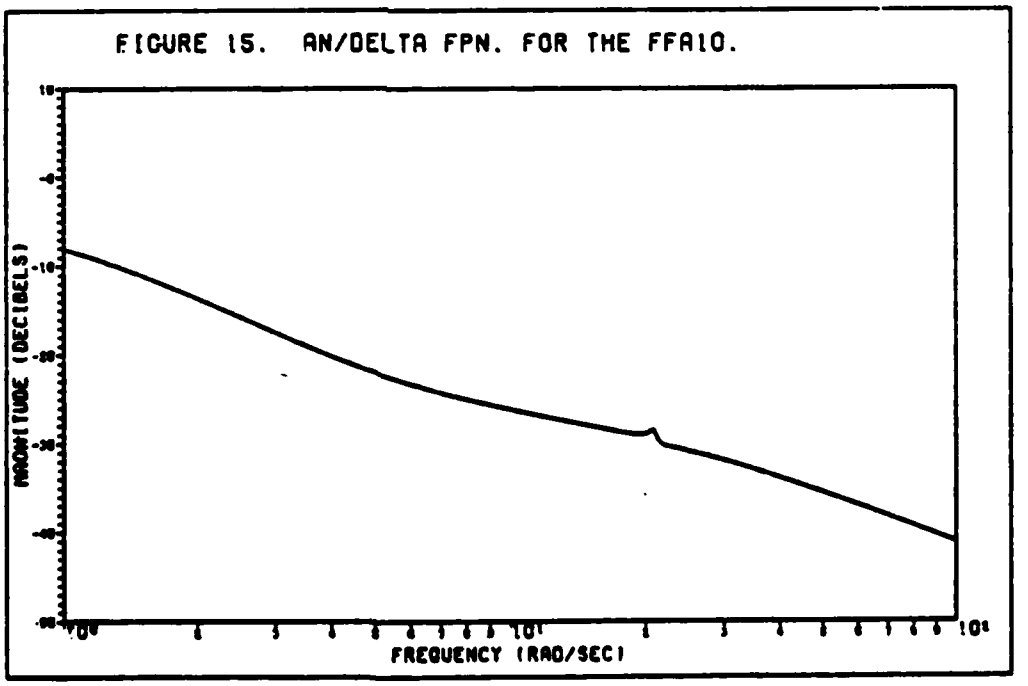

and A_{n_p}/δ_f, respectively, using Equation (4-1), which are represented as FFA10.

To further examine these effects, the χ_1 and χ_2 coefficients are increased by a factor of 100 which is shown in Equation (4-2):

$$A_{n_p} = [0.000002229 \quad 0.001337 \quad 0.3817 \quad -0.001943 \quad -0.0547 \quad 0.04469 \quad -0.005056 \quad -0.003118]\ \underline{x} \qquad (4\text{-}2)$$

Figures 16 and 17 are the results using the output Equation (4-2). The new aircraft model is represented as FFA100.

The output Equation A_{n_p} is originally computed by Equation (2.25) as $A_{n_{cg}} + l_x(\dot{q})$, as described in Chapter II. As a further modification of the aircraft model the χ_1 and χ_2 factors found in the $\dot{q}$ equation are increased by the same amount as in the output equation. Figures 18 and 19, represented as FFA10q, are the responses A_{n_p}/δ_e and A_{n_p}/δ_f, respectively, using Equation (4-1) for A_{n_p} and increasing the χ_1 and χ_2 factors in the $\dot{q}$ equation by 10. Figures 20 and 21, are the results of increasing the χ_1 and χ_2 factors in the $\dot{q}$ equation by 100 and using the output Equation (4-2) for A_{n_p}. These figures represent the aircraft model FFA100q.

Time Responses

This section examines the digital flight control design for the rigid body and for the five different flexible-fighter models performing the q-command pull-up maneuver

FIGURE 16. AN/DELTA ELV. FOR THE FFA100.

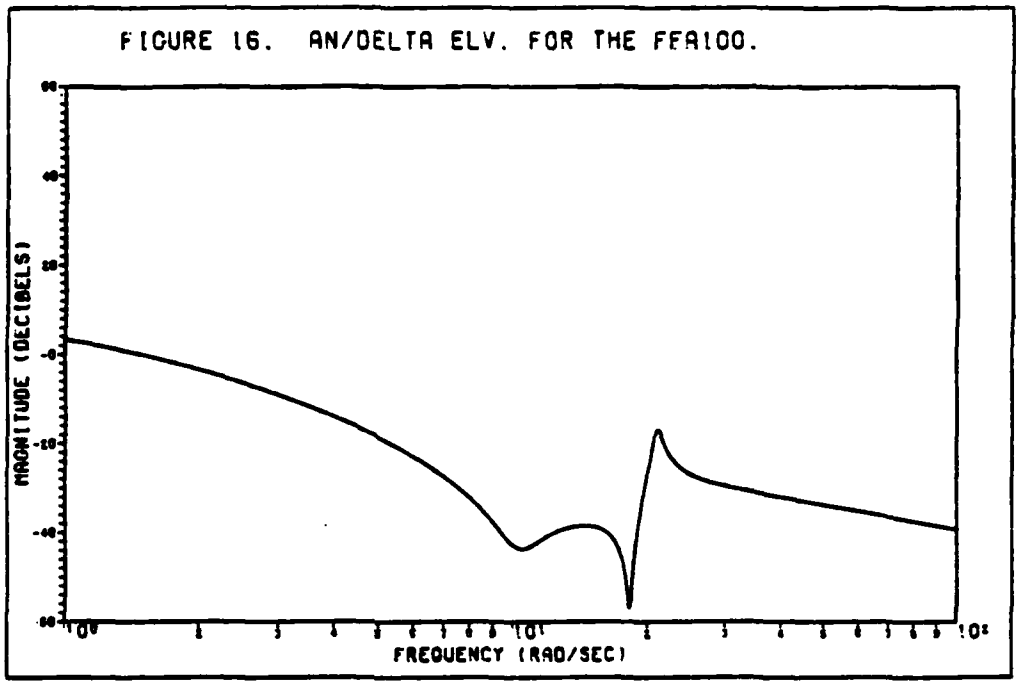

FIGURE 17. AN/DELTA FPN. FOR THE FFA100.

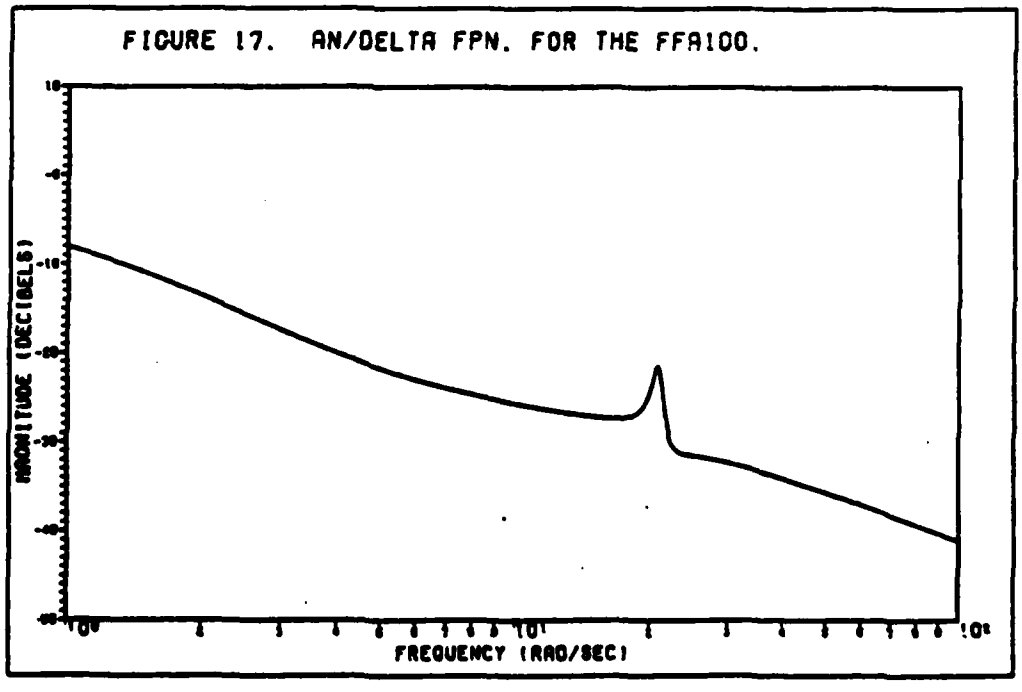

FIGURE 18. AN/DELTA ELV. FOR THE FFA100.

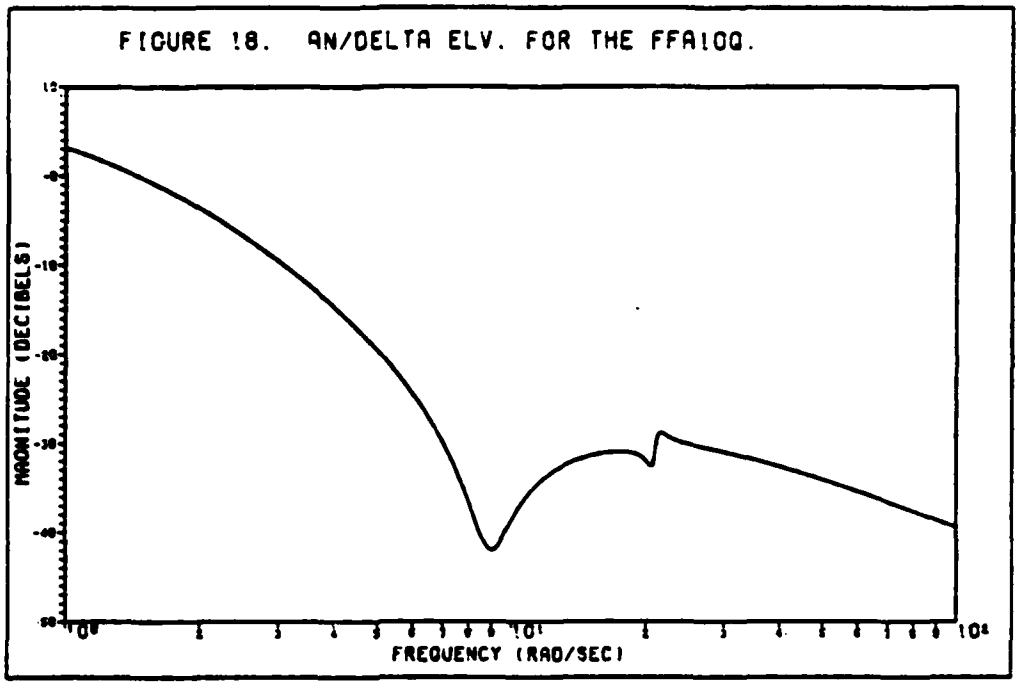

FIGURE 19. AN/DELTA FPN. FOR THE FFA100.

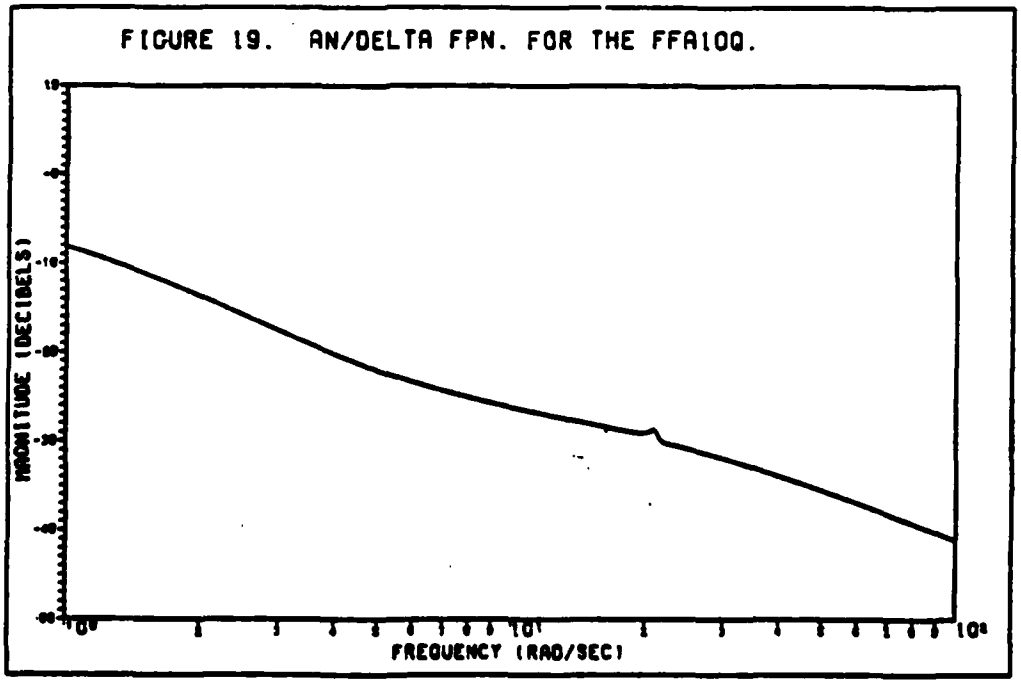

FIGURE 20. AN/DELTA ELV. FOR THE FFA100Q.

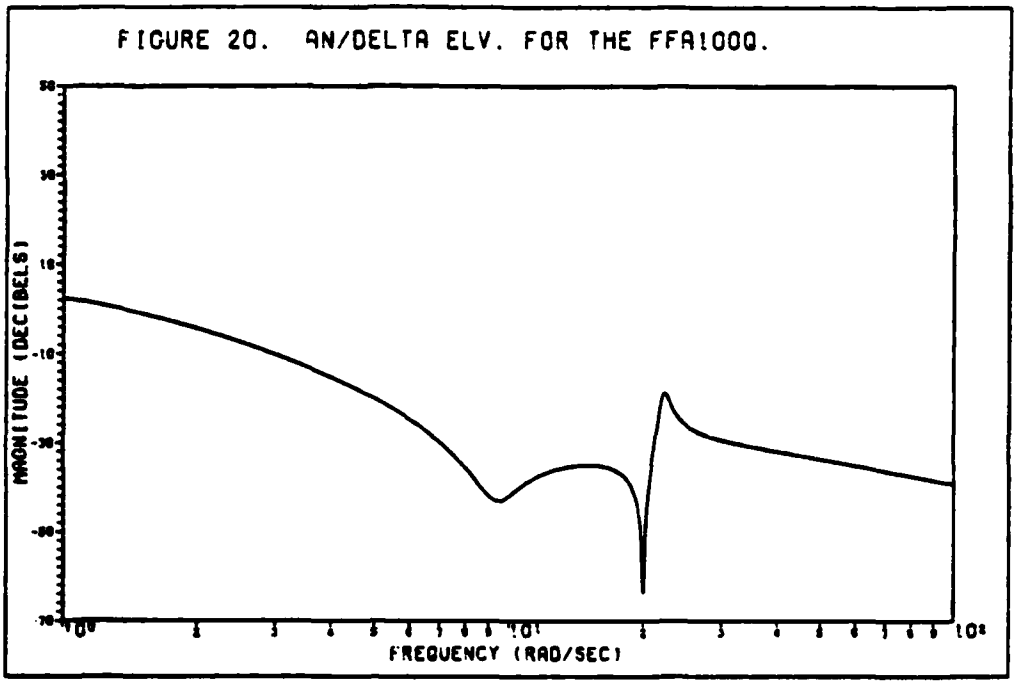

FIGURE 21. AN/DELTA FPN. FOR THE FFA100Q

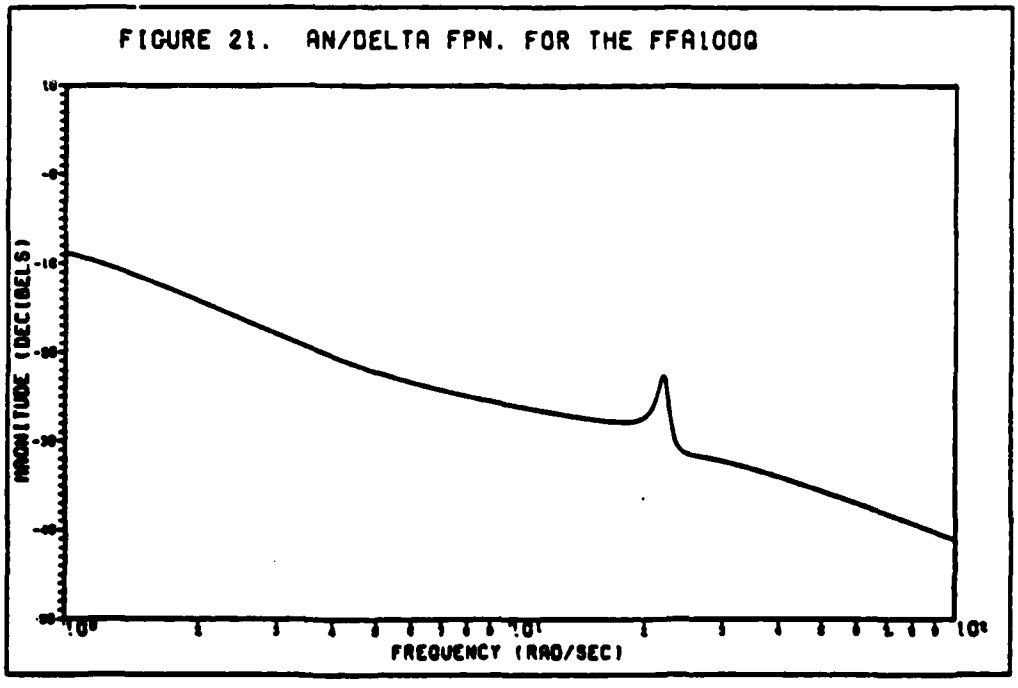

and the pitch-pointing maneuver. The five flexible-fighter models are those described in the first sections of this chapter.

The following design data is used to develop the simulation time responses:

Design Data for the G-Command System

Flight Condition: 0.8 Mach 30,000 feet

$T = 0.02$

Computational Delay: 0

$\bar{\alpha} = 0.2$

$$\underline{\Sigma} = \begin{bmatrix} 0.025 & 0 \\ 0 & 2.0 \end{bmatrix}$$

$\epsilon = 2.0$

Rigid Body Model

$$\underline{M} = \begin{bmatrix} 0 & 0 & 0 & 0 \\ 0 & 0 & 0 & 0.1 \end{bmatrix}$$

Flexible-Fighter Models

$$\underline{M} = \begin{bmatrix} 0 & 0 & 0 & 0 & 0 & 0 \\ 0 & 0 & 0 & 0.1 & 0 & 0 \end{bmatrix}$$

$$K_0 = \begin{bmatrix} -0.002013 & -0.02664 \\ 0.008724 & -0.03260 \end{bmatrix}$$

$$K_1 = \begin{bmatrix} -0.01007 & -0.1332 \\ 0.04362 & -0.1630 \end{bmatrix}$$

Input ramp-up time: 0.4 seconds

Input commands: A_{n_p} = 1g step

$$q = \frac{1845}{U} A_{n_p} = 2.32 \text{ deg/sec}$$

NOTE: Step inputs are "ramped-up" to the steady-state value over a specified time. This time is designated as the "input ramp-up time" given above.

Design Data for the Pitch-Pointing System

Fight Condition: 0.8 Mach 30,000 feet

$T = 0.02$

Computational Delay: 0

$\bar{\alpha} = 0.5$

$$\underline{\Sigma} = \begin{bmatrix} 1.5 & 0 \\ 0 & 1.0 \end{bmatrix}$$

$\epsilon = 2.5$

Rigid Body Model

$$\underline{M} = \begin{bmatrix} 0 & 0 & 0 & 0 \\ 0 & 0 & 0 & 0.1 \end{bmatrix}$$

Flexible-Fighter Models

$$\underline{M} = \begin{bmatrix} 0 & 0 & 0 & 0 & 0 & 0 \\ 0 & 0 & 0 & 0.1 & 0 & 0 \end{bmatrix}$$

$$K_0 = \begin{bmatrix} -0.3774 & -0.04162 \\ 1.636 & -0.05094 \end{bmatrix}$$

$$K_1 = \begin{bmatrix} -0.7549 & -0.08324 \\ 3.272 & -0.1019 \end{bmatrix}$$

Input ramp-up time: 0.0 seconds

Input command: $A_{n_p} = 0.0$

$q = 1.0$ deg/sec step

NOTE: Step commands are ramped-up to the steady-state value over a specified time. This time is designated as the "input ramp-up time" given above.

NOTE: The pitch-pointing maneuver is usually thought of as a pilot commanding a certain angle, θ, without changing its flight path. Actually, the pilot commands a pitch rate, q, and when it reaches the angle, θ, the pitch rate is brought to zero. This is the reason that the design for the pitch rate maneuver commands a pitch rate, q, and not an angle, θ.

Figures 30a-d and 31a-e are the results of commanding one degree of pitch-pointing for the rigid body and the flexible-fighter aircraft (FFA). That is:

Input Ramp-up time: 0.0 seconds

Input command: $A_{n_p} = 0.0$

$q = 1.0$ deg/sec pulse for 1 sec duration

Maximum Command Responses

This section contains responses to maximum estimated commands which have been used to select system gains so that control surface position limits are not exceeded. The g-command system design includes only the rigid body and the flexible-fighter model as stated in Table 6 of Chapter II.

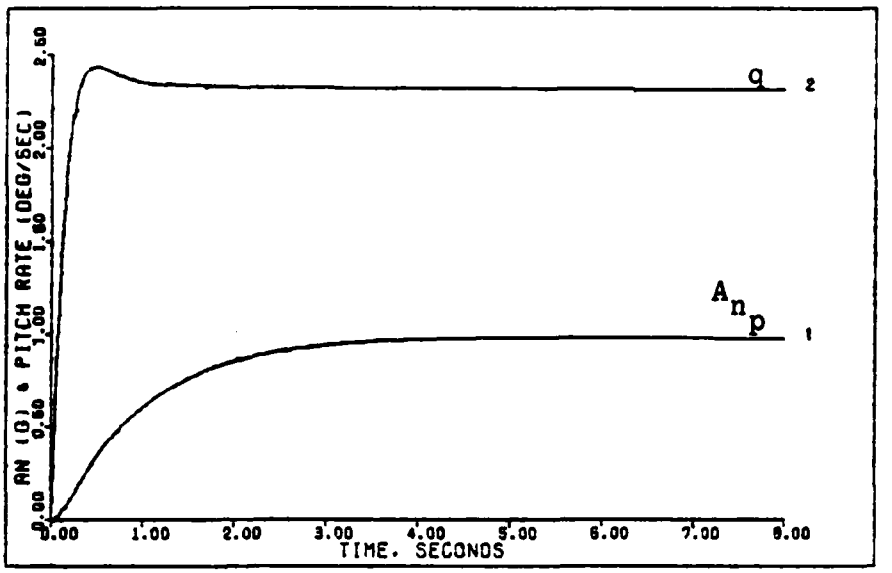

Figure 22a. G-Command System Response to a 1g Step Command for the Rigid Body Aircraft. (0.8 Mach 30,000 ft)

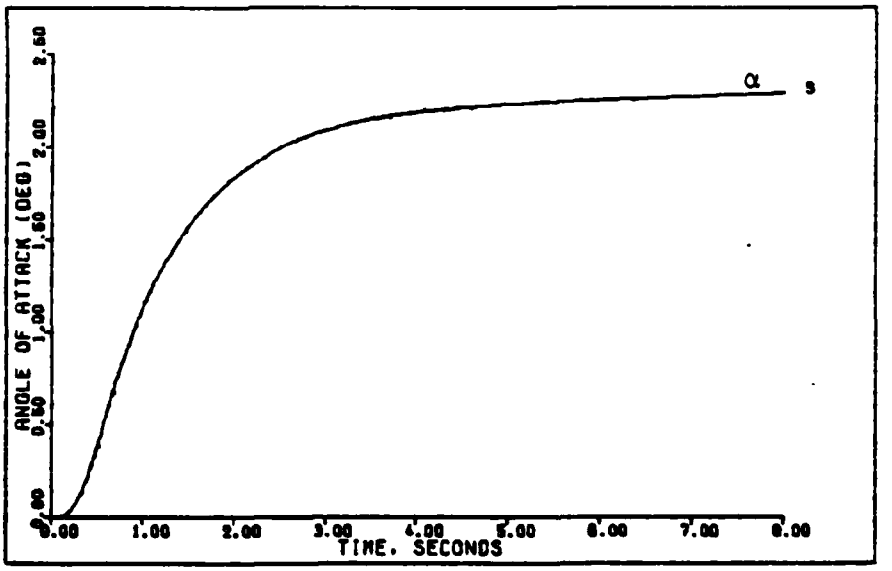

Figure 22b. G-Command System Response to a 1g Step Command for the Rigid Body Aircraft. (0.8 Mach 30,000 ft)

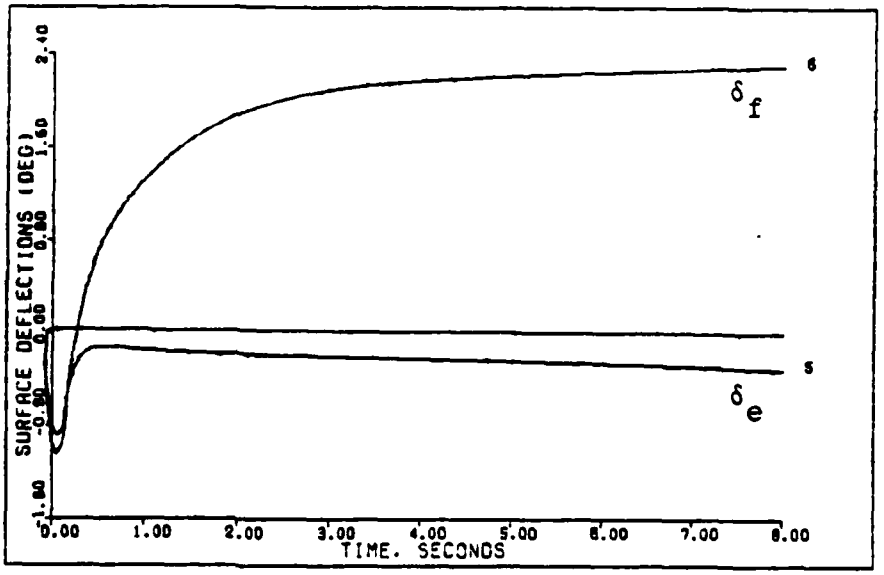

Figure 22c. G-Command System Response to a 1g Step Command for the Rigid Body Aircraft. (0.8 Mach 30,000 ft)

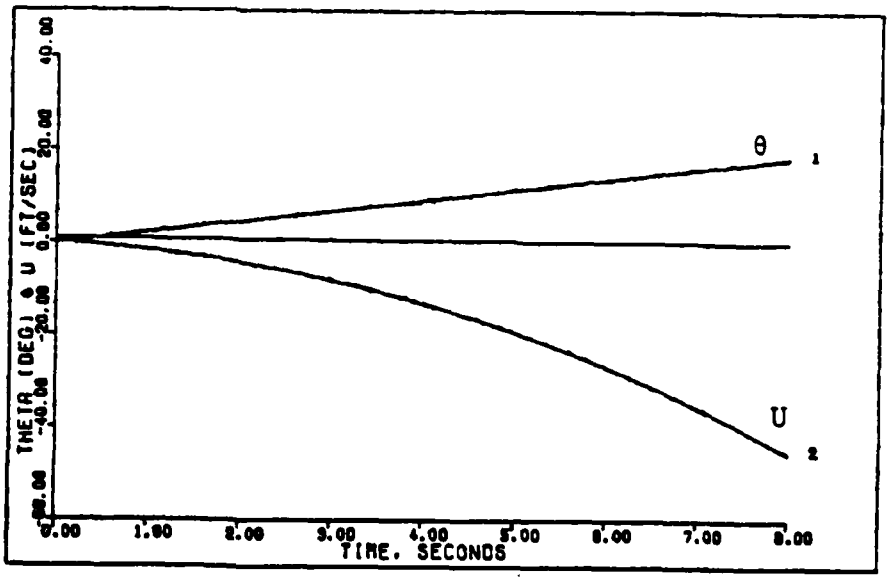

Figure 22d. G-Command System Response to a 1g Step Command for the Rigid Body Aircraft. (0.8 Mach 30,000 ft)

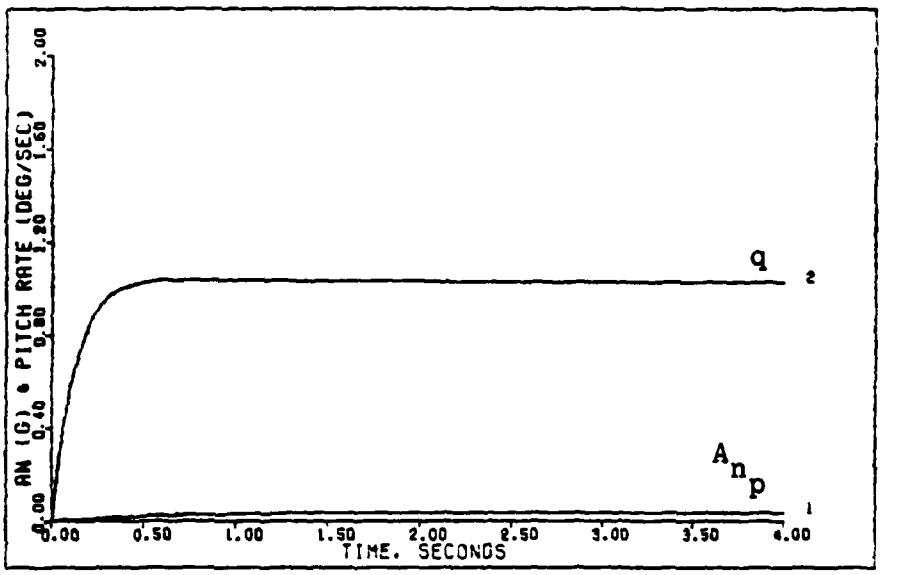

Figure 23a. Pitch-Pointing System Response to a 1 deg/sec Step Command for the Rigid Body Aircraft. (0.8 Mach 30,000 feet)

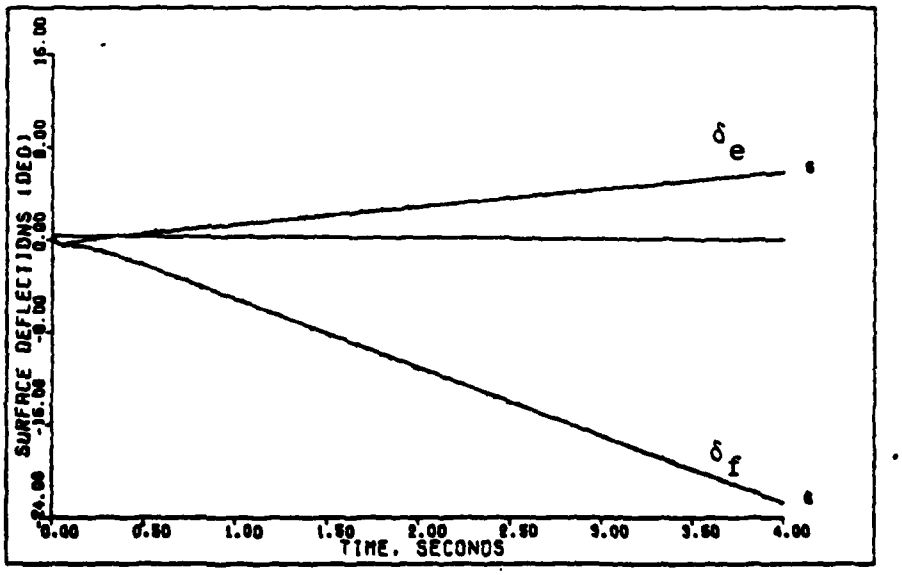

Figure 23b. Pitch-Pointing System Response to a 1 deg/sec Step Command for the Rigid Body Aircraft. (0.8 Mach 30,000 feet)

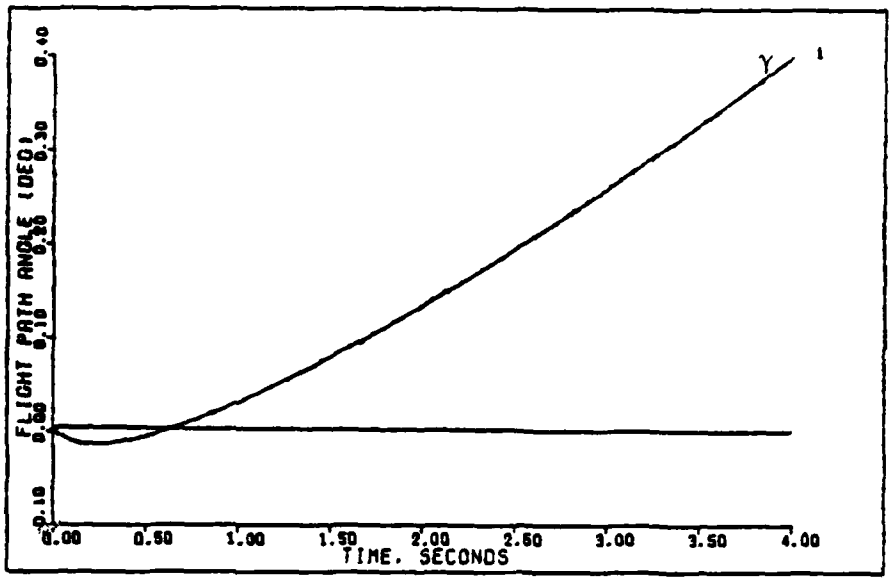

Figure 23c. Pitch-Pointing System Response to a 1 deg/sec Step Command for the Rigid Body Aircraft. (0.8 Mach 30,000 feet)

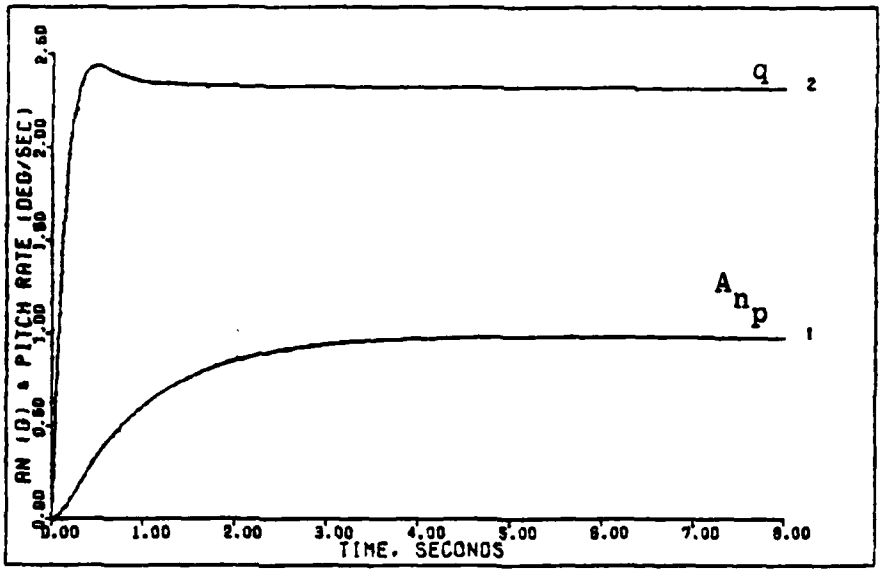

Figure 24a. G-Command System Response to a 1g Step Command for the FFA, for the FFA10, and for the FFA10q. (0.8 Mach 30,000 feet)

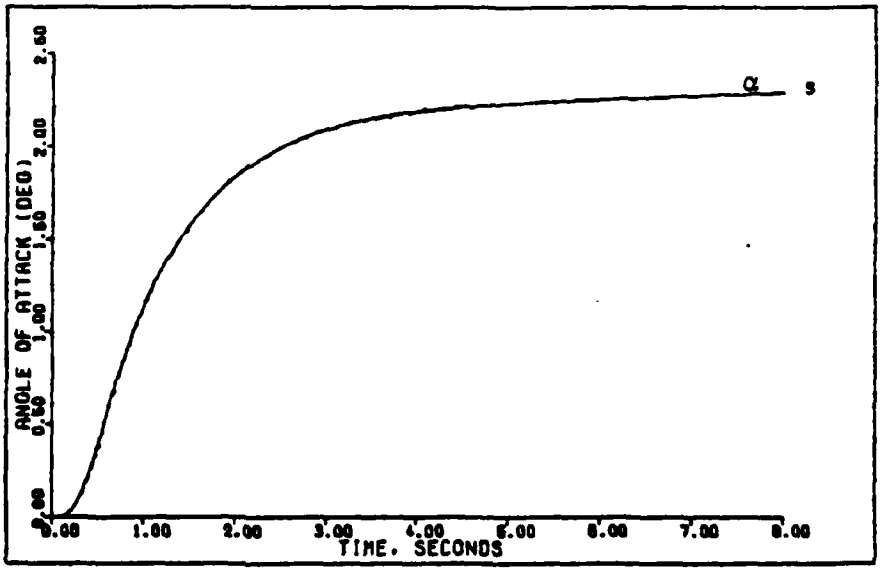

Figure 24b. G-Command System Response to a 1g Step Command for the FFA, for the FFA10, and for the FFA10q. (0.8 Mach 30,000 feet)

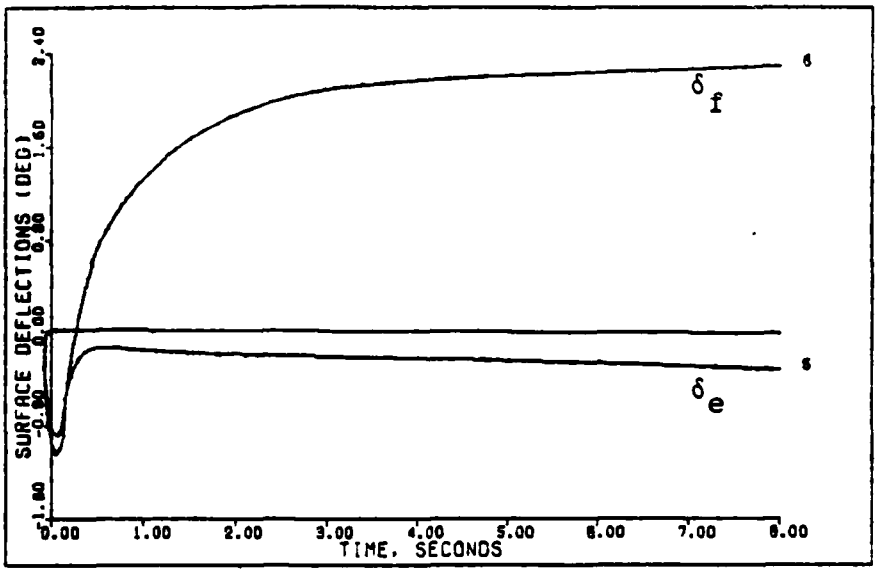

Figure 24c. G-Command System Response to a 1g Step Command for the FFA, for the FFA10, and for the FFA10q. (0.8 Mach 30,000 feet)

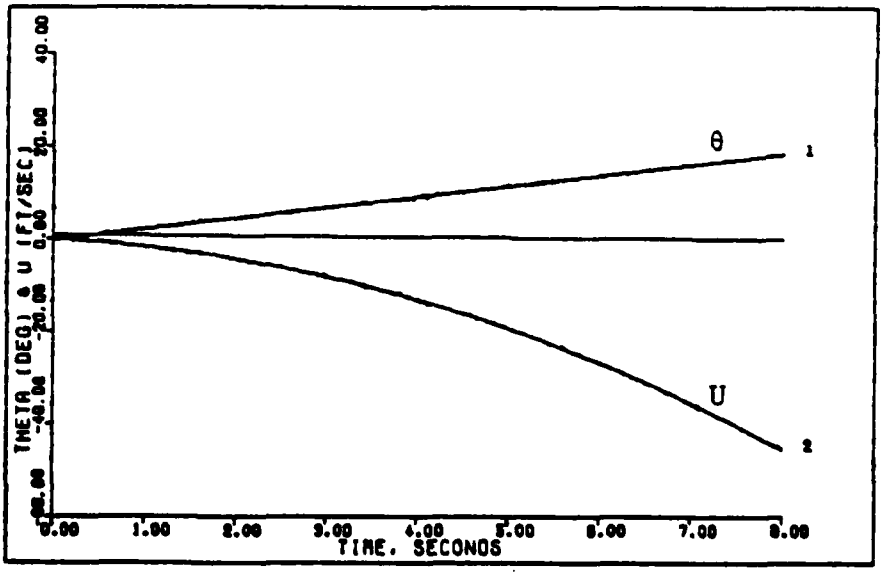

Figure 24d. G-Command System Response to a 1g Step Command for the FFA, for the FFA10, and for the FFA 10q. (0.8 Mach 30,000 feet)

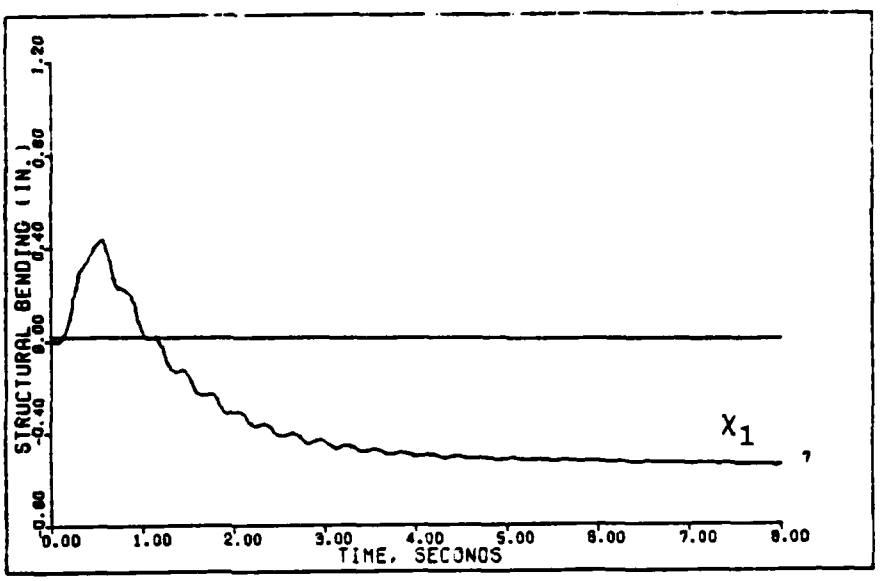

Figure 24e. G-Command System Response to a 1g Step Command for the FFA, for the FFA10, and for the FFA 10q. (0.8 Mach 30,000 feet)

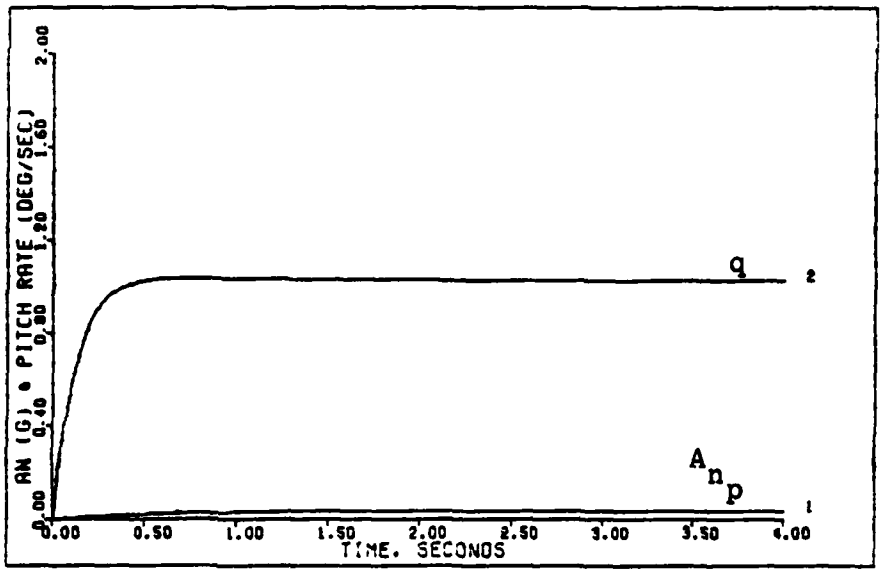

Figure 25a. Pitch-Pointing System Response to a 1 deg/sec Step Command for the FFA, for the FFA10, and for the FFA10q. (0.8 Mach 30,000 feet)

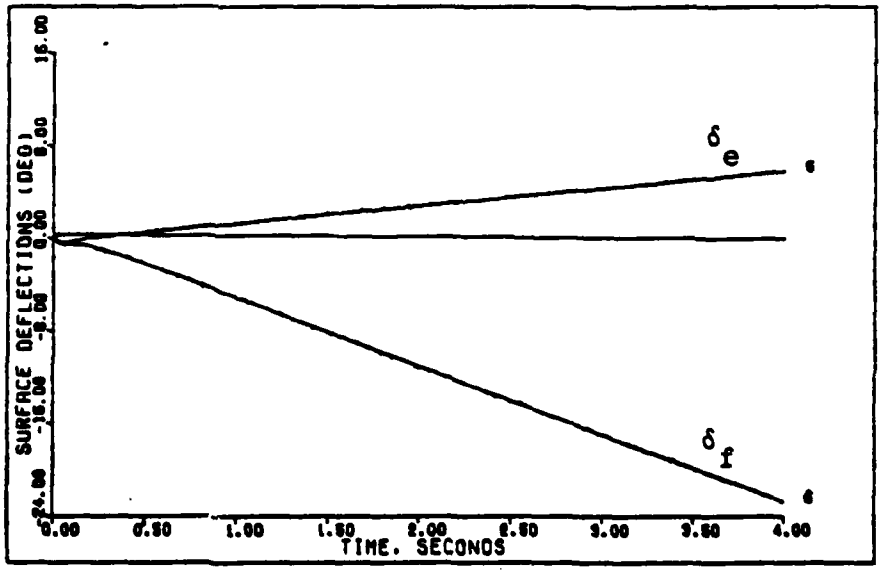

Figure 25b. Pitch-Pointing System Response to a 1 deg/sec Step Command for the FFA, for the FFA10, and for the FFA10q. (0.8 Mach 30,000 feet)

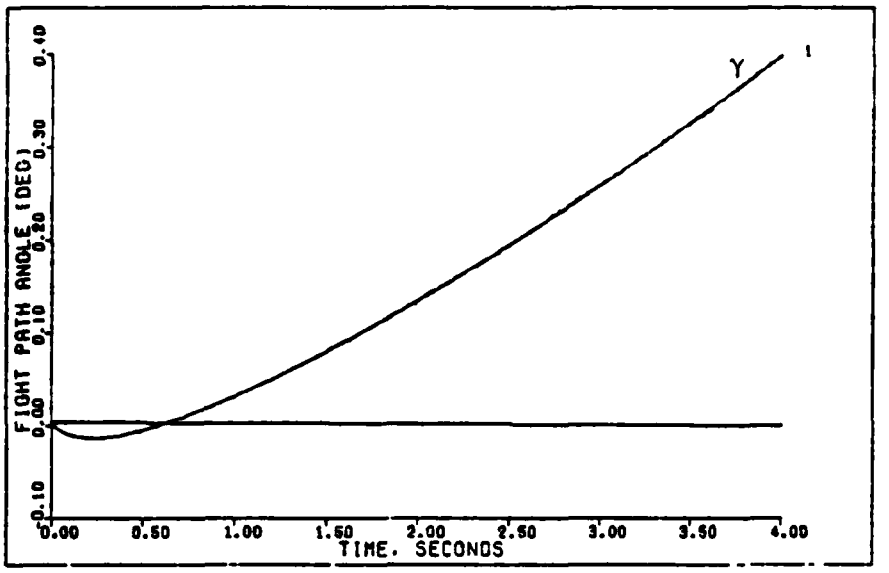

Figure 25c. Pitch-Pointing System Response to a 1 deg/sec Step Command for the FFA, for the FFA10, and for the FFA10q. (0.8 Mach 30,000 feet)

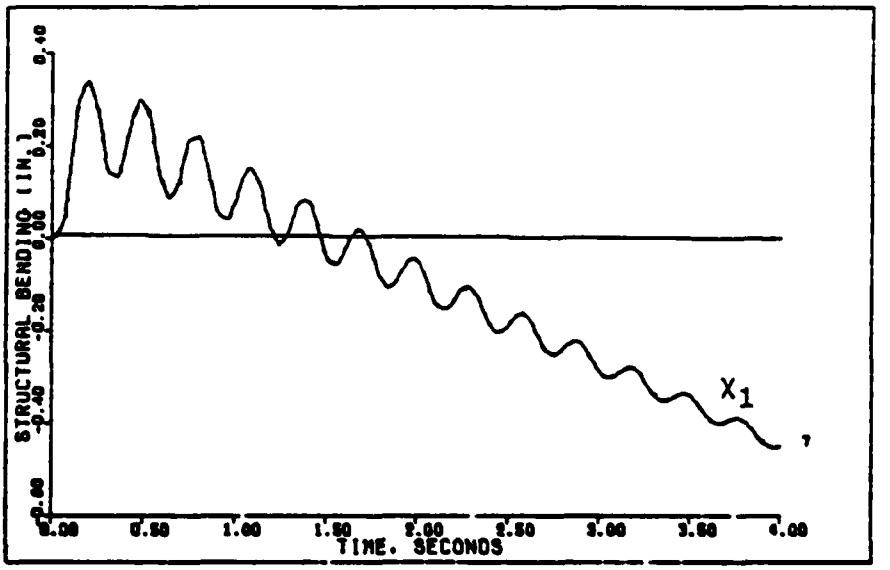

Figure 25d. Pitch-Pointing System Response to a 1 deg/sec Step Command for the FFA, for the FFA10, and for the FFA10q. (0.8 Mach 30,000 feet)

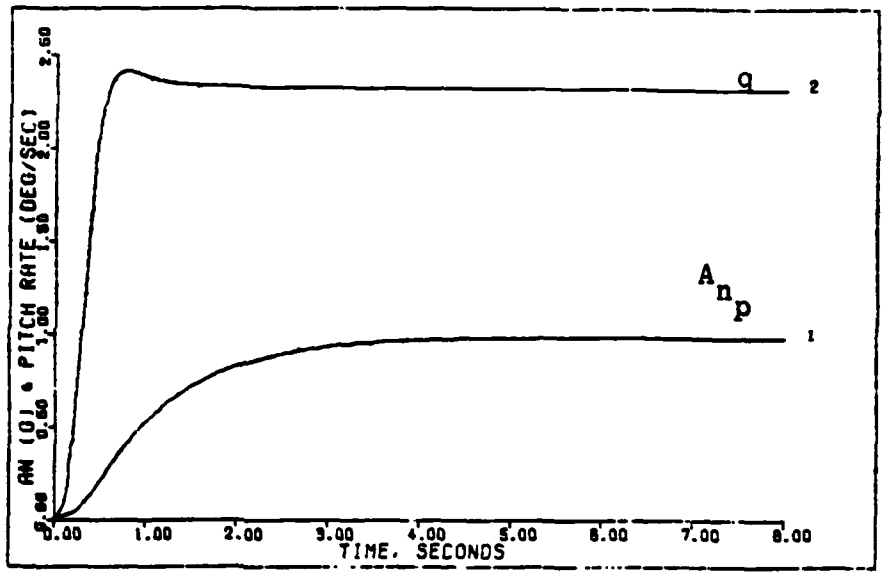

Figure 26a. G-Command System Response to a 1g Step Command for the FFA100. (0.8 Mach 30,000 feet)

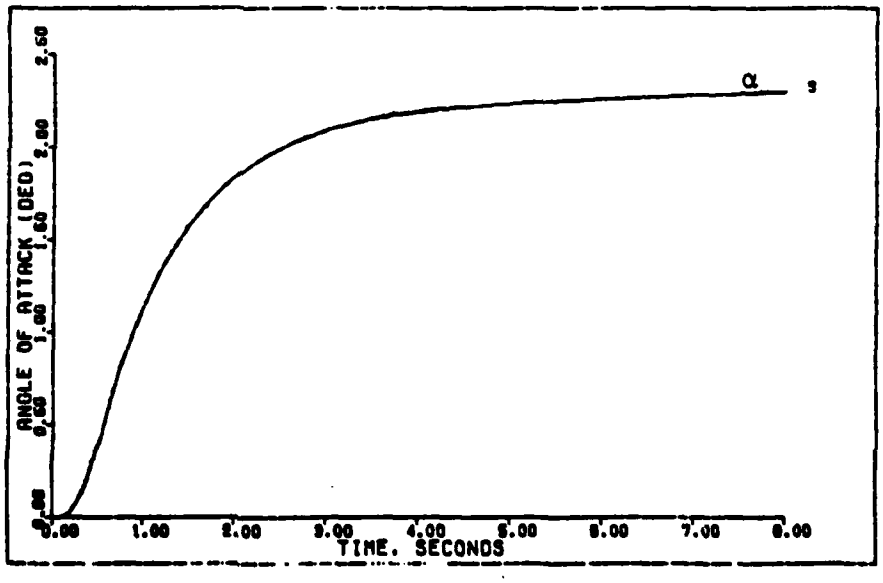

Figure 26b. G-Command System Response to a 1g Step Command for the FFA100. (0.8 Mach 30,000 feet)

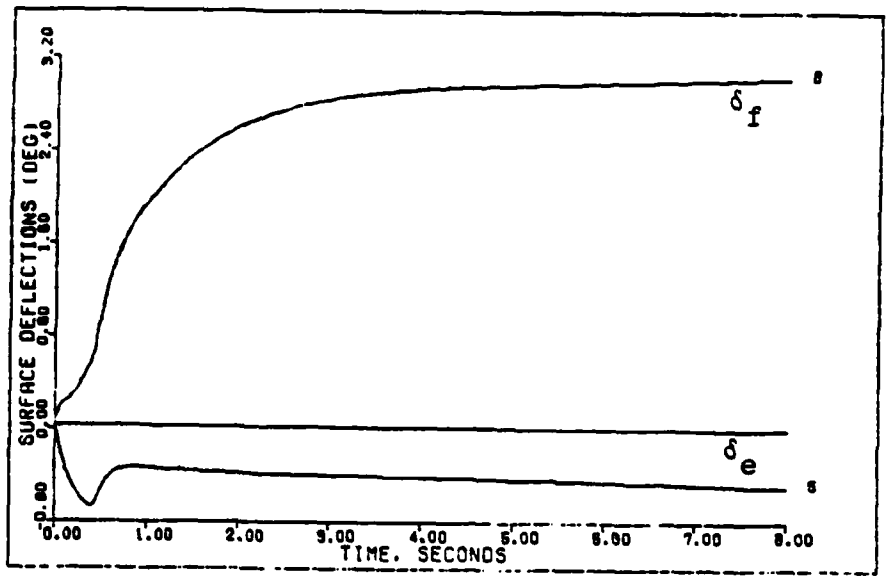

Figure 26c. G-Command System Response to a 1g Step Command for the FFA100. (0.8 Mach 30,000 Feet)

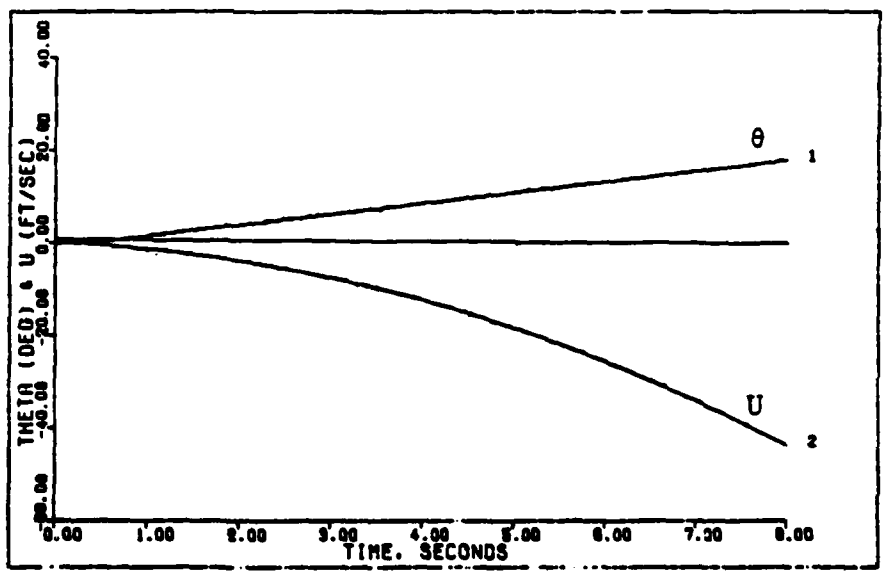

Figure 26d. G-Command System Response to a 1g Step Command for the FFA100. (0.8 Mach 30,000 feet)

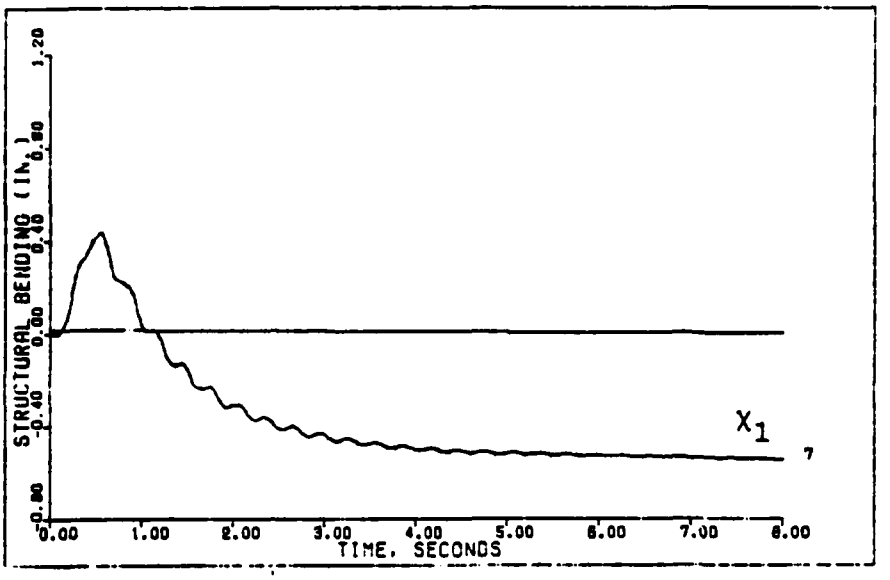

Figure 26e. G-Command System Response to a 1g Step Command for the FFA100. (0.8 Mach 30,000 feet)

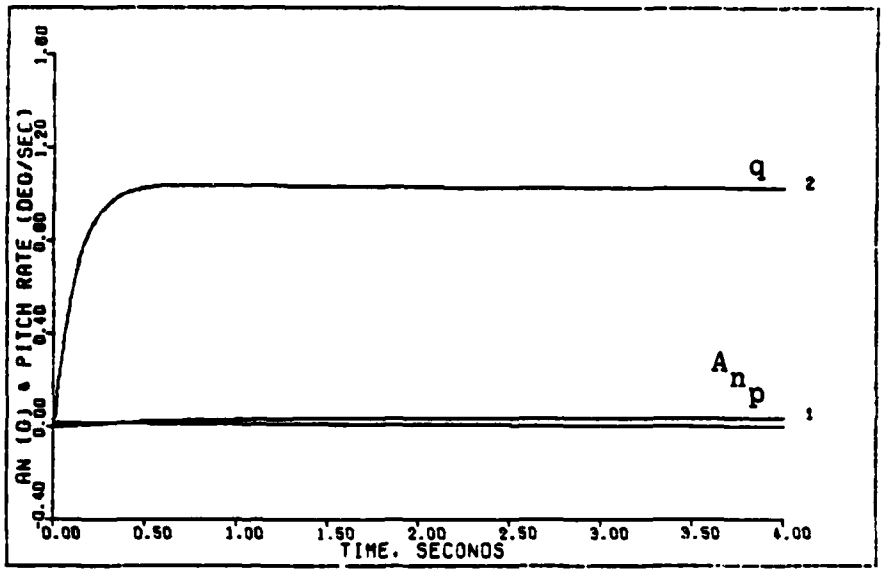

Figure 27a. Pitch-Pointing System Response to a 1 deg/sec Step Command for the FFA100. (0.8 Mach 30,000 feet)

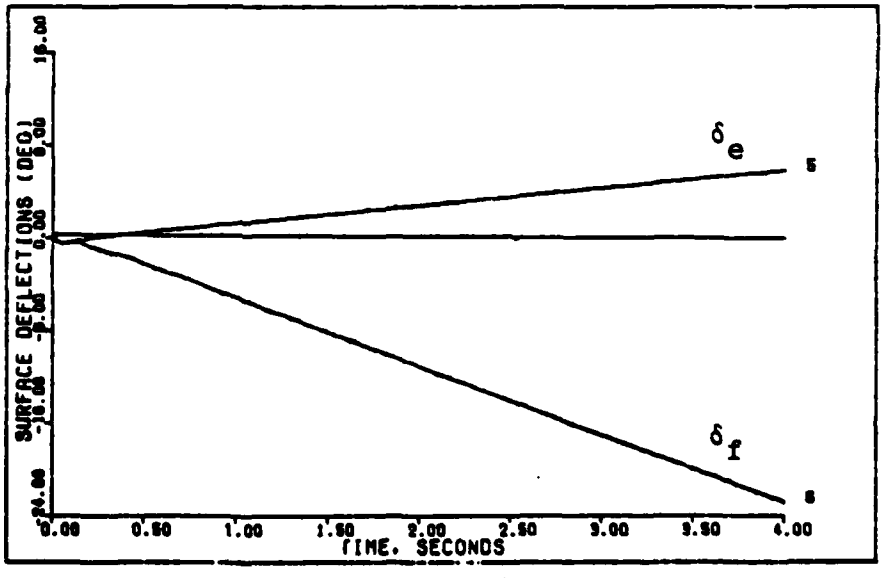

Figure 27b. Pitch-Pointing System Response to a 1deg/sec Step Command for the FFA100. (0.8 Mach 30,000 feet)

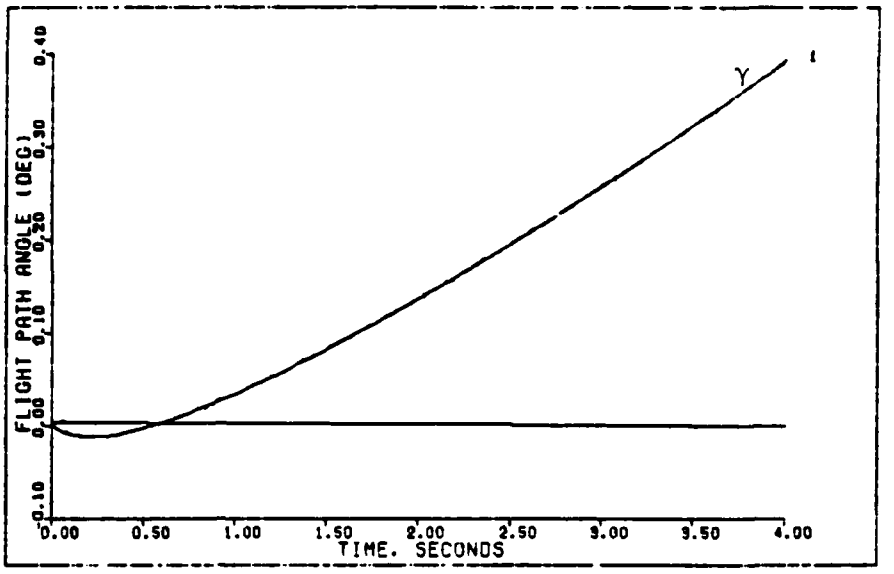

Figure 27c. Pitch-Pointing System Response to a 1 deg/sec Step Command for the FFA100. (0.8 Mach 30,000 feet)

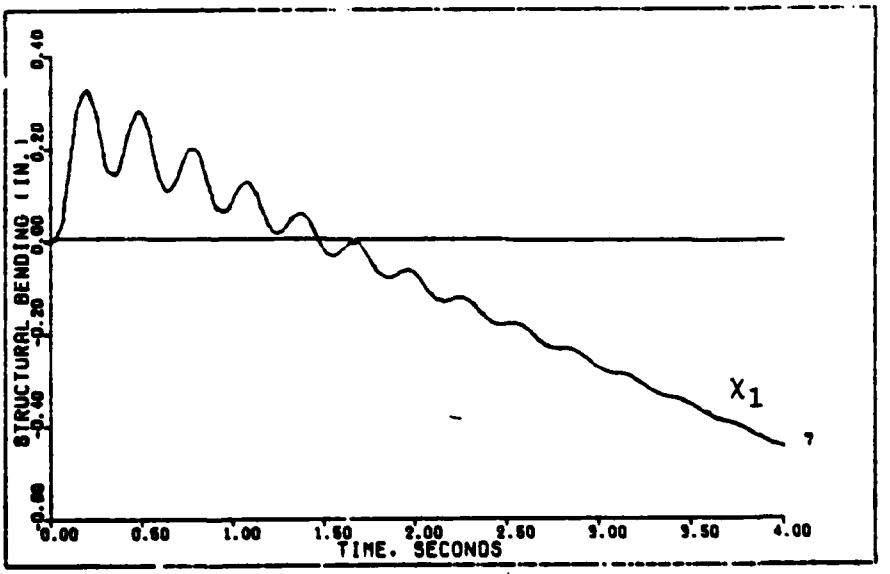

Figure 27d. Pitch-Pointing System Response to a 1 deg/sec Step Command for the FFA100. (0.8 Mach 30,000 feet)

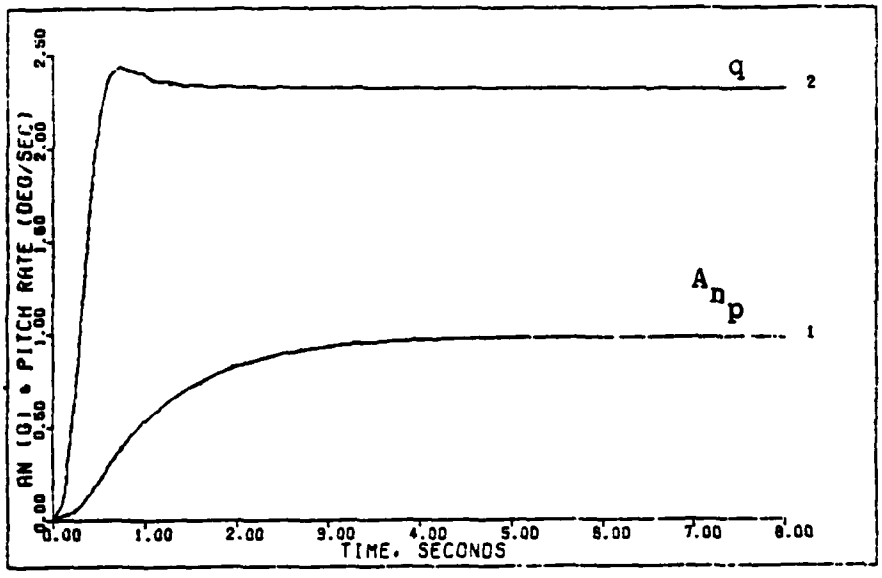

Figure 28a. G-Command System Response to a 1g Step Command for the FFA100q. (0.8 Mach 30,000 feet)

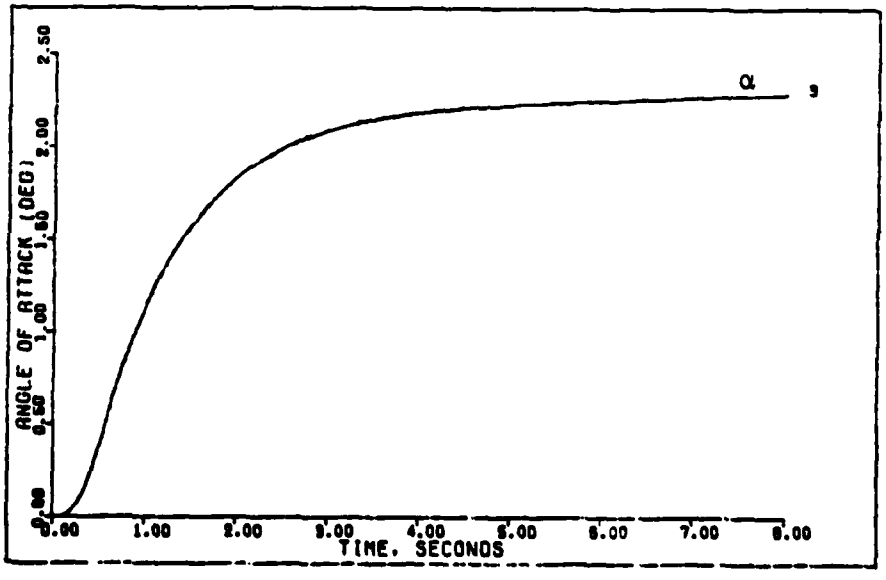

Figure 28b. G-Command System Response to a 1g Step Command for the FFA100q. (0.8 Mach 30,000 feet)

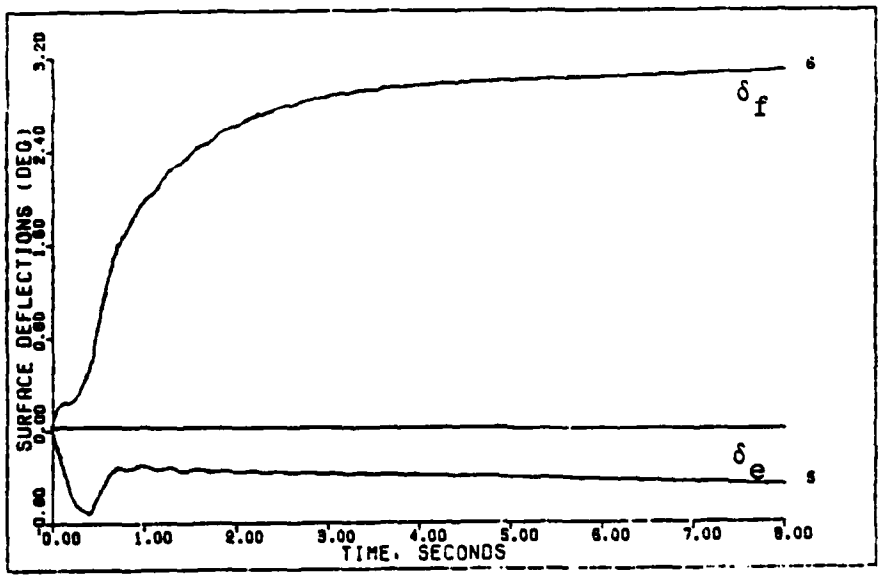

Figure 28c. G-Command System Response to a 1g Step Command for the FFA100q. (0.8 Mach 30,000 feet)

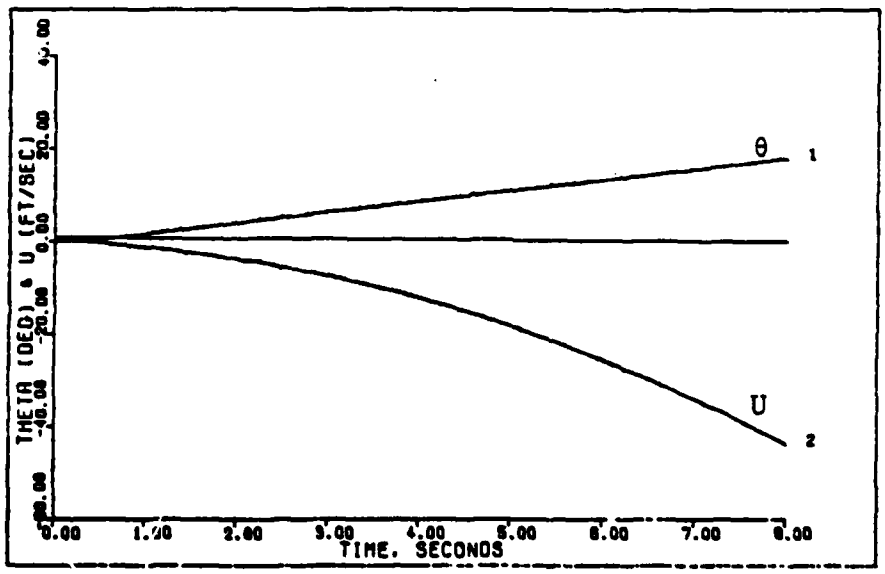

Figure 28d. G-Command System Response to a 1g Step Command for the FFA100q. (0.8 Mach 30,000 feet)

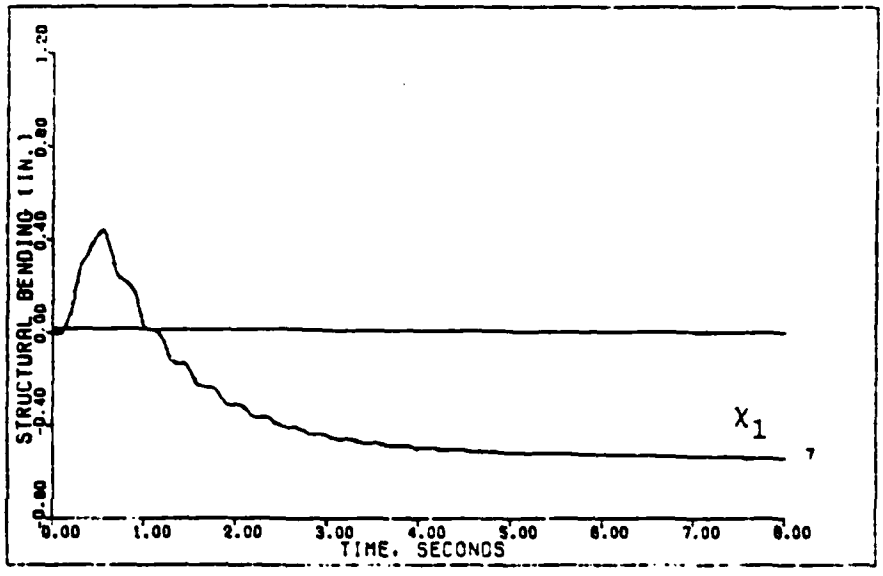

Figure 28c. G-Command System Response to a 1g Step Command for the FFA100q. (0.8 Mach 30,000 feet)

AD-A138 269 EVALUATION OF A DIGITAL FLIGHT CONTROLLER FOR A FLEXIBLE-FIGHTER AIRCRAFT(U) AIR FORCE INST OF TECH WRIGHT-PATTERSON AFB OH SCHOOL OF ENGINEERING

2/2

UNCLASSIFIED M L HOFFMAN DEC 82 AFIT/GE/EE/83D-30 F/G 1/4 NL

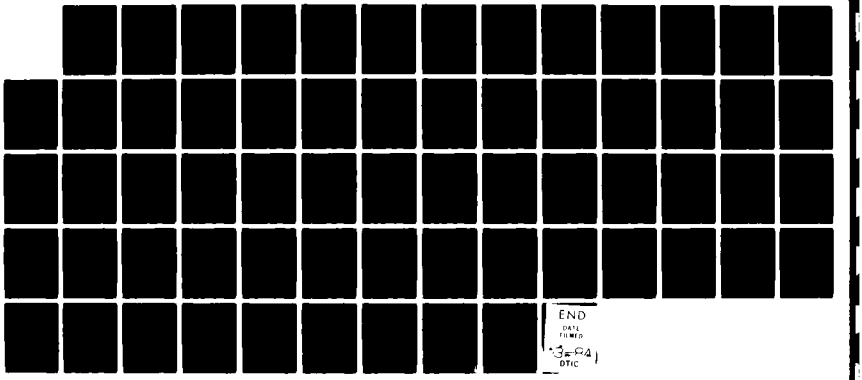

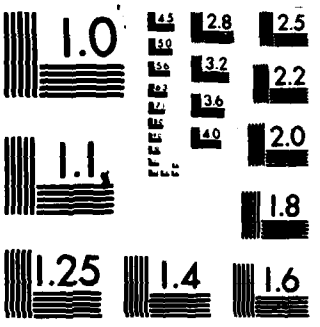

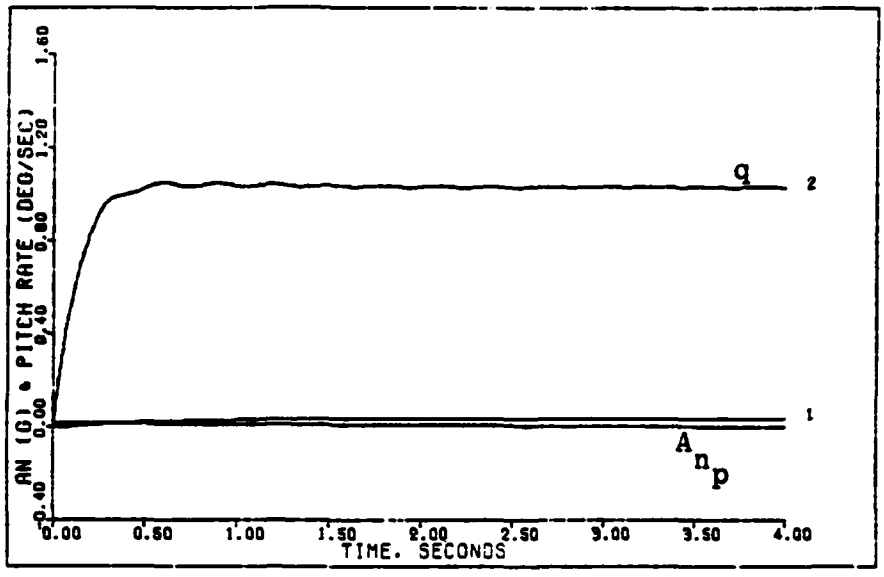

Figure 29a. Pitch-Pointing System Response to a 1 deg/sec Step Command for the FFA100q. (0.8 Mach 30,000 feet)

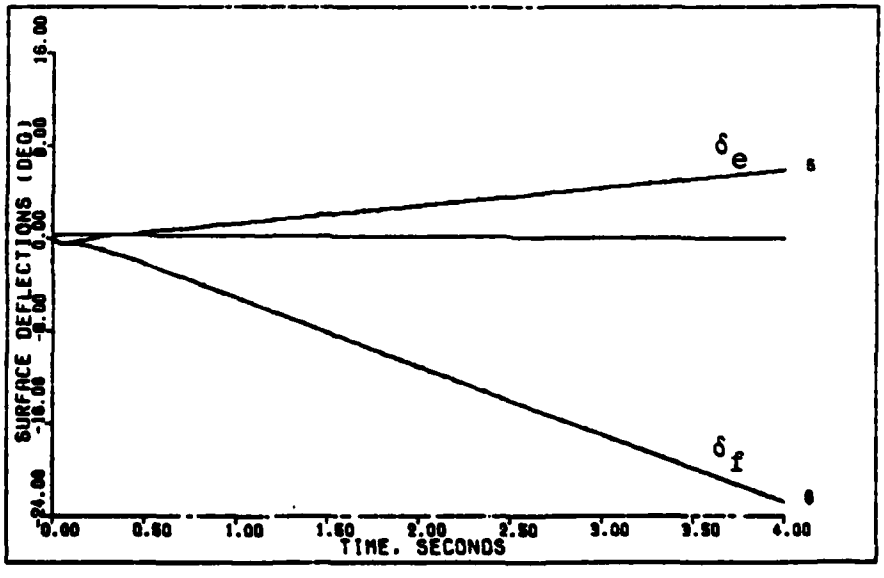

Figure 29b. Pitch-Pointing System Response to a 1 deg/sec Step Command for the FFA100q. (0.8 Mach 30,000 feet)

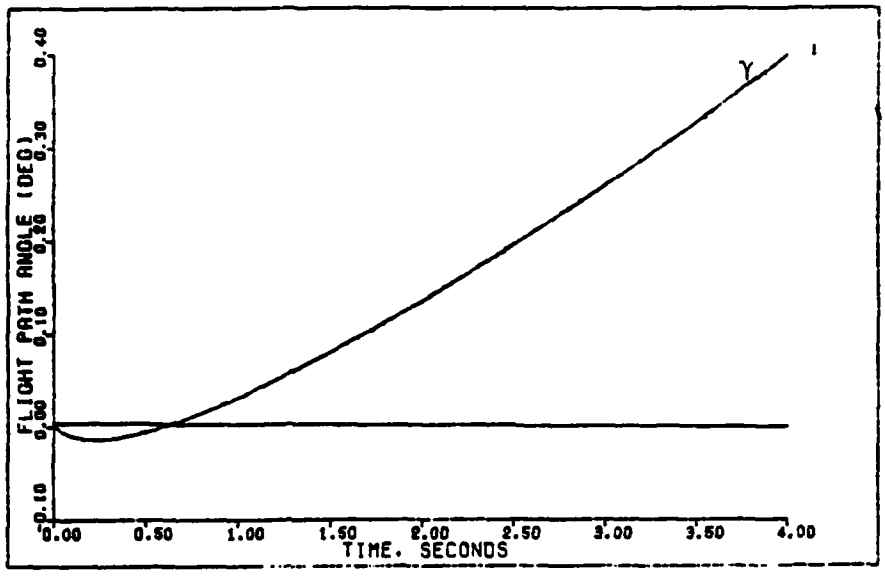

Figure 29c. Pitch-Pointing System Response to a 1 deg/sec Step Command for the FFA100q. (0.8 Mach 30,000 feet)

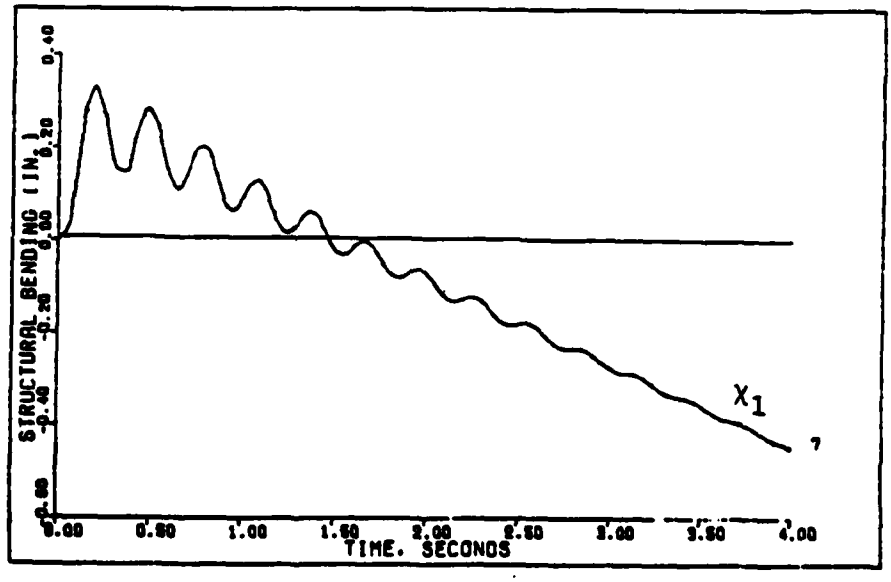

Figure 29d. Pitch-Pointing System Response to a 1 deg/sec Step Command for the FFA100q. (0.8 Mach 30,000 feet)

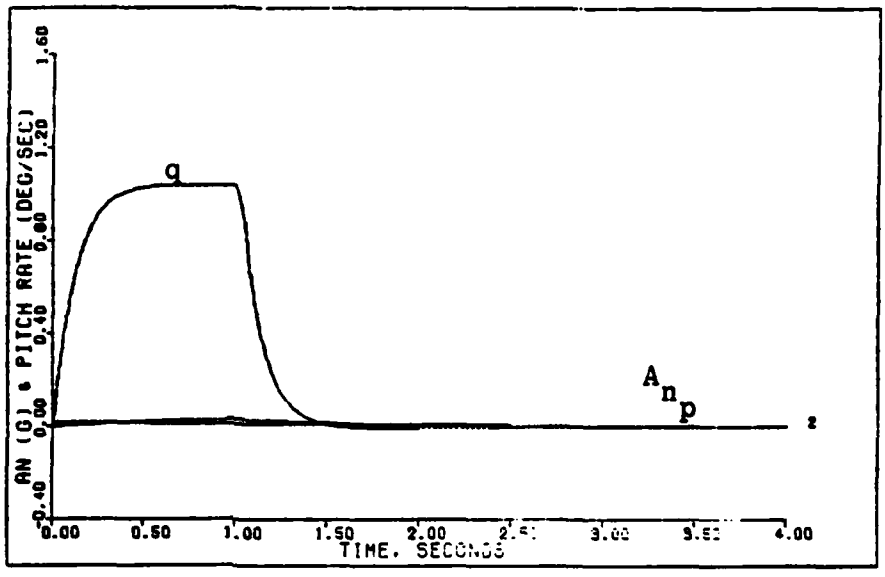

Figure 30a. Pitch-Pointing Command System Response to a 1 deg/sec pulse of 1 sec duration for the Rigid Body Aircraft.

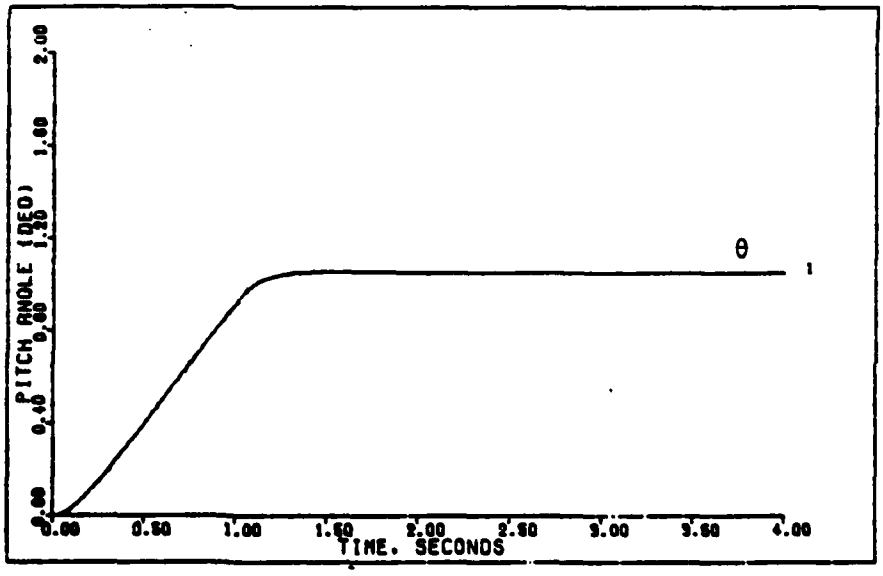

Figure 30b. Pitch-Pointing Command System Response to a 1 deg/sec pulse of 1 sec duration for the Rigid Body Aircraft.

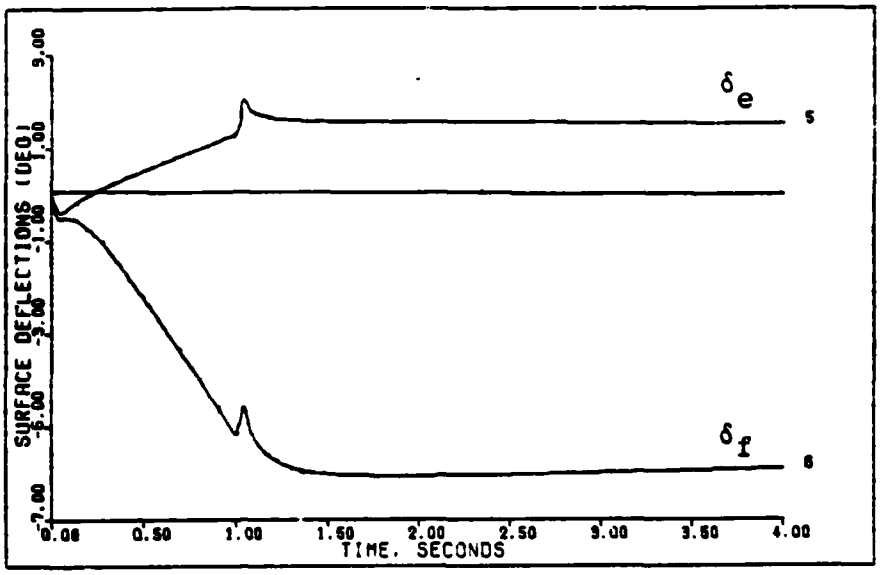

Figure 30c. Pitch-Pointing Command System Response to a 1 deg/sec pulse of 1 sec duration for the Rigid Body Aircraft.

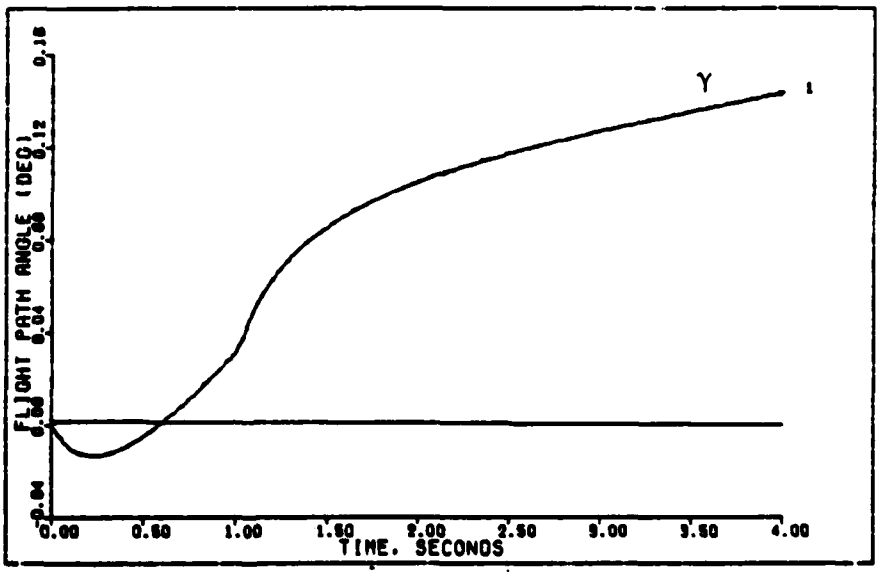

Figure 30d. Pitch-Pointing Command System Response to a 1 deg/sec pulse of 1 sec duration for the Rigid Body Aircraft.

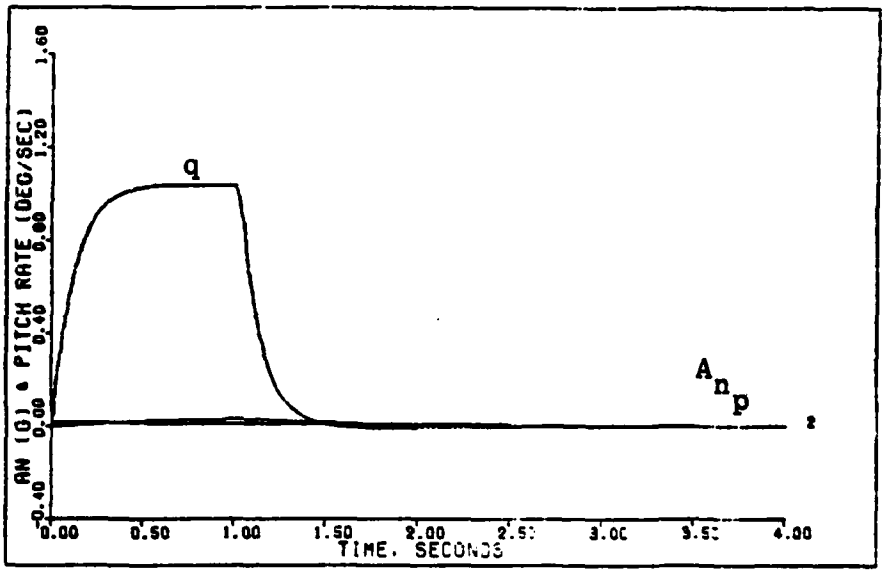

Figure 31a. Pitch-Pointing Command System Response to a 1 deg/sec pulse of 1 sec duration for the FFA.

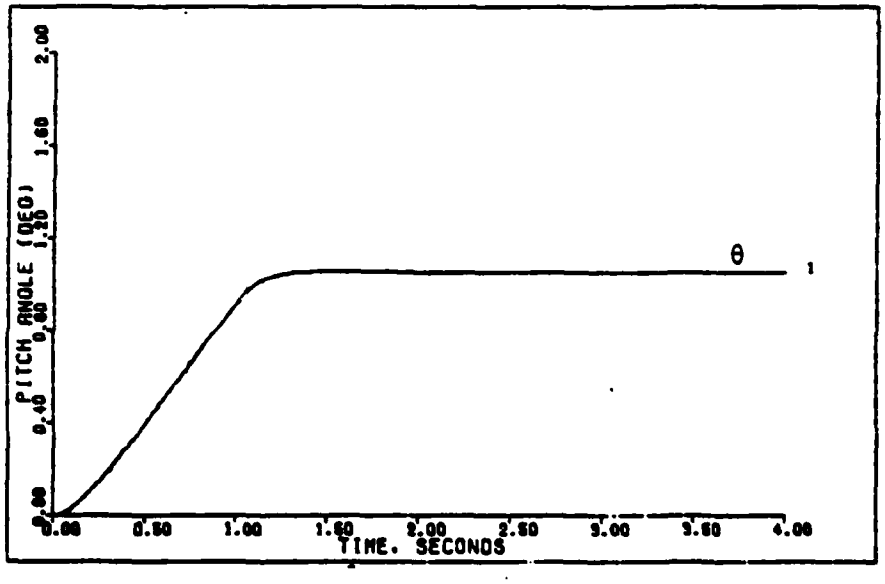

Figure 31b. Pitch-Pointing Command System Response to a 1 deg/sec pulse of 1 sec duration for the FFA.

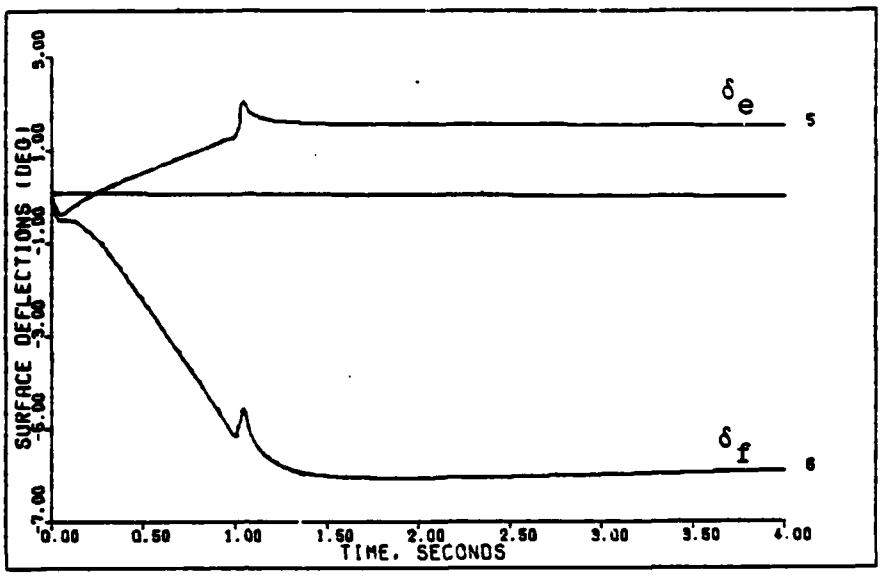

Figure 31c. Pitch-Pointing Command System Response to a 1 deg/sec pulse 1 sec duration for the FFA.

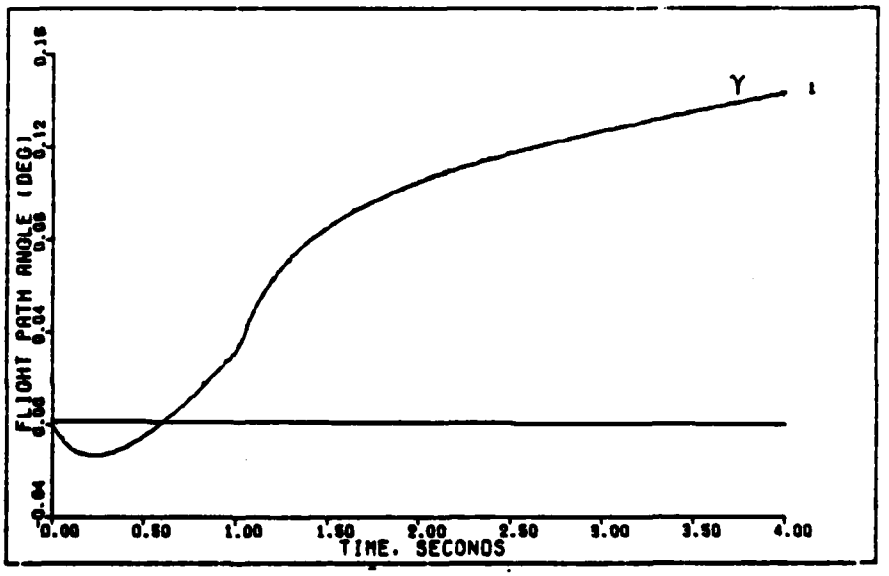

Figure 31d. Pitch-Pointing Command System Response to a 1 deg/sec pulse of 1 sec duration for the FFA.

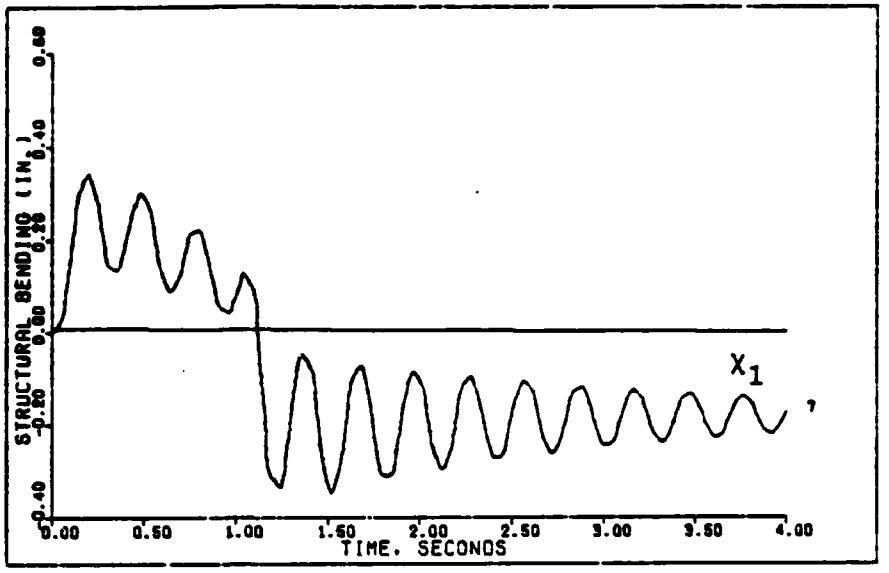

Figure 31e. Pitch-Pointing Command System Response to a 1 deg/sec pulse of 1 sec duration for the FFA.

The responses, Figures 32a-d and 33a-e, of this section are not intended to indicate adequacy of both the rigid body or the flexible-fighter models in properly representing such large maneuvers. They are simply used as a guideline in establishing realistic gains. The design parameters given in the last section apply to these responses with the exception that the inputs have been appropriately increased.

Computational Delay Responses

This section contains the time responses, Figures 34 through 37, of the design that has a computational delay incorporated. The time delay in the design represents the expected microprocessor computational time delay in generating the control law. The simulation time responses are for both the rigid body and the flexible-fighter aircraft (FFA).

The design parameters are the same as stated in the second section except that there is a computational delay of 1 sampling period.

The evaluation and conclusions that are drawn from the design are discussed in Chapter V and VI, respectively. The evaluation is based on a pilot's expected rating for the flight controller.

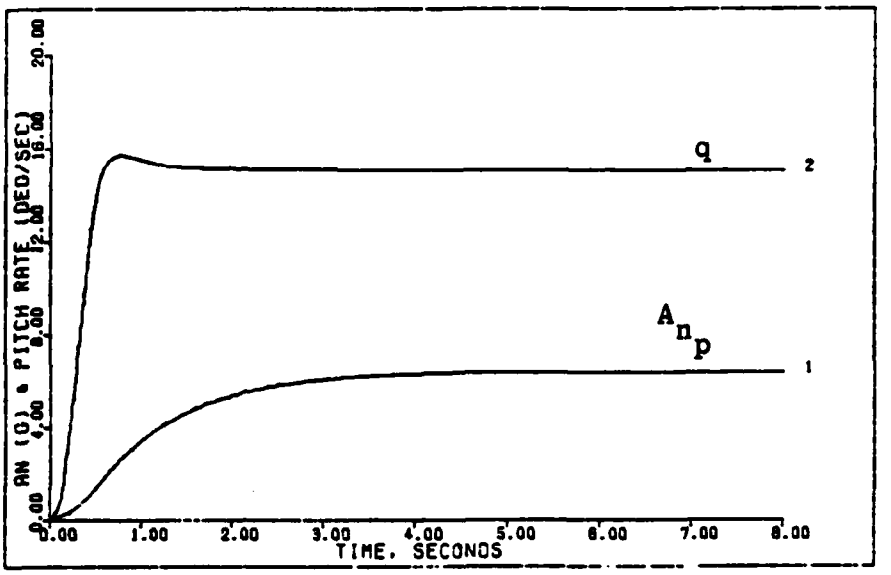

Figure 32a. G-Command System Response to a 6.5g Step Command for the Rigid Body. (0.8 Mach 30,000 feet)

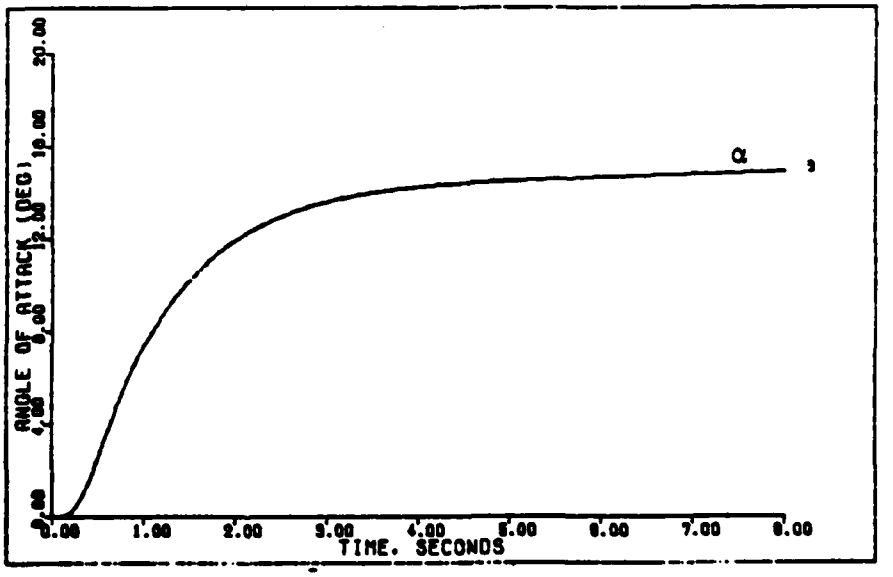

Figure 32b. G-Command System Response to a 6.5g Step Command for the Rigid Body. (0.8 Mach 30,000 feet)

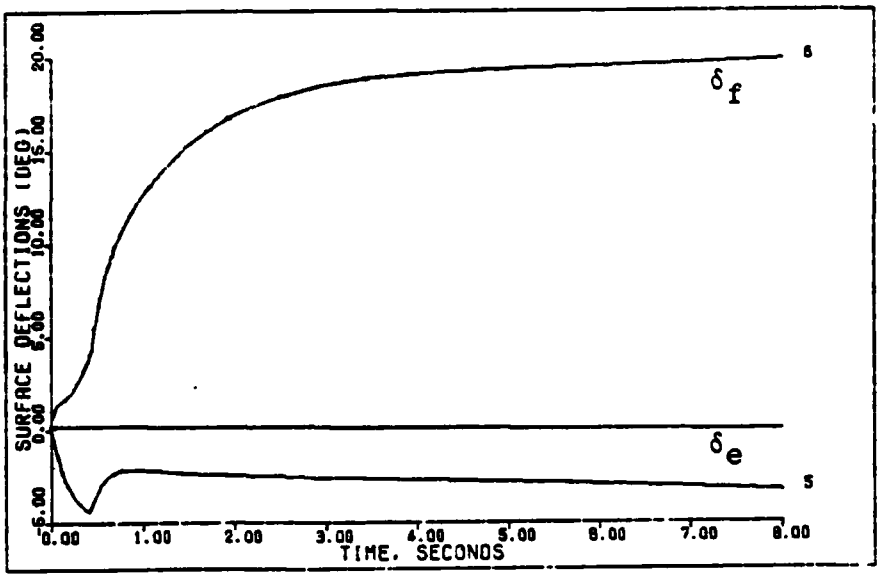

Figure 32c. G-Command System Response to a 6.5g Step Command for the Rigid Body. (0.8 Mach 30,000 feet)

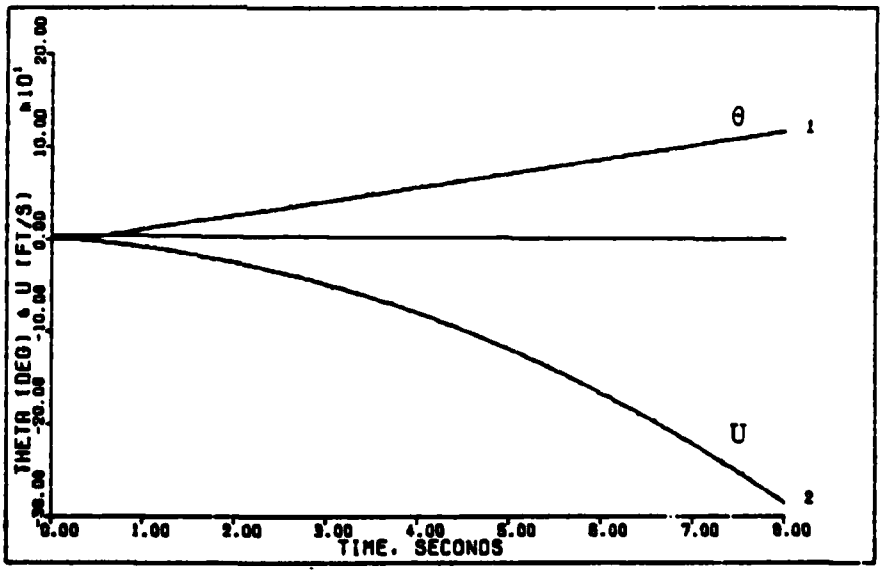

Figure 32d. G-Command System Response to a 6.5g Step Command for the Rigid Body. (0.8 Mach 30,000 feet)

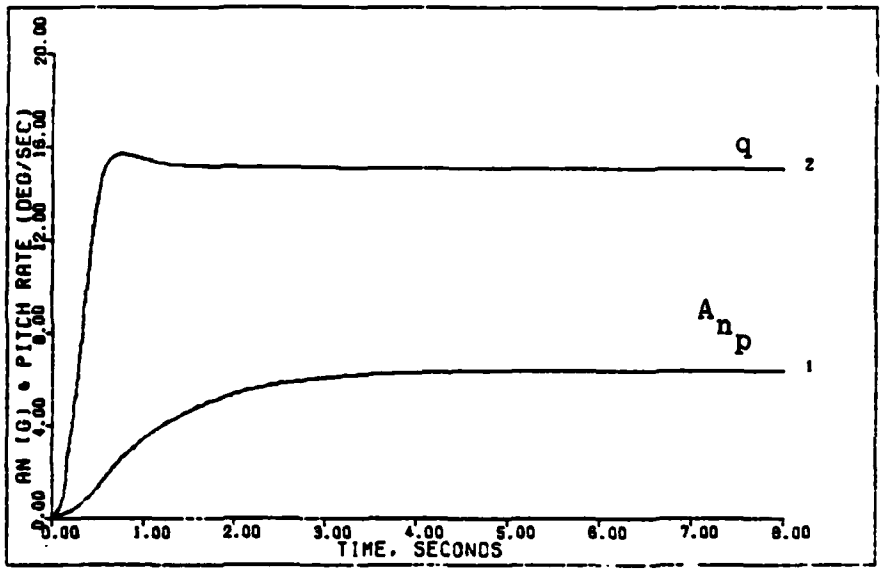

Figure 33a. G-Command System Response to a 6.5g Step Command for the FFA. (0.8 Mach 30,000 feet)

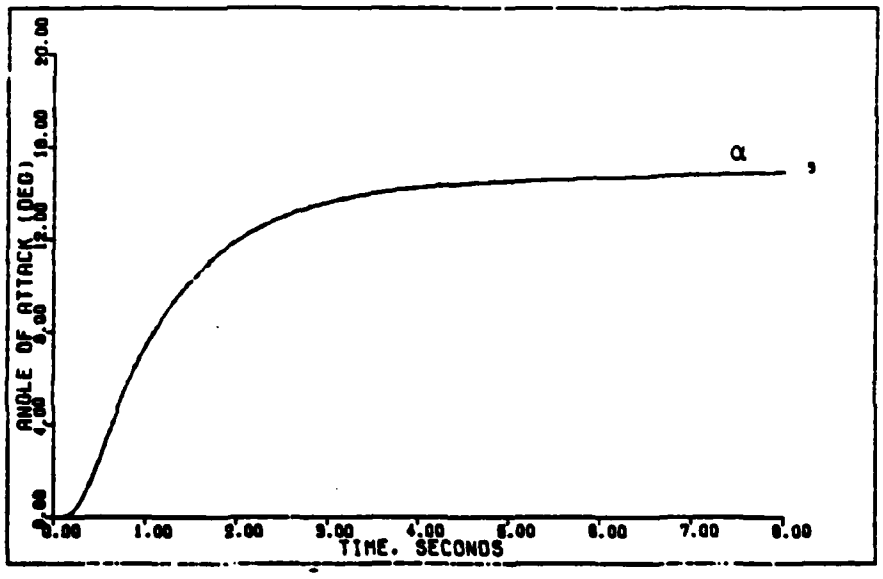

Figure 33b. G-Command System Response to a 6.5g Step Command for the FFA. (0.8 Mach 30,000 feet)

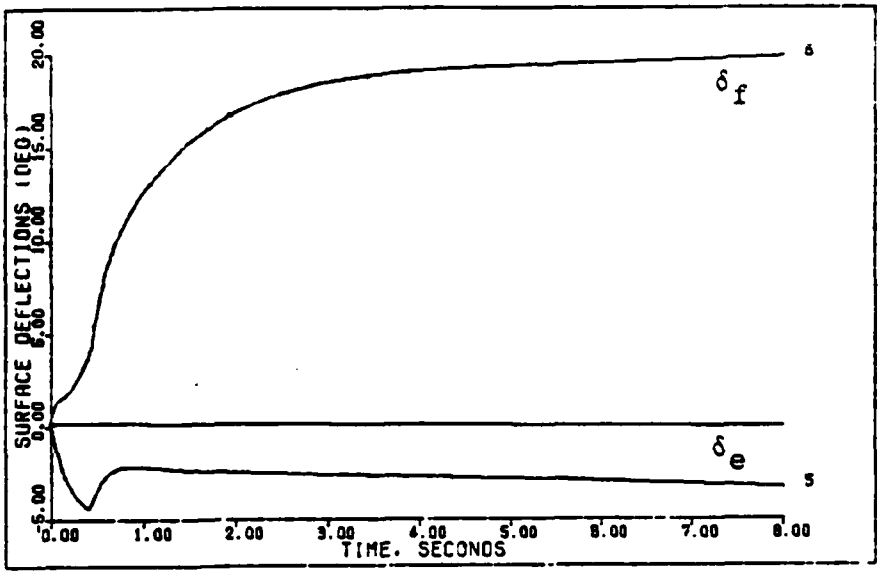

Figure 33c. G-Command System Response to a 6.5g Step Command for the FFA. (0.8 Mach 30,000 feet)

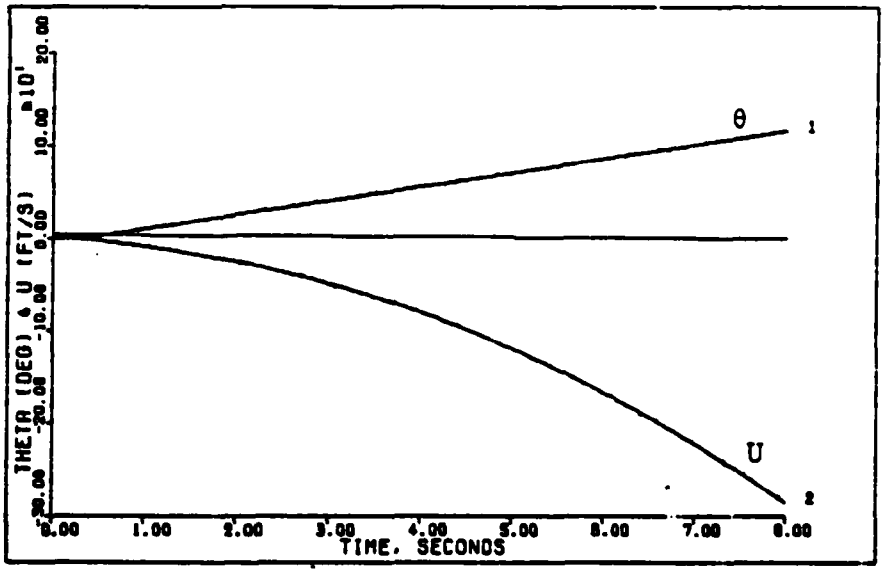

Figure 33d. G-Command System Response to a 6.5g Step Command for the FFA. (0.8 Mach 30,000 feet)

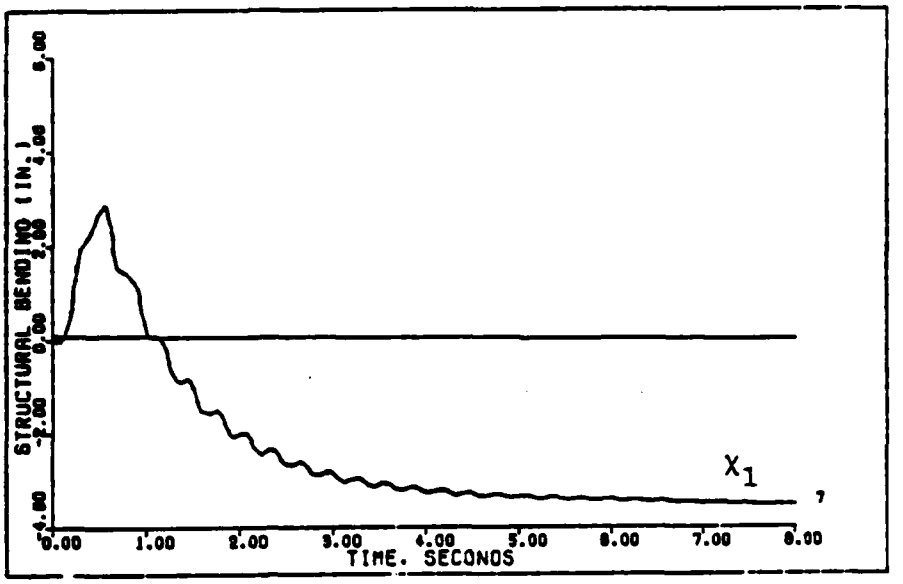

Figure 33e. G-Command System Response to a 6.5g Step Command for the FFA. (0.8 Mach 30,000 feet)

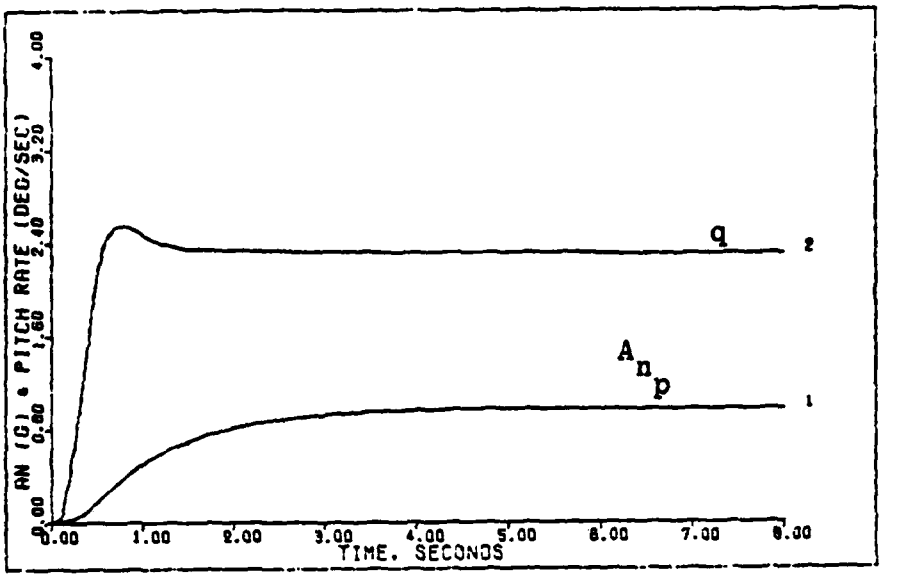

Figure 34a. G-Command System Response to a 1g Step Command with a Computational Delay of 1 for the Rigid Body. (0.8 Mach 30,000 feet)

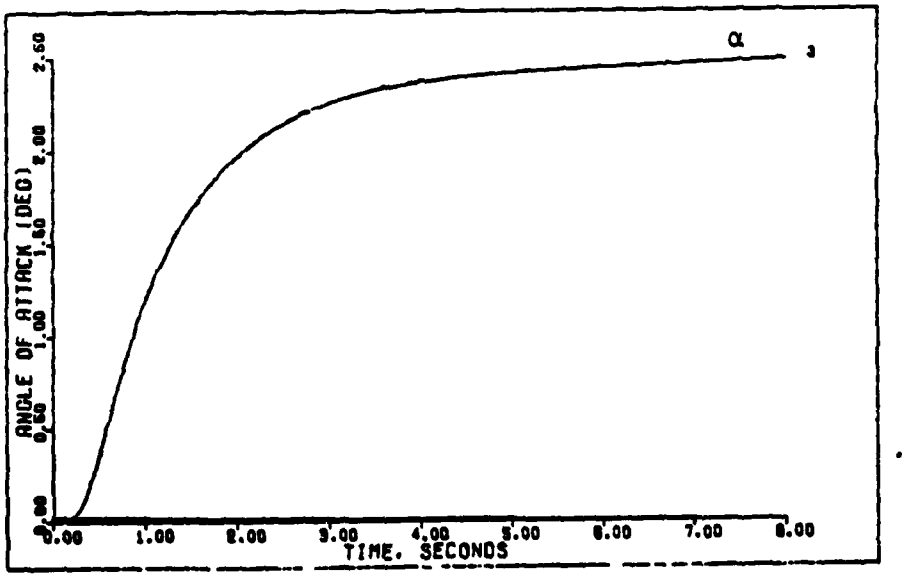

Figure 34b. G-Command System Response to a 1g Step Command with a Computational Delay of 1 for the Rigid Body. (0.8 Mach 30,00 feet)

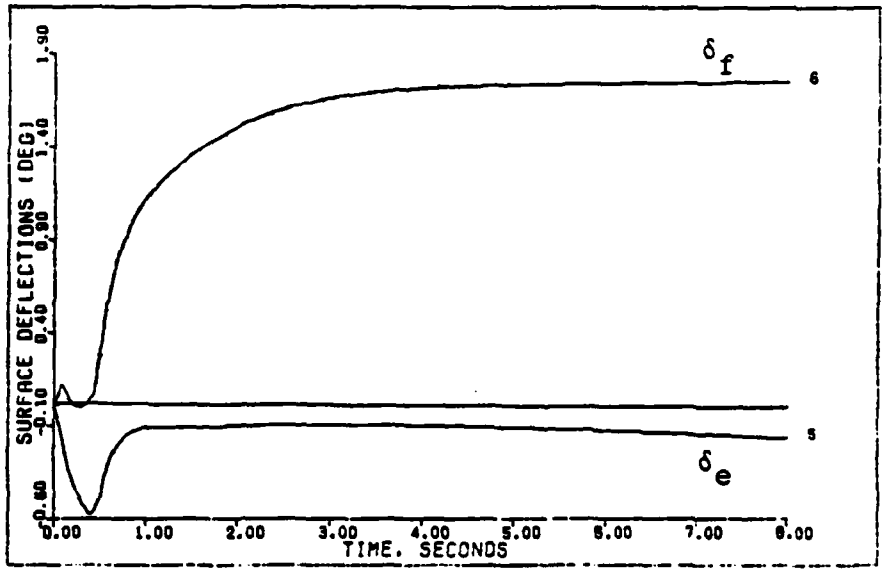

Figure 34c. G-Command System Response to a 1g Step Command with a Computational Delay of 1 for the Rigid Body. (0.8 Mach 30,000 feet)

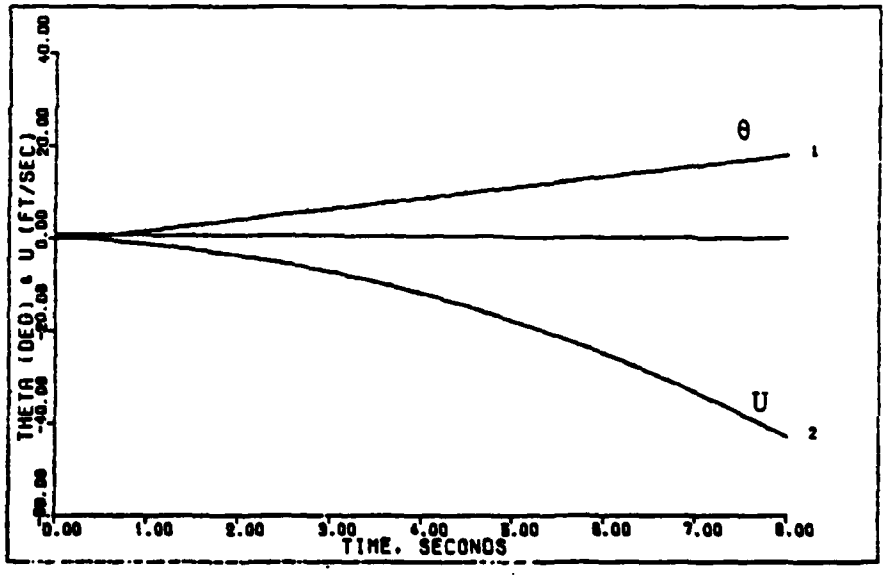

Figure 34d. G-Command System Response to a 1g Step Command with a Computational Delay of 1 for the Rigid Body. (0.8 Mach 30,000 feet)

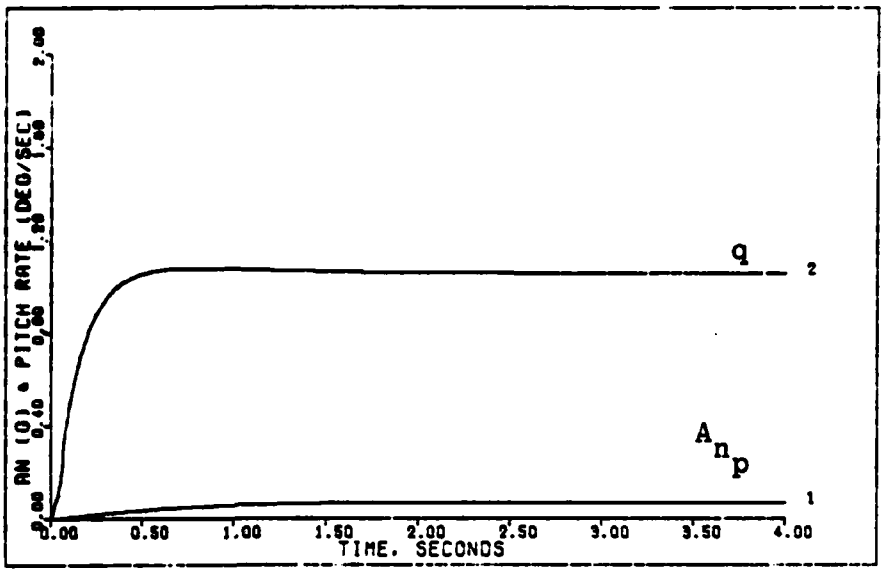

Figure 35a. Pitch-Pointing Command System Response to a 1 deg/sec Step Command with a Computational delay of 1 for the Rigid Body. (0.8 Mach 30,000 feet)

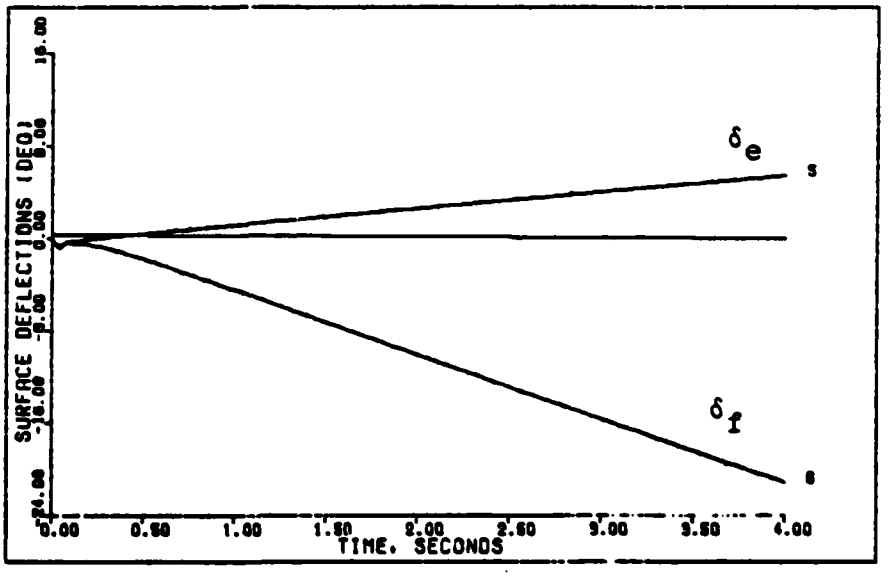

Figure 35b. Pitch-Pointing Command System Response to a 1 deg/sec Step Command with a Computational delay of 1 for the Rigid Body. (0.8 Mach 30,000 feet)

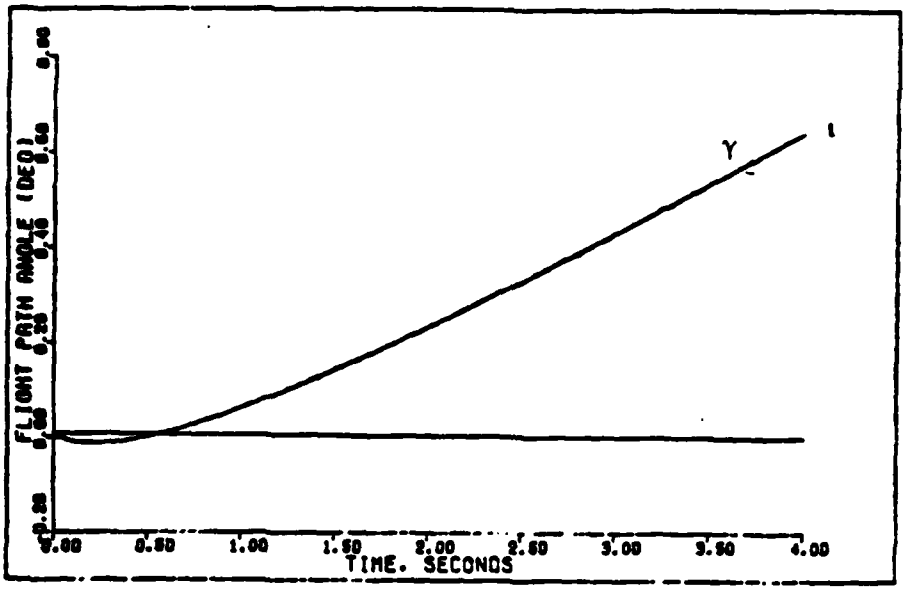

Figure 35c. Pitch-Pointing Command System Response to a 1 deg/sec Step Command with a Computational delay of 1 for the Rigid Body. (0.8 Mach 30,000 feet)

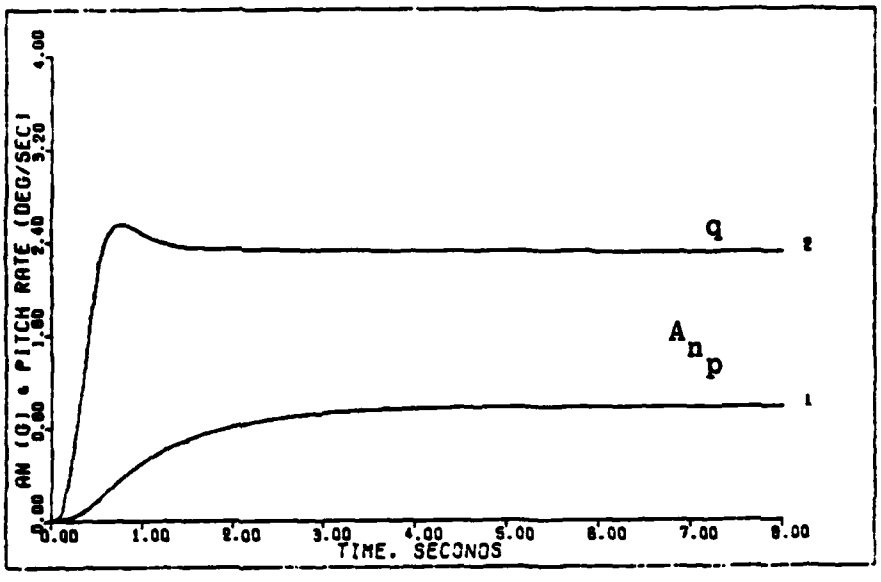

Figure 36a. G-Command System Response to a 1g Step Command with a Computational delay of 1 for the FFA. (0.8 Mach 30,000 feet)

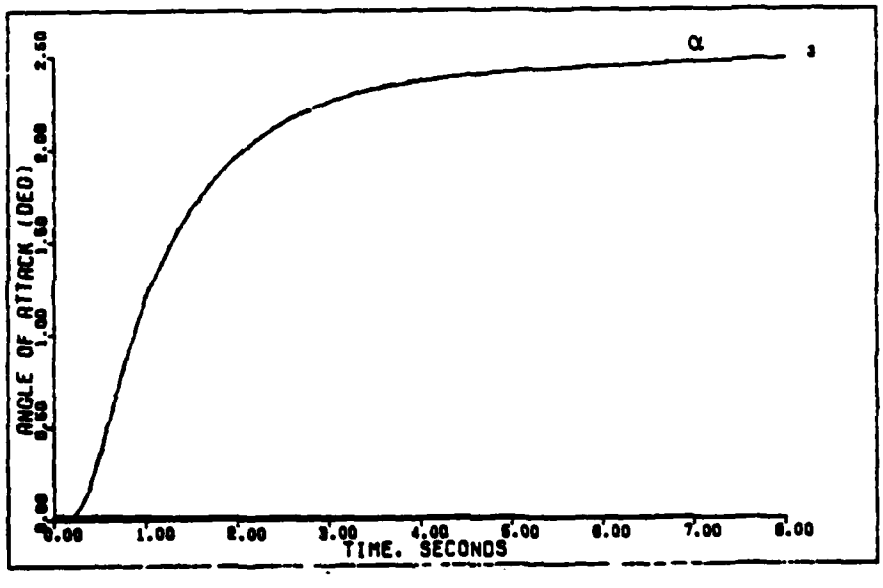

Figure 36b. G-Command System Response to a 1g Command with a Computational delay of 1 for the FFA. (0.8 Mach 30,000 feet)

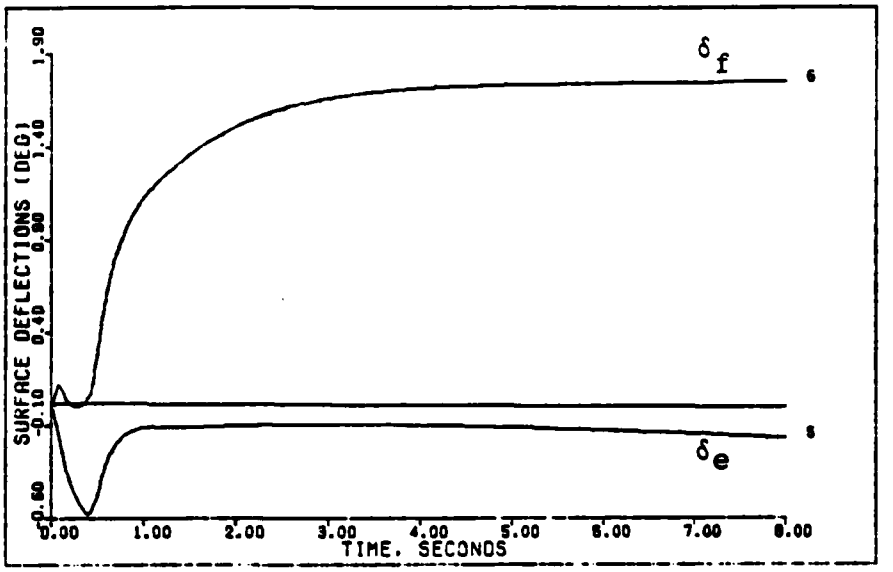

Figure 36c. G-Command System Response to a 1g Step Command with a Computational delay of 1 for the FFA. (0.8 Mach 30,000 feet)

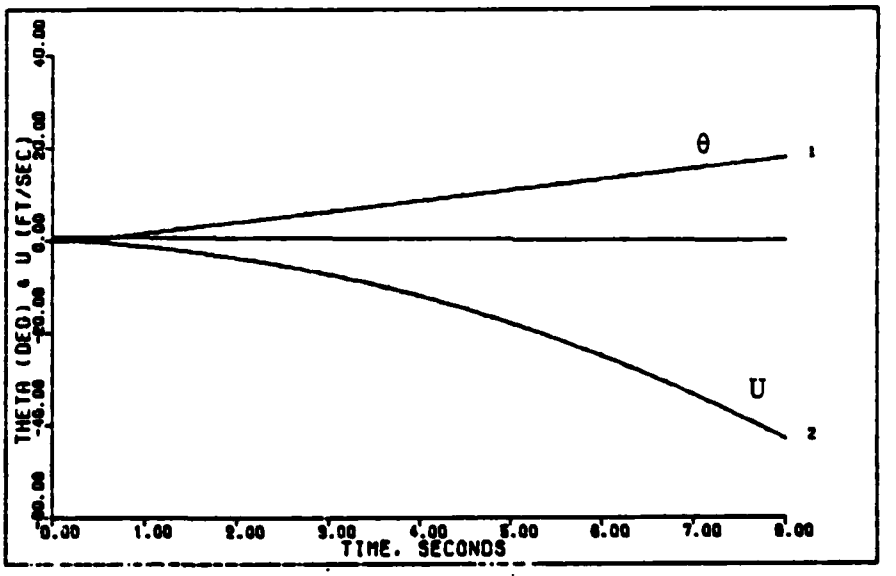

Figure 36d. G-Command System Response to a 1g Command with a Computational delay of 1 for the FFA. (0.8 Mach 30,000 feet)

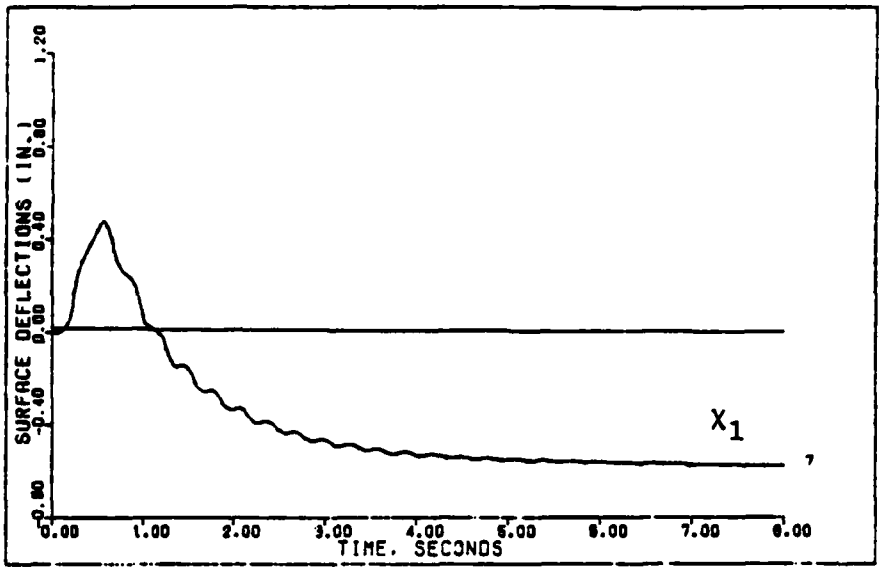

Figure 36e. G-Command System Response to a 1g Command with a Computational delay of 1 for the FFA. (0.8 Mach 30,000 feet)

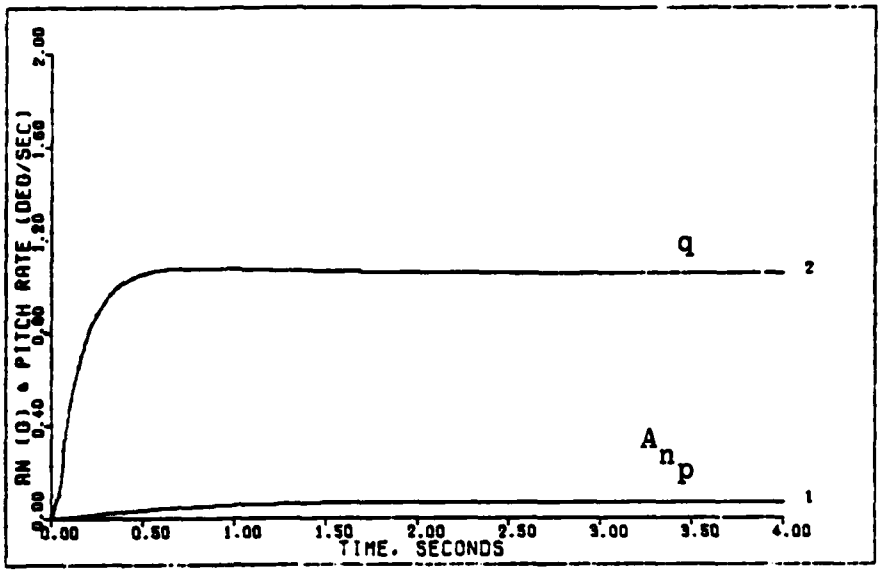

Figure 37a. Pitch-Pointing System Response to a 1 deg/sec Step Command with a Computational Delay of 1 for the FFA. (0.8 Mach 30,000 feet)

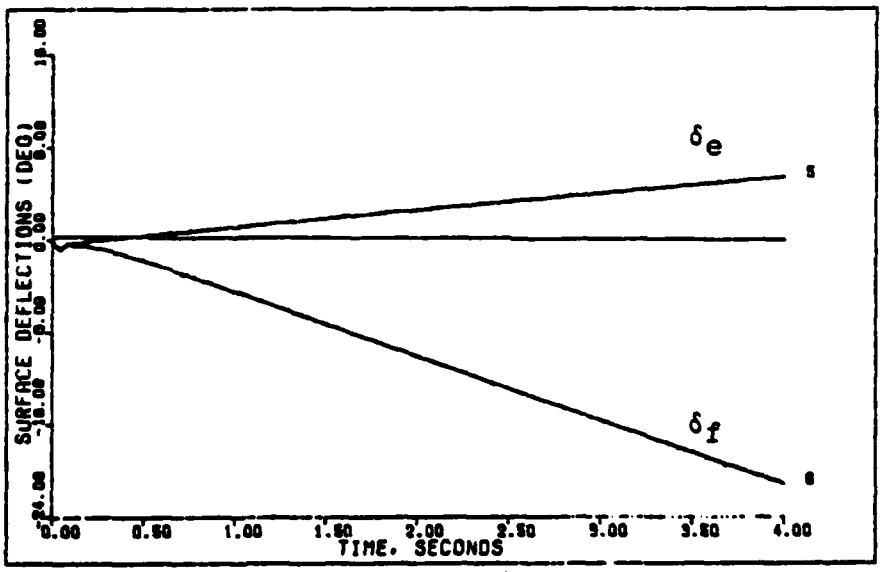

Figure 37b. Pitch-Pointing System Response to a 1 deg/sec Step Command with a Computational Delay of 1 for the FFA. (0.8 Mach 30,000 feet)

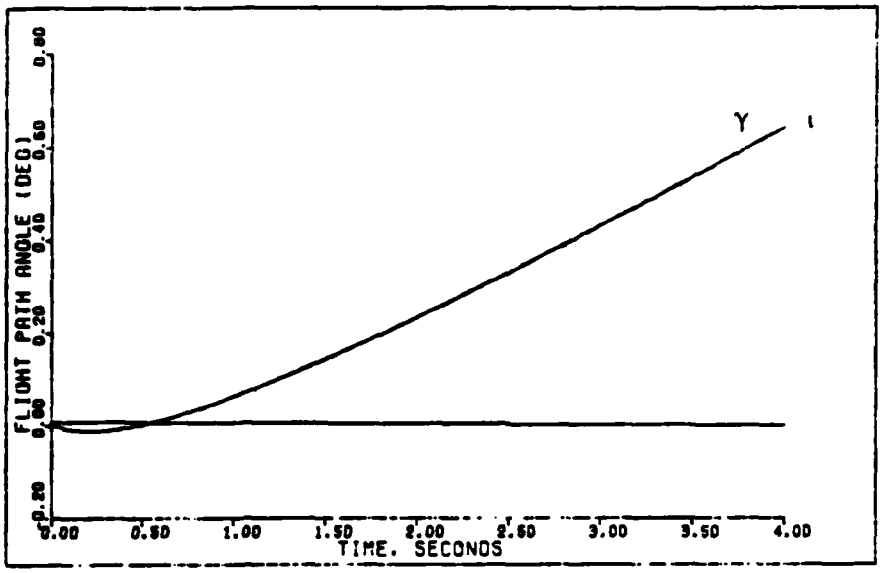

Figure 37c. Pitch-Pointing System Response to a 1 deg/sec Step Command with a Computational Delay of 1 for the FFA. (0.8 Mach 30,000 feet)

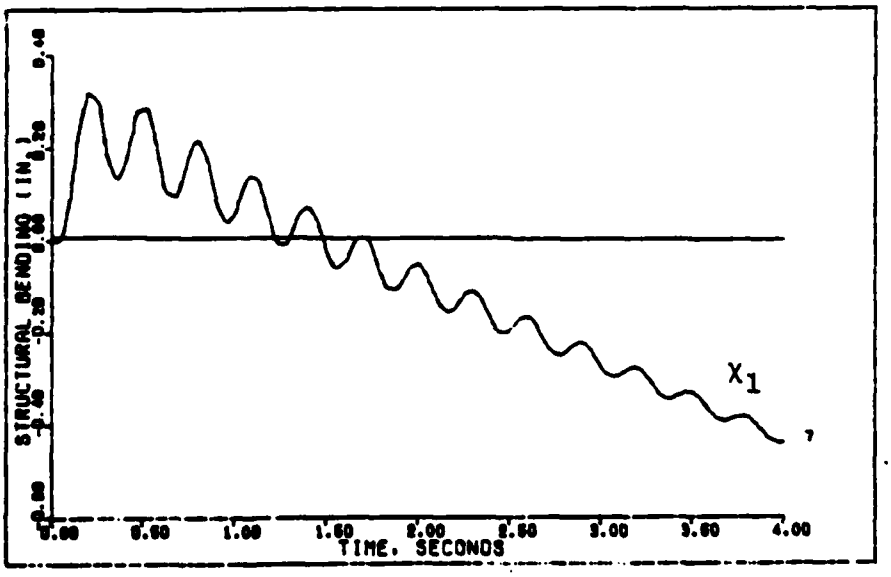

Figure 37d. Pitch-Pointing System Response to a 1 deg/sec Step Command with a Computational Delay of 1 for the FFA. (0.8 Mach 30,000 feet)

V. Pilot Rating Evaluation

Neal-Smith Criterion

After a digital flight controller is designed a means of determining its acceptability by a pilot is needed. One method of predicting a pilot's acceptance for a longitudinal compensatory tracking task has been suggested by Peter Neal and Roger Smith. The complete theoretical basis and the data used for the development of this criterion are provided in Reference 8. A summary of the Neal-Smith Criterion for predicting pilot rating is presented in this section.

An assumption is made when using the criterion; that is, the acceptability of an aircraft's maneuvering response in performing a specific task can be expressed in terms of a function representing a pilot's compensation needed to achieve some "minimum standard of performance" with the least tendency to develop a pilot induced oscillation (PIO). The standard of performance is established by the maneuver which the pilot is performing. For fighter aircraft the precise control of pitch attitude is assumed to be the critical task in the reference. The control of pitch attitude is modeled as shown in Figure 38. The model and definitions presented in the figure are direct extracts from Reference 8.

In order to use the Neal-Smith criterion, the engineer

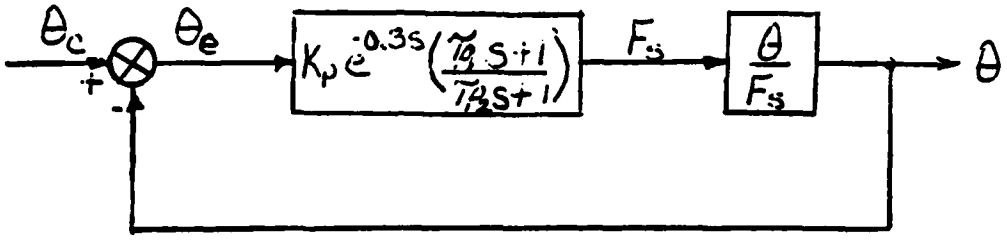

Using this model, the following terms are defined:

Bandwidth (BW): Bandwidth is defined as the frequency for which the closed-loop Bode phase, $\angle(\theta/\theta_c)$, is equal to -90 degrees. It is a measure of how quickly the pilot can move the airplane's nose toward the target.

Droop: Droop is defined as the maximum excursion of closed-loop Bode amplitude, $|\theta/\theta_c|$, below the 0 dB line for frequencies less than BW. In the absence of large oscillations, droop is a measure of how slowly the nose settles down on target.

Standard of Performance: A minimum bandwidth, $(BW)_{min}$, of 3.5 rad/sec, and a maximum droop of 3 dB:

$\left.\begin{array}{l}\angle(\theta/\theta_c) \text{ greater than } (-90) \text{ degree} \\ \text{and } |\theta/\theta_c| \text{ greater than } (-3) \text{ dB}\end{array}\right\}$ for ω less than 3.5

PIO Tendency: The tendency to oscillate or PIO is defined in terms of the Bode magnitude of any closed-loop resonant peak, $|\theta/\theta_c|_{max}$, that results from the pilot's efforts to achieve the performance standards.

Pilot Compensation: The pilot's physical and mental workload required to achieve the standard of performance is defined in terms of the phase of his compensation at $\omega = (BW)_{min}$:

$$\angle_{pc} = \angle\left(\frac{j\omega\tau_{p_1}+1}{j\omega\tau_{p_2}+1}\right)_{\omega=(BW)_{min}}$$

Figure 38. Neal-Smith Model for Pitch Attitude Control.

selects values for K_p, τ_{p1}, and τ_{p2} in the pilot compensation model that yield the smallest maximum value for $|\theta/\theta_c|$ for the closed-loop system while maintaining a minimum bandwidth of 3.5 radians per second, and a maximum droop of 3dB. The procedure for selecting the values are covered later.

The Nichols chart is used to determine the maximum value of $|\theta/\theta_c|$ and the phase angle at the frequency of 3.5 rad/sec for each of the pilot model parameter selections. The value of K_p and the pilot compensation angle determined by the τ_{p1} and τ_{p2} values are plotted in Figure 39. This figure is used to evaluate the design, that is, to determine a predicted pilot rating (PR) and the acceptability of the design.

To apply this method, the airframe plus flight control system transfer function, θ/F_s, must first be determined for the longitudinal system, where F_s is the stick force applied by the pilot. Equation (5.1) represents the control system transfer function matrix $\underline{G}(s)$.

$$\underline{G}(s) = \begin{bmatrix} \frac{A_{n_p}}{v_1} & \frac{A_{n_p}}{v_2} \\ \frac{q}{v_1} & \frac{q}{v_2} \end{bmatrix} \qquad (5.1)$$

Application

Since the normal acceleration A_{n_p} and q are related

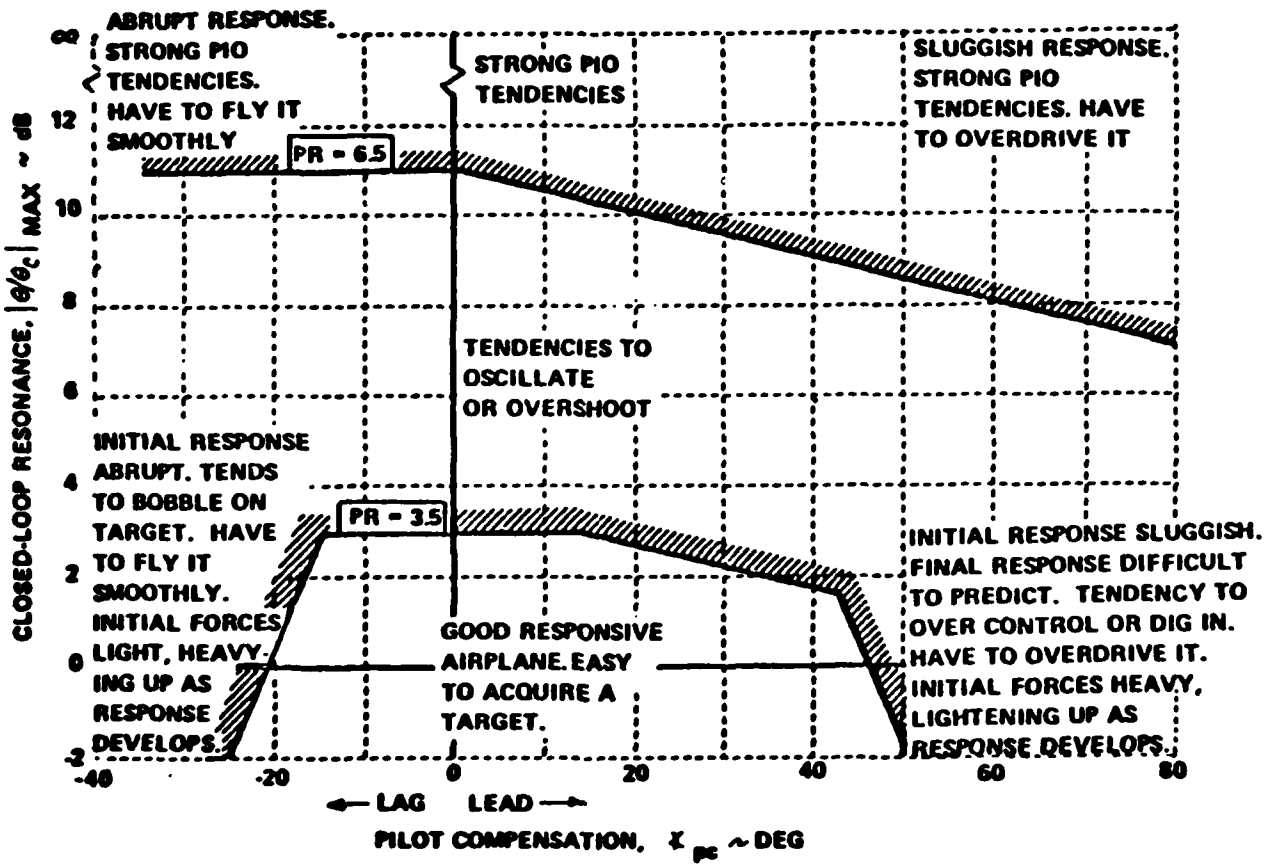

Figure 39. Neal-Smith Criterion for Fighter Maneuvering Dynamics

quantities, both inputs must be considered in the pitch attitude output. Figure 40 relates stick force input (F_s) to the control commands v_1 and v_2 for both the g-command and pitch-pointing maneuvers. For the g-command maneuver

$$v_1 = F_s \text{ and } v_2 = (\frac{1845}{U})(F_s) \tag{5.2}$$

Thus

$$q = \frac{q}{v_1} v_1 + \frac{q}{v_2} v_2 = \frac{q}{v_1} (F_s) + \frac{q}{v_2} (\frac{1845}{U})(F_s) \tag{5.3}$$

and

$$\frac{q}{F_s} = \frac{q}{v_1} + \frac{q}{v_2} (\frac{1845}{U}) \tag{5.4}$$

$$\frac{\theta}{F_s} = \frac{1}{s} \{\frac{q}{v_1} + \frac{q}{v_2} (\frac{1845}{U})\} \tag{5.5}$$

For the pitch-pointing maneuver

$$v_1 = 0.0 \text{ and } v_2 = F_s \tag{5.6}$$

thus

$$\frac{\theta}{F_s} = \frac{1}{s} (\frac{q}{v_2}) \tag{5.7}$$

Equations (5.8) and (5.9) are the transfer function θ/F_s, obtained for Equation (5.5), of the rigid body and the flexible-fighter aircraft, respectively, performing the q-command maneuver.

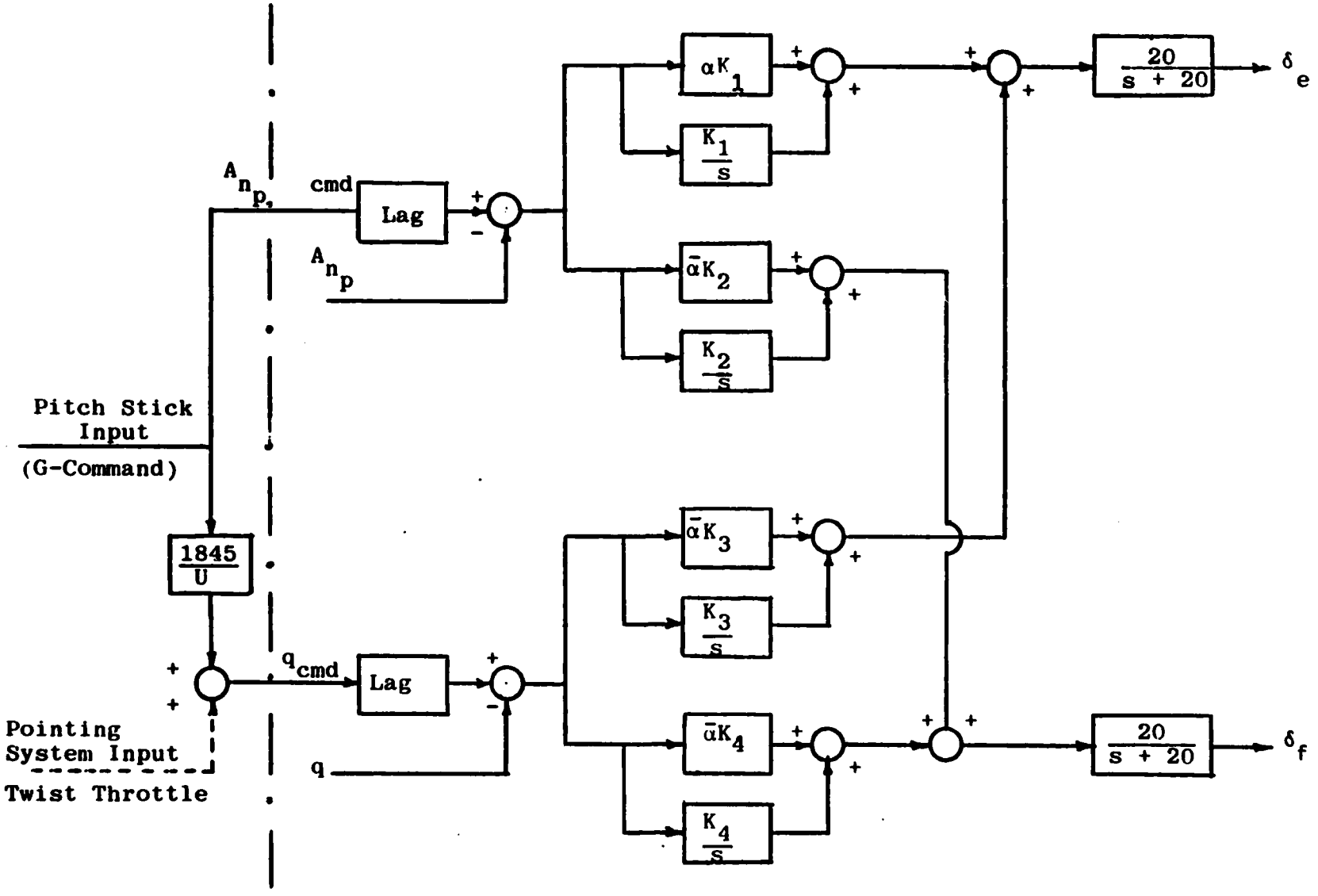

Figure 40. Block Diagram of Longitudinal G-Command System With Pilot Interface Addition and Including the Pitch Pointing System

$$\frac{\theta}{F_s} = \frac{927.3(s+0.00036\pm j0.0034)(s+0.0094)}{s(s-0.00075)(s+0.0037)(s+0.0073)(s+1.012)} \frac{(s+0.986)(s+5.0)}{(s+5.79\pm j2.54)(s+48.82)} \quad (5.8)$$

$$\frac{\theta}{F_s} = \frac{927.3(s+0.521\pm j20.99)(s+0.0088\pm j0.00874)}{s(s+0.528\pm j20.99)(s-0.00155\pm j0.0075)(s+0.01324)} \frac{(s-0.0076)(s+0.984)(s+5.0)}{(s+1.01)(s+5.79\pm j2.54)(s+48.82)} \quad (5.9)$$

Equations (5.10) and (5.11) represent the transfer functions of θ/F_s, obtained from Equation (5.7), of the rigid body and the flexible-fighter aircraft, respectively, for the pitch-pointing maneuver.

$$\frac{\theta}{F_s} = \frac{625.0(s+2.0)(s+1.818)(s+0.0025+j0.00703)}{s(s+72.8)(s+8.12)(s+1.965)(s+1.898)(s+0.0037\pm j0.005)} \frac{(s+0.016)}{(s+0.0139)} \quad (5.10)$$

$$\frac{\theta}{F_s} = \frac{625.0(s+0.5242\pm j20.99)(s+2.0)(s+1.817)(s-0.0075)}{s(s+0.529\pm j20.99)(s+72.8)(s+8.12)(s+1.966)(s+1.897)} \frac{(s+0.014\pm j0.0123)}{(s+0.0201\pm j0.0234)(s-0.0196)} \quad (5.11)$$

The magnitude and phase values are calculated for the frequency response for the transfer functions in equation (5.8) through (5.11). The values of the rigid body and the flexible-fighter aircraft responses are practically the same. Table 8 illustrates this point.

Table 8

Frequency Response

	G-COMMAND MANEUVER				PITCH-POINTING MANEUVER			
FREQ. RAD/SEC	RIGID BODY		FFA		RIGID BODY		FFA	
	1dB	ANGLE	dB	ANGLE	dB	ANGLE	dB	ANGLE
0.2	21.3	-90.9	21.3	-90.8	14.2	-91.3	14.2	-91.2
0.4	15.3	-92.0	15.3	-92.0	8.23	-92.8	8.22	-92.7
0.8	9.34	-94.4	9.34	-94.4	2.2	-95.7	2.2	-95.7
1.6	3.42	-99.8	3.42	-99.8	-3.88	-101.7	-3.88	-101.7
2.2	0.69	-104.2	0.69	-104.2	-6.76	-106.2	-6.76	-106.2
3.5	-3.45	-114.4	-3.45	-114.4	-11.2	-115.5	-11.2	-115.5
5.0	-7.0	-126.1	-7.0	-126.1	-14.9	-125.1	-14.9	-125.1

The next step is to select values for the pilot model that allow the standard of performance to be met.

The phase angle from the exponential term in the pilot model, $(57.3)(-0.3)(\omega)$, is added to the phase values of θ/F_s for both maneuvers. This establishes the open-loop θ/θ_e magnitude and phase information. Figures 41 and 42 represent the open-loop amplitude-phase plot of θ/θ_e for the g-command and pitch-pointing maneuvers, respectively, of the rigid body and the flexible-fighter aircraft (FFA) with τ_{p_1} and τ_{p_2} equal to zero. The standard of performance (closed-loop) boundaries are established in both figures on the Nichols chart.

First examining the g-command open-loop plot of θ/θ_e

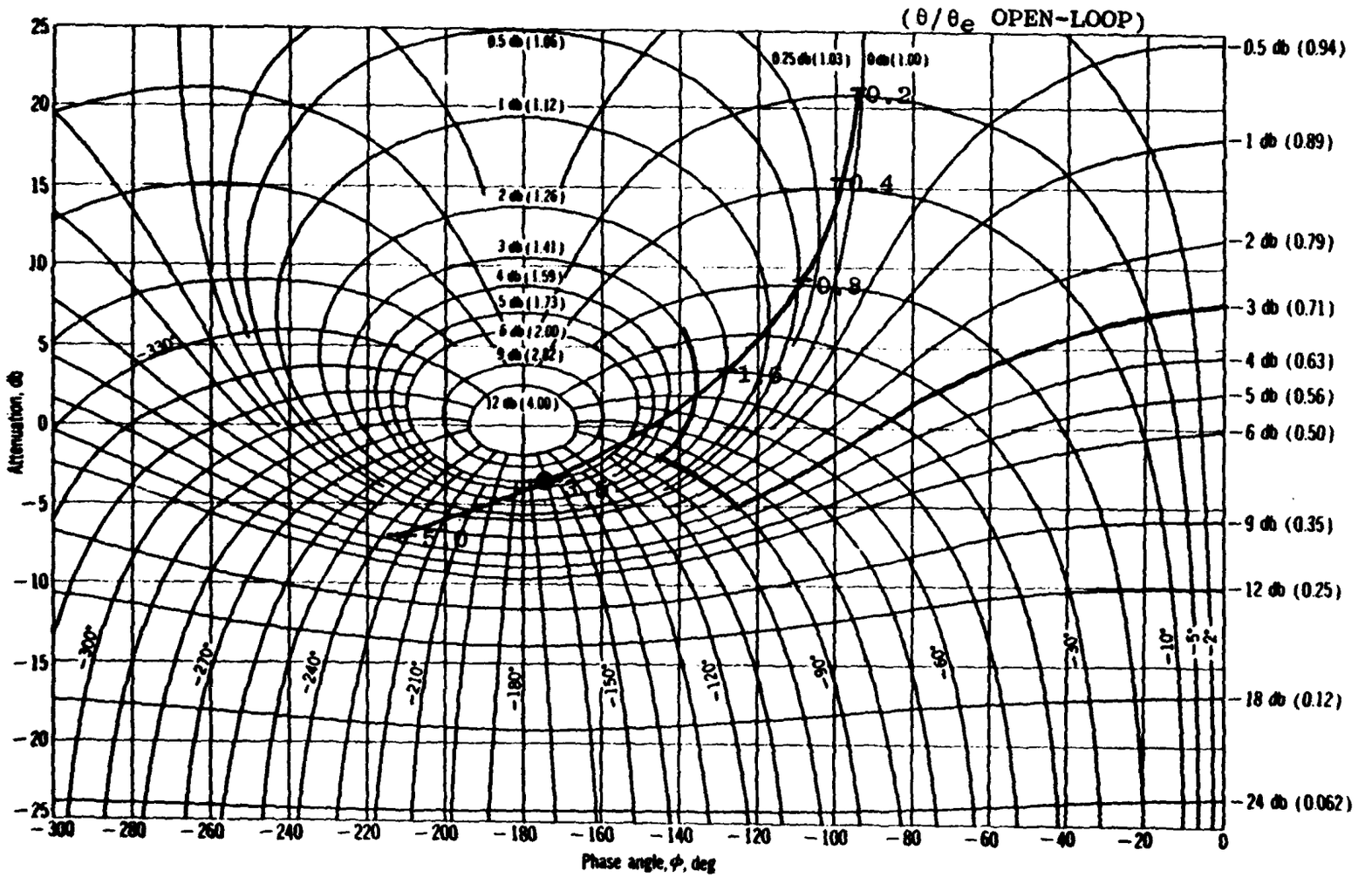

Figure 41. Nichols Chart with Performance Standard Boundaries and Overlay of Amplitude-Phase of θ/θ_e ($\tau_{p1} = \tau_{p2} = 0$) for the Rigid Body and the FFA Performing the G-Command Maneuver.

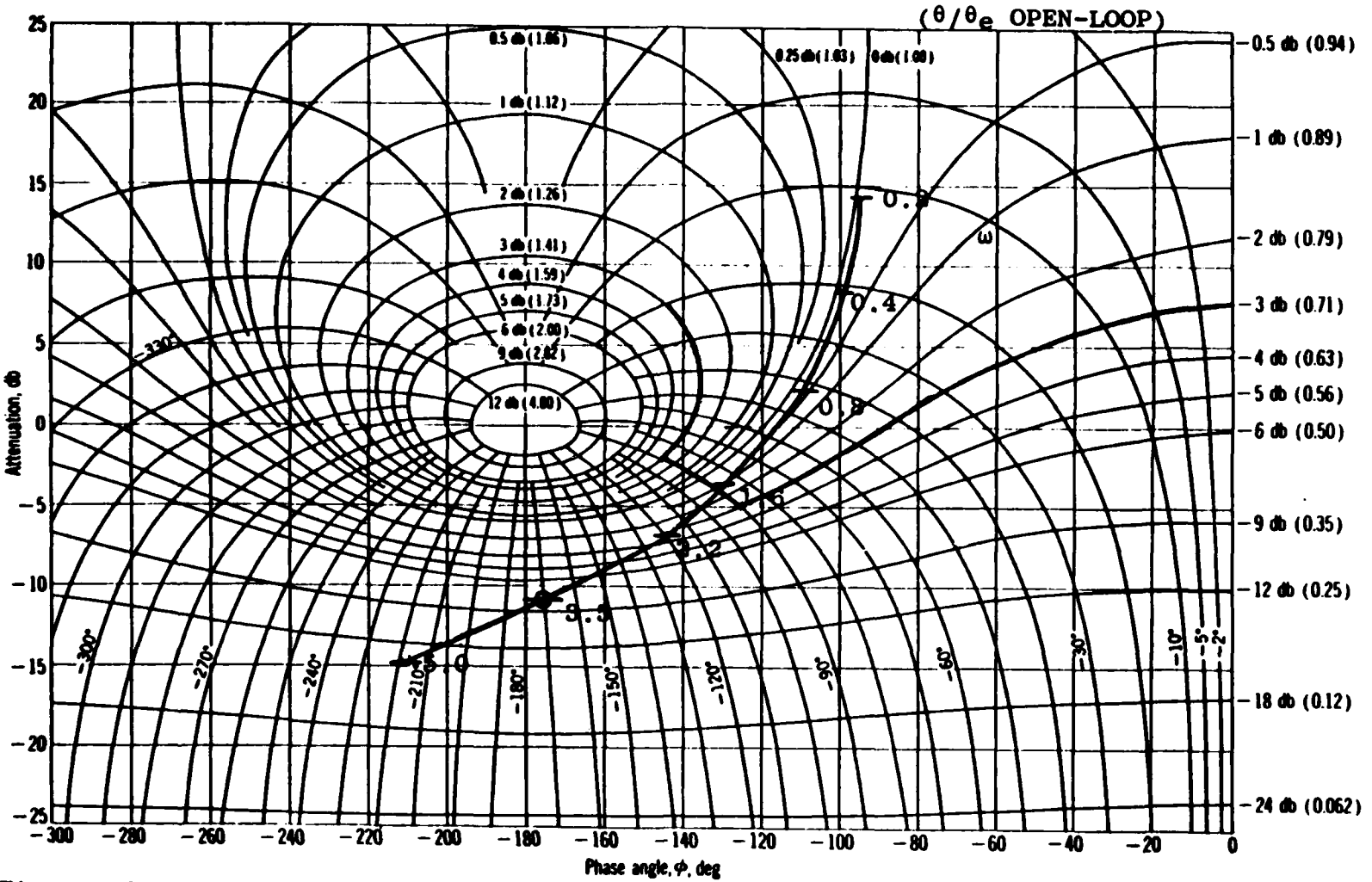

Figure 42. Nichols Chart with Performance Standard Boundaries and, Overlay of Amplitude-Phase Plot of θ/θ_e ($\tau_{p1} = \tau_{p2} = 0.0$) for the Rigid Body and the FFA Performing the Pitch-Pointing Maneuver.

(Figure 41), the value of K_p alone can not meet the standard for the closed-loop tracking system θ/θ_c. The 3.5 radians per second point on the amplitude-phase plot requires an increase in phase angle, indicating lead compensation that must be added by the pilot. Figure 43 from Reference 7 provides a plot of amplitude-phase curves for optimum pilot compensation which simplifies the selection of τ_{p_1} and τ_{p_2}. Selecting $\tau_{p_1} = 0.8$ and $\tau_{p_1} = 0.0$ meets both the bandwidth and droop requirements. These values indicate that the pilot must generate about 39 degrees of lead at a frequency of 3.5 rad/sec. The resulting $|\theta/\theta_c|$ max is plotted (as a dot) verses the pilot compensations angle on the criterion graph in Figure 44. The point falls within the desired PR boundary.

Examining the pitch-pointing open-loop plot of θ/θ_e (Figure 42), the value of K_p alone can not meet the standard for the closed-loop tracking system θ/θ_c. Again lead compensation by the pilot is needed according to the amplitude-phase plot. Selecting $\tau_{p1} = 0.9$ and $\tau_{p2} = 0.0$ meets the bandwidth and droop requirement. These values indicate that the pilot must generate about 42 degrees of lead at 3.5 rad/sec frequency. This point is also plotted (as a triangle) in Figure 44. According to the point on the figure, the design of pitch-pointing maneuver would not be acceptable to the pilot.

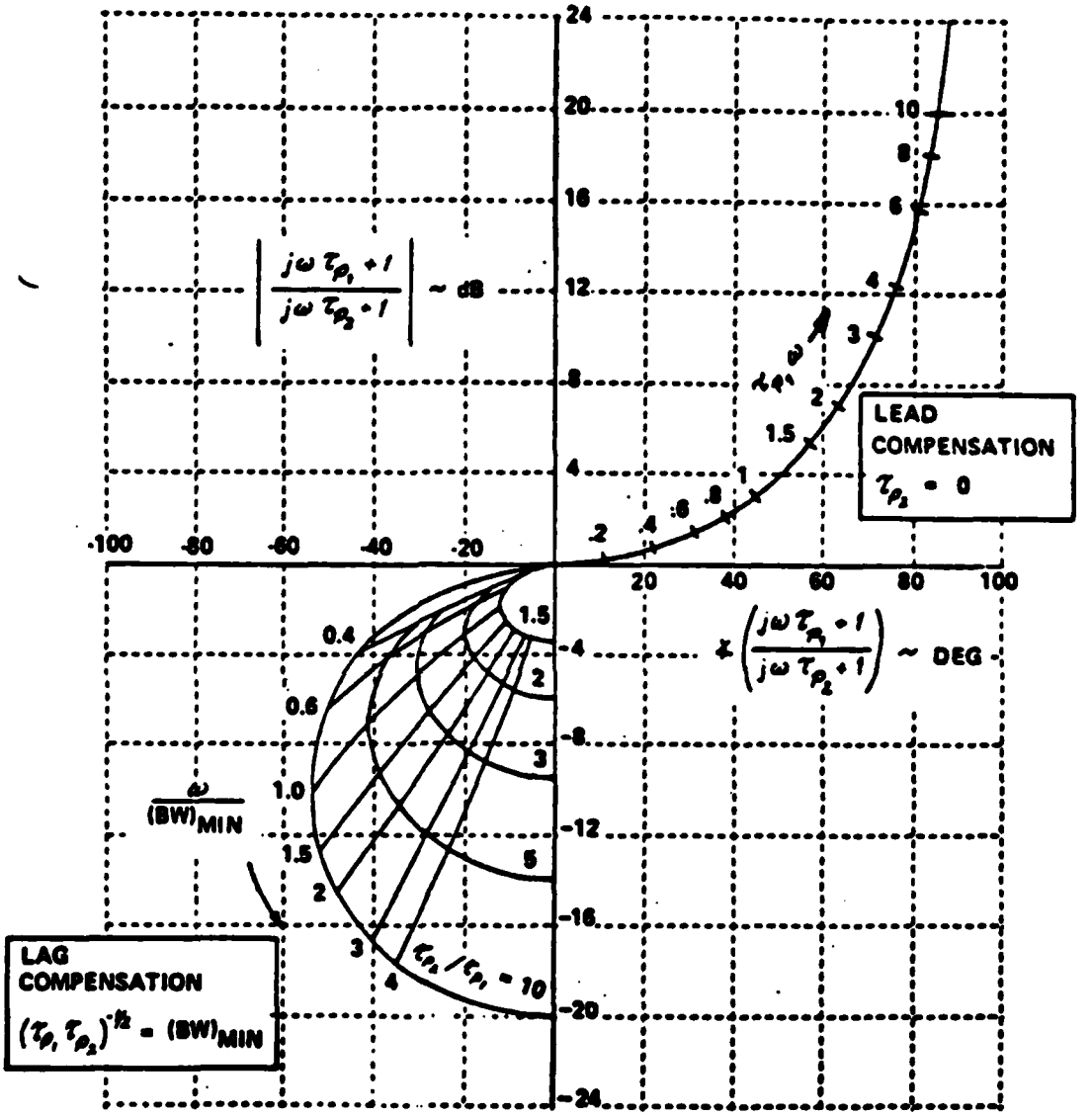

Figure 43. Amplitude-Phase Curves for "Optimum" Pilot Compensation

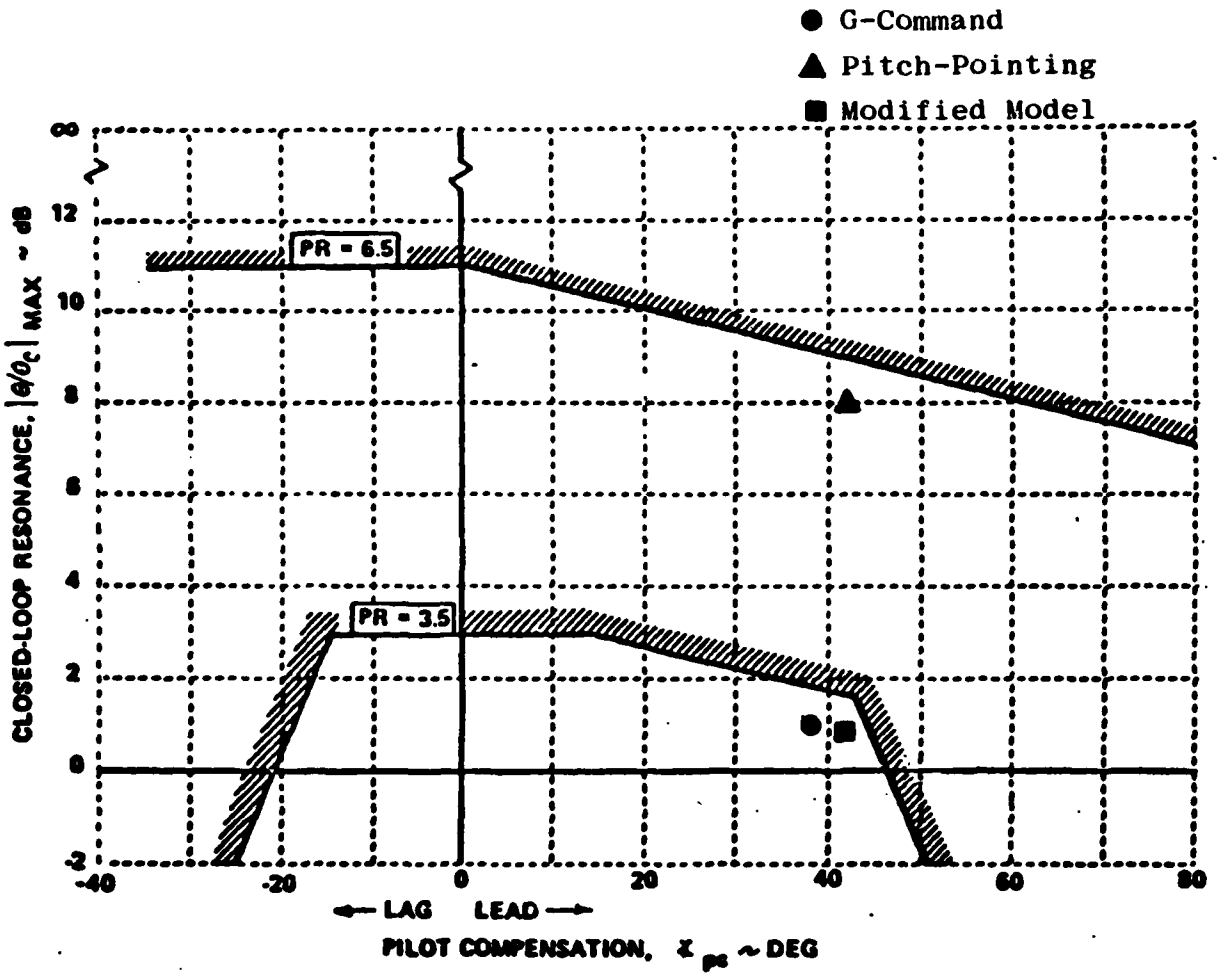

Figure 44. Criterion Graph with Design Evaluation Points

The closed-loop resonance gain, $|\theta/\theta_c|_{MAX}$, that is plotted in Figure 44 comes from the magnitude of K_p and the gain established by the $(\tau_{p1}s+1)(\tau_{p2}s+2)$. That is

$$K = K_p \left[\frac{(\tau_{p1}\omega)^2 + 1}{(\tau_{p2}\omega)2 + 1} \right]^{\frac{1}{2}} \qquad (5.12)$$

where K is the closed-loop resonance gain. Therefore, the gain that is plotted versus the pilot compensation angle comes from the pilot model only. If the gain from the pilot model can be reduced, the pitch-pointing design is acceptable by the pilot. A suggestion was made by Mr. Finley Barfield of the Flight Dynamics Laboratory at Wright-Patterson AFB, Ohio, to modify the Neal-Smith model in Figure 38. The modified model is shown in Figure 45.

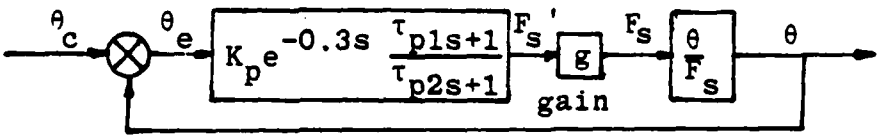

Figure 45. Modified Neal-Smith Model for Pitch Attitude Control.

This modified model decreases the effort required by the pilot to perform a pitch rate maneuver. This reduces the tendency to produce a PIO when performing a longitudinal maneuver.

Using the values of τ_{p1} and τ_{p2} selected previously for the pitch-pointing open-loop plot of θ/θ_e, and setting g = 10.0dB, the point plotted (as a square) in Figure 44

falls within the desired PR boundary. This is true only if the gain plotted in Figure 44 comes from the pilot model alone.

If the new model is a fair representation of the original Neal-Smith model, the only Standard that is needed to be met is that the pilot compensation angle must be between -20 and 50 degrees. The reason is that the gain g may be increased or decreased to ensure that the gain required from the pilot model falls within the acceptable PR boundary.

VI. Conclusion

The major objective of this thesis has been to determine how a flexible-fighter aircraft can react to a design that is originally developed for a rigid body aircraft. The result found in this thesis is that this flexible-fighter aircraft, as described in Chapter II, responds the same as the rigid body aircraft when using the same controller design. Even when the flexible-fighter model is changed through a range of dynamic properties, as described in Chapter IV, the time responses are nearly the same as for the rigid body model.

The performance obtained from the digital controller developed with Professor Porter's technique is very good. Both the g-command and pitch-pointing maneuvers shown excellent performance with their individual controllers. Even when a time delay is incorporated to represent the controller implementation, both the rigid body and the flexible-fighter aircraft simulation time responses are not significantly affected and the aircraft performance is very satisfactory.

According to the Neal-Smith Criterion, the g-command controller is a pilot acceptable design. Evaluating the pitch-pointing controller, the results show initially that the design is not acceptable. After modifying the model (Figure 45), the pitch-pointing controller is again evaluated using the new model and the results show that it

is a pilot acceptable design.

Equations (5.8) and (5.9) for the g-command transfer function θ/F_s of the rigid body and the flexible-fighter aircraft, respectively, have an unstable real pole or complex pole pair. Since the maneuver only lasts 8 seconds, the unstable poles for both aircraft do not affect the time response. Because the poles are very close to the origin, the pilot is able to control the unstable response. Also, a g-command maneuver typically may probably not last more than 8 seconds.

The transfer function θ/F_s of the flexible-fighter aircraft performing the pitch-pointing maneuver has one unstable pole as indicated in Equation (5.11). The maneuver lasts 4 seconds and the unstable pole does not affect the response. If the maneuver lasts longer than 10 seconds, the unstable pole can probably start to influence the aircraft's response, but the pilot can still be able to control the aircraft, that is, to break off the maneuver. Usually, as in a dog fight, a pitch-pointing maneuver may not last longer than 10 seconds, especially if the aircraft is in a turn pulling over 4 g's.

Appendix A

Subroutine Fix

Introduction

The purpose of the Subroutine Fix is to make the program MULTI user friendly when inputing matrices. The way this works is that the user will no longer have to input the matrix from beginning to end if an error is made. All the user has to do now is to give the row and column number along with the new value. This is explained in more detail in the User's Guide.

User's Guide

The options which ask for the input of certain matrices have the same format and the user enters the data by row after the prompt (>). After each matrix is entered, its values are automatically echoed back for checking (Ref. 9). The checking tool used is the following:

IS THIS CORRECT....YES, NO, $...>

In this case of a "$" reply the option is terminated. although the option is terminated, the values just entered are still in memory. The reply "N " gives the following message (the user can also enter a simple "Y" or "N"):

ENTER THE NUMBER OF CORRECTIONS BEING MADE...>

The number of corrections correspond to the number of

wrong values in the matrix. After entering the number of corrections, another message appears along with a prompt (>).

```
ENTER THE ROW, COLUMN, AND NEW VALUE FOR EACH CORRECTION
EX-> 1,2,-1.5...PRESS RETURN.
>
```

Only one correction can be entered at a time. Once the row, column, and new value for that single correction is entered the user must press the return key. The prompt (>) appears according to the number of corrections being made. After the corrections have been made, the matrix is echoed back with the new values for checking. The same checking tool is used again.

Programmer's Guide

The Subroutine Fix is used to make MULTI user friendly. The subroutine is located in the Main Executive Overlay. The following fortran statements are found in the Subroutine Fix:

```
SUBROUTINE FIX (TS,IS,ID)
DIMENSION TS(10,10)
```

This initializes the subroutine that has three parameters that are described below:

TS - A real matrix of maximum dimension 10 x 10

TS - An integer value denoting the # of rows of the matrix.

ID - An integer valued denoting the # of columns of the matrix.

These parameters are transferred from the previously entered matrix.

```
      PRINT '(/A)', 'ENTER THE NUMBER OF CORRECTIONS
                     BEING MADE...>'
      READ*, K
```

First the statement is printed out, then the reply is read that will be used in a DO Loop

```
      PRINT*,   'ENTER THE ROW, COLUMN, AND NEW VALUE FOR
                 EACH CORRECTION.'
      PRINT*,   'EX->1,2,-1.5 ... PRESS RETURN.'
      DO 60 L=1,K
      PRINT '(/A)', ' >'
 60   READ*,I,J,TS(I,J)
      PRINT*, '  '
      END
```

This is the main part of the subroutine which actually corrects the errors in the matrix. The Subroutine Fix has been added to MULTI throughout the program. Everyplace a matrix is inputted the Subroutine Fix has been added. Below is the program before the fix was added: (this is not an actual matrix)

```
      1 PRINT*,  'ENTER "Y" MATRIX... ,N,' ROWS WITH ',K,
                 ' ELEMENTS EACH'
      DO 2 I=1,N
      PRINT*,   'ROW ',I,' >'
      2 READ*, (Y(I,J),J=1,K)
```

```
     + CALL ANSWER (*1,*8001)
       CALL MATPR(Y,N,K)
       PRINT*,  'Y MATRIX...'
```

+ NOTE- 1st* - line number denoting inccorect data directing return to number given. (*1)
(Ref. 9)

2nd* - line number denoting option abort directing return to end of option (*8001)

This is how the program looks with the subroutine daded.

```
       PRINT*, 'ENTER "Y" MATRIX...;N,' ROWS WITH,',K,
              ' ELEMENTS EACH'
       DO 2 I1,N
       PRINT*, 'ROW ',I,' >'
     2 READ*, (Y(I,J),J=1,K)
       GO TO 5
     1 CALL FIX (Y,N,K)
     5 PRINT*, 'Y MATRIX...'
       CALL MATPR (Y,N,K)
       CALL ANSWER (*1,*8001)
```

Appendix B

Combination of States

Introduction

The output equation, $\underline{y}=\underline{C}\underline{x}$, can be considered to be the combination of states formed by the "C" matrix. The output for a MIMO system can be evaluated from the state and output equations (Ref 1.):

$$\dot{\underline{x}} = \underline{A}\underline{x} + \underline{B}\underline{u} \tag{B-1}$$

$$\underline{y} = \underline{C}\underline{x} \tag{B-2}$$

Taking the Laplace transform of Equations (B-1) and (B-2) yields

$$s\underline{x}(s) - \underline{x}(0) = \underline{A}\underline{x}(s) + \underline{B}\underline{U}(s) \tag{B-3}$$

$$Y(s) = \underline{C}\underline{x}(s) \tag{B-4}$$

Solving for x(s) in Equation (B-3)

$$\underline{X}(s) = \underline{\Phi}(s)\underline{x}(0) + \underline{\Phi}(s)\underline{B}\underline{U}(s) \tag{B-5}$$

where $\Phi(s) = [\,s\underline{I}-\underline{A}\,]^{-1}$. Substituting in Equation (B-5) into Equation (B-4) yields

$$Y(s) = \underline{C}\underline{\Phi}(s)\underline{x}(0) + \underline{C}\underline{\Phi}(s)\underline{B}\underline{U}(s) \tag{B-6}$$

The output equation above is actually the combination of states, but that is only true because of the output

equation $\underline{Y}(s) = \underline{Cx}(s)$. If the output equation happened to be $\underline{Y}(s) = \underline{Cx}(s) + \underline{DU}(s)$ it can no longer be just the combination of states. This is one of the reasons for developing a routine that takes the states in Equation (B-5) and forms only state combinations. This is accomplished by forming a new matrix "Z" and multiplying it by the states determined in Equation (B-5). Another reason for this routine is that the Program MULTI deals with only equal number of inputs and outputs. Therefore, until now only the combination of states $\underline{y} = \underline{Cx}$ appearing in the output could be observed.

User's Guide

The routine for combination of states is now contained in Options 31 and 32 for terminal plots, and Options 34 and 35 for calcomp plots. The first part of the User's Guide deals with Options 31 and 34. The second part covers the use of Options 32 and 35.

After 31 or 34 are entered, either option gives the reply (after stating whether the option produces a terminal plot or a calcomp plot):

```
PLEASE CHOOSE ONE OF THE FOLLOWING:

FOR A SINGLE SAMPLING TIME
  1...A PLOT OF UP TO 2 INPUT AND OUTPUT PAIRS
  2...A PLOT OF UP TO 4 INPUTS OR OUTPUTS OR STATES
  3...A PLOT OF UP TO 4 DIFFERENT SIMULATIONS
       (FOR ANY SINGLE INPUT OR OUTPUT)
OR 4...A PLOT OF UP TO 4 COMBINATION OF STATES
```

ENTER CHOICE DESIRED >4

Choice number 4 is the routine that enables the user to form conbinations of states. When choice 4 is entered the statement below is obtained.

CHOCIE #4...YOU'VE CHOSEN TO PLOT COMBINATION OF STATES

After the statement is given, the following question appears:

ENTER THE NUMBER OF COMBINATIONS OF STATES>

This is asking for the number of different combinations the user wants to plot. Choice number 4 permits the user to enter as many as four (no more than four) different combinations of states. When the number of combinations is entered, a "Z" matrix must be formed by the user. This "Z" matrix must contain the combinations the user wants to see. This, like the other matrices, has the same format and the user enters the data by row following the prompt (>). Below is an example of a 5 state model in which the user wants to add states 2 and 4 together:

ROW>0,1,0,1,0

After the matrix is entered, its values are automatically echoed back for checking. The chekcing tool used is the

same one described in Appendix A.

After the "Z" matrix is entered, the following reply is given:

FOR GRID ON PLOT ENTER "0", FOR A GRID ENTER "1">

This reply is self explanatory. After the user decides whether or not a grid is needed, the plot for the combinations of states is printed out on the terminal for Option 31, or for Option 34 a calcomp plot is developed.

The following message is given to the user when Option 31 or 32 is used:

DO YOU WANT A LIST OF POINTS USED IN PLOTTING?

ENTER...YES OR NO...>

In case of a "NO" reply the option is terminated. The reply "YES" gives a table of the points used in plotting. The user can also enter a simple "Y" or "N". The following is a sample format of a table produced by the program.

TIME	COMB 1	COMB 2
0.000	0.	0.
.040	-.8704E-01	-.7894E-01
.080	-.7281E-01	-.6307E-01
.120	-.4229E-01	-.4558E-01

The maximum number of points used in plotting is one hundred.

Now Options 32 and 35 deal with the short version for plotting either on the terminal or developing a calcomp plot. The statement below is given for either option.

ENTER SHORT VERSION CHOICE...1,2,3,4...>

These numbers represent the same numbers found in both Options 31 and 34. Choice 4 is the number that plots up to four combinations of states. From there on, Options 31, 32, 34, and 35 have the same format. That is, the same statements are given as before according to the option entered.

Programmer's Guide

This guide does not cover the exact location of the changes made or the additions made to the Program MULTI. It just gives the changes and their approximate locations. The numbers that were changed or moved are not mentioned. Therefore, the main concern of this guide is to explain what is added and what their purpose is. The reference numbers given (located on the right side on the page) are their positions relative to each other from the point of location.

In the overlay that contains the Options 30 thru 39 the following changes are added.

```
DIMENSION Z(10,10)                                    3
COMMON /B  2 / M                                      6
```

These statements are added in the first part of the program OPTPLT. The statements below are added after the comment "SET DATA FOR SHORT VERSION PLOT". This enables

The user to use the short version to plot.

```
PRINT*, 'ENTER SHORT VERSION CHOICE...1,2,3,4...>'  3
IF (ICODE.EQ.4) GO TO 1486                          6
```

From the comment "SET ICODE" the following choice is added with some of the minor changes that are made.

```
PRINT*, 'OR 4...A PLOT OF UP TO 4 COMBINATION OF
        STATES'                                     7
IF (ICODE.LT.1.OR.ICODE.GT.4) GO TO 1415           10
GO TO (1425,1430,1435,1440) ICODE                  12
```

Above the comment statement "SET CHOICE, SET NUM, PRINT MESSAGES (1)" the following are added.

```
1440 PRINT*, 'CHOICE #4...YOU'VE CHOSEN TO PLOT
             COMBINATION OF STATES'
     GO TO 1486
```

The next few groups of fortran statements belong to the main part of the routine that combines states. These statements are located three lines below the comment "OUTPUT(3)".

```
1486 PRINT '(/A)', 'ENTER THE NUMBER OF COMBINATIONS
                   OF STATES>'
     READ*, K
     PRINT*, '  '
```

The first two statements are to set the number of combinations of states, up to four, that can be performed. The next four statements are used to generate a "Z" matrix

that combines the states. The variable "M" is a common statement in which the number of states in the system is stored.

```
      PRINT*, 'ENTER "Z" MATRIX...,'K,' ROWS WITH ',
             M,' ELEMENTS EACH'
      DO 1490 I-1,K
      PRINT*, 'ROW ',I,' >'
1490  READ*, (Z(I,J),J-1,M)
      PRINT*, '  '
```

The next statements call different subroutines and their placement in the routine has in the same format shown at the end of Appendix A.

```
      GO TO 190
1495  CALL FIX (Z,K,M)
 190  PRINT*, 'COMBO MATRIXZ...'
      CALL MATPR (Z,K,M)
      CALL ANSWER (*1945,*8010)
```

The statements below are the actual steps used in performing the combinations of states.

```
      DO 1510 I = 1,N
      DO 1505 J = 1,K
      S = 0
      DO 1500 L = 1,M
1500  S - S + X(I,L+1)*Z(J,L)
1505  PLMAT(I,J) = S
1510  CONTINUE
      ICLM = K
      CHOICE = ' COMBO'
```

Figures B-1 through B-4 show the actual set ups for each matrix.

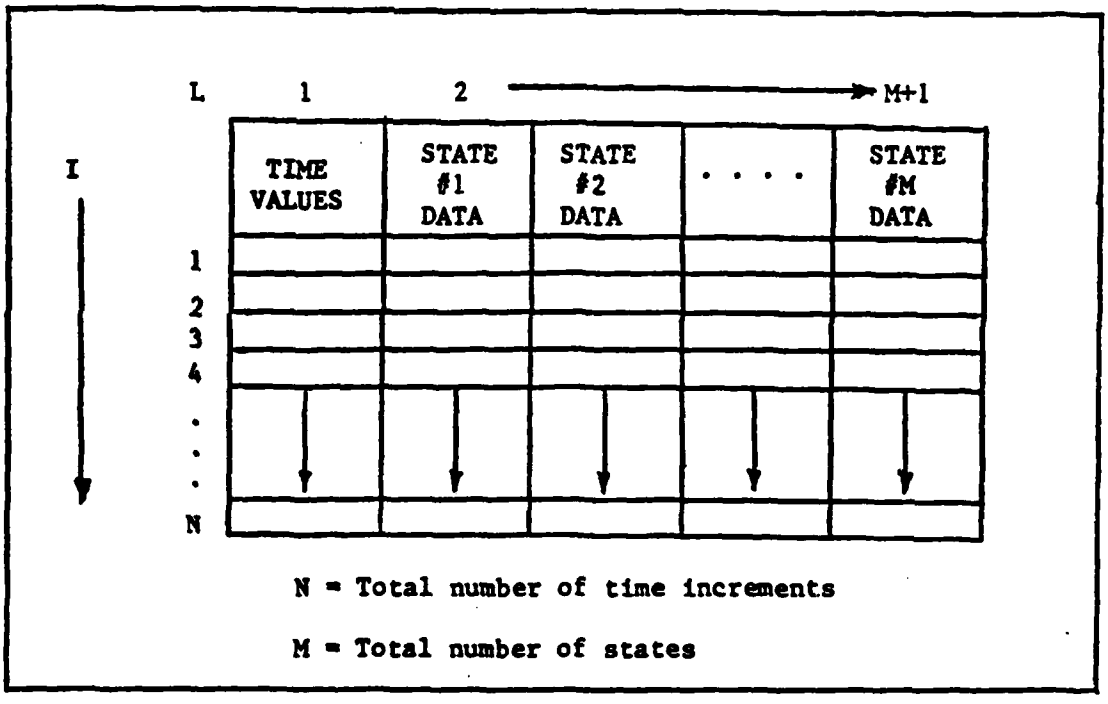

Figure B-1. Representation of the State Matrix X(I,L) (REF.10)

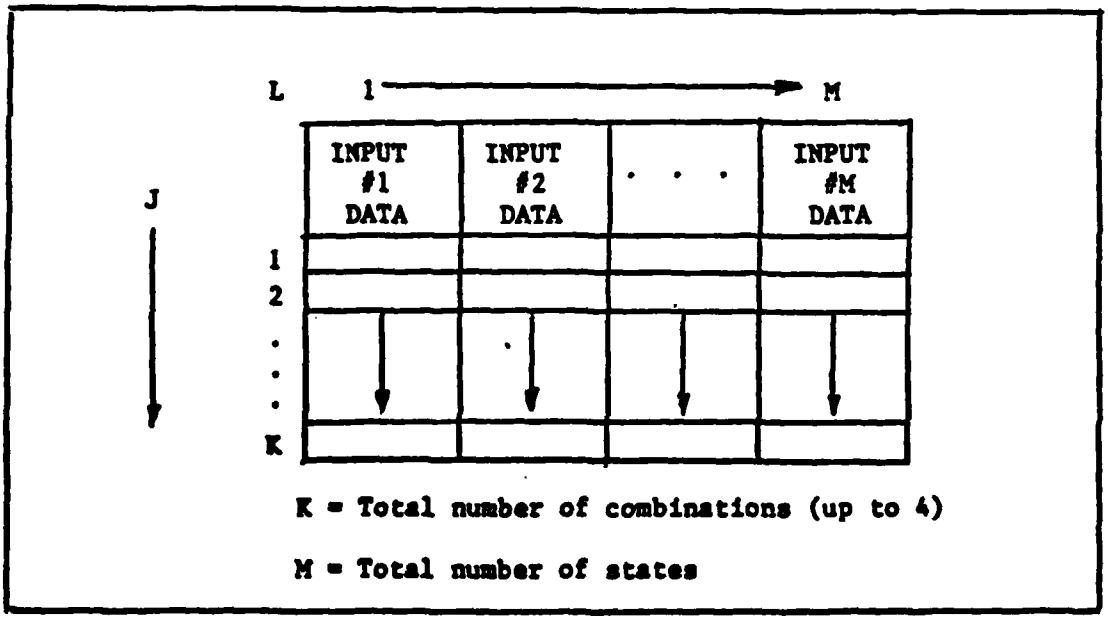

Figure B-2. Representation of the Combination Matrix Z(J,L).

$$[PLMAT] = \begin{bmatrix} X_{12} & X_{13} & X_{14} & \cdots & X_{1M} \\ X_{22} & X_{23} & \cdots & & \cdot \\ X_{32} & \cdot & \cdot & & \cdot \\ \cdot & \cdot & \cdot & & \cdot \\ \cdot & \cdot & & & \cdot \\ \cdot & & & & \cdot \\ X_{N2} & \cdot & \cdots & & X_{NM} \end{bmatrix} \begin{bmatrix} Z_{11} & \cdots & Z_{1M} \\ \cdot & \cdots & \cdot \\ Z_{K1} & \cdots & Z_{KM} \end{bmatrix}$$

N = Total number of data increments

M = Total number of states

K = Total number of combinations (up to 4)

Figure B-3. Representation of the multiplication of X(I,L+1) and Z(J,L).

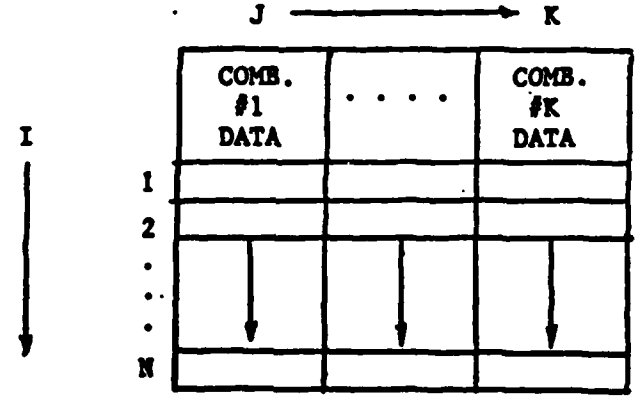

N = Total number of data increments

K = Total number of combinations (up to 4)

Figure B-4. Representation of the matrix PLMAT(I,J).

Figure B-4 is the format of matrix PLMAT in order for the terminal or calcomp plot to be developed. The statement CHOICE = ' COMBO' is added so that identification of the combination can be made after the terminal plot is printed out.

The next statements are in the overlay for terminal plots. One common statement is needed along with two character string. These two statements are needed if the table described in the User's Guide is going to be printed.

```
      COMMON N/1B 13C/ 13C/ V(101,11),X(101,11)
      CHARACTER CHECK, H(5)*6
```

The statements below are needed to identify the different combinations the terminal plot illustrates. These statements are located after the comment "EXIT TO PRINT STATEMENTS WHEN PLOT IS DISPLAYED".

```
      IF (ICODE.EQ.4) GO TO 1630                              4
1630  PRINT*,' CURVE ',STRING(i:I),' ABOVE IS ',              5
     1      choice,' ', I
```

The following statements are used to print the table that contains the data for plotting.

```
1636  PRINT*, '  '                                           13
      PRINT*, 'DO YOU WANT A LIST OF POINTS USED
     1     IN PLOTTING?'
      PRINT '(/A)', 'ENTER...YES OR NO...>'                   15
```

```
      READ '(A)', CHECK                                          16
      IF (CHECK.EQ.'N') GO TO 1650                               17
      PRINT*, ' '                                                18
      H(1) = 'COMB 1'                                            19
      H(2) = 'COMB 2'                                            20
      H(3) = 'COMB 3'                                            21
      H(4) = 'COMB 4'                                            22
      PRINT 5005, 'TIME', (H(I),I=1,ICLM)                        23
      PRINT*, ' '                                                24
      DO 1638 I-1,N                                              25
1638  PRINT 5010, X(I,1), (PLMAT(I,K),K=1,ICLM)                  26
      GO TO 1650                                                 27
5005  FORMAT (2X,A4,4X,4(A6,7X))                                 28
5010  FORMAT (1X,F6.3,1X,4(1E10.4,3X)                            29
      IF (CHOICE.EQ.'COMB') GO TO 1636                           33
1650  IENTRY = 0                                                 34
```

The next two statements are in the overlay for the calcomp plot. Their location is after the statement SYS = 'SIM '//STRING(J:J)// ' '.

```
      ELSEIF (ICODE.EQ.4) THEN
          SYS = STRING(J:J)//' '
```

Appendix C

Forming the Measurement Matrix And Changing the K_0 and K_1 Matrix For the Irregular Method

Introduction

The program MULTI is used for designing Digital Flight Control Systems (DFCS). This is accomplished by inputting the plant matrices and all the design parameters (epsilon, sigma matrix, alpha, measurement matrix, etc.) into MULTI, calculating the $\underline{K}_0$ and $\underline{K}_1$ matrices, and then running the simulation option. Option 26 uses the measurement matrix $\underline{M}$ and the calculated $\underline{K}_0$ and $\underline{K}_1$ matrices to run the simulation for the DFCS. It would be helpful in the design to be able to change one of the design matrices without changing the others. Option 14 did allow the user to change the measurement matrix $\underline{M}$ but it would then recalculate the $\underline{K}_0$ and $\underline{K}_1$ matrices. Therefore, Option 16 is created to input just the measurement matrix, and Option 114 is changed to allow the user to change either the $\underline{K}_0$ or $\underline{K}_1$ matrix, or both. Option 14 for the irregular method is still used in the initial calucation of the $\underline{K}_0$ and $\underline{K}_1$ matrices.

Option 118 is changed to 116 to allow the user to see the measurement matrix without changing it.

User's Guide

Option 16, which is used to input the measurement matrix

$\underline{M}$, uses the same format as the other matrices and the user enters the data by row after the prompt (>). After the matrix is entered, its values are automatically echoed back for checking. The checking tool used is the same one that is described in Appendix A.

Option 114 initially prints out the $\underline{K}_0$ and $\underline{K}_1$ matrices. Then the following statements appear:

```
DO YOU WANT TO CHANGE K0, OR K1, OR BOTH?
ENTER 1 FOR K0, 2 FOR K1, 3 FOR BOTH, OR 4 FOR NONE.>
```

In case of a "4" reply the option is terminated. The "1" reply gives the following statements:

```
THIS IS TO CORRECT K0
ENTER THE NUMBER OF CORRECTIONS BENING MADE>
```

The number of corrections corresponds to the number of values the user wants to change in the matrix. After entering the number, another message appears along with a prompt (>).

```
ENTER THE ROW, COLUMN, AND NEW VALUE FOR EACH
               CORRECTION
EX->1,2,-1.5...PRESS RETURN.

>
```

Only one correction can be entered at a time. Once the row, column, and new value for that single correction is entered, the user must press the return key. The prompt (>) appears according to the number of corrections being

made. After the corrections have been made, the following statement appears:

NEW KO MATRIX...

When the statement appears the corrected matrix is echoed back for checking. The checking tool used is the same as described in Appendix A.

The "2" reply is the same format as "1", and the reply "3" contains both $\underline{K}_0$ and $\underline{K}_1$.

Programmer's Guide

The fortran statements used for inputting the measurement matrix $\underline{M}$ are deleted from the original MULTI program. The following fortran statements are found in Option 16 for the inputting of the measurement matrix:

```
2016 PRINT '(A/)', 'THIS OPTION FORMS THE MEASUREMENT
        MATRIX'
     PRINT*, ' '
     PRINT*, 'ENTER THE M MATRIX...',P,' ROWS WITH ',N-M,
             ' COLUMNS'
     DO 550 I = 1,P
 550 PRINT*, 'ROW ',I,'>'
     GO TO 560
 555 CALL FIX (MM,P,N-M)
 560 PRINT '(/A/)', 'MEASUREMENT MATRIX...'
     CALL MATPR (MM,P,N-M)
     CALL ANSWER (*555,*8002)
     FLAG (16) = 1
     GO TO 8002
```

The IFLAG (16) = 1 is an error message used to determine if the matrix has been inputted when Option 116 is

used. The overlay for the error statements is changed in two places to the following:

```
3016 PRINT*, 'MEASUREMENT MATRIX MISSING... SEE
             OPTION #16 OR #18'
3018 PRINT*, 'ERROR #18 STATEMENT'
```

Option 114 is changed to allow the user to change either the $\underline{K}_0$ or $\underline{K}_1$ matrix or both. The following statements are found in Option 114.

```
C     OPTION #114
2114  IF  (METHOD.EQ.'X')  GOT TO 1824
      IF  (METHOD.EQ.'U')  PLTYPE = 'UNKNOWN'
      IF  (METHOD.EQ.'R')  PLTYPE = 'REGULAR'
      IF  (METHOD.EQ.'I')  PLTYPE = 'IRREGULAR'
      IF  (METHOD.EQ.'B')  PLTYPE = 'BSTAR'
      PRINT*, 'CONTROL MATRICES ARE FOR PLANTS WHICH ARE',
              PLTYPE
1824  PRINT '(/A/)', ' K0 MATRIX...'
      CALL MATPR (K0,M,P)
      IF (IFLAG(10).NE.1) GO TO 1825
      PRINT '(/A/)', ' K1 MATRIX...'
      CALL MATPR (K1,M,P)
      GO TO 1827
1825  IF (ALPHA.EQ.1.AND.METHOD.NE.'B') THEN
        PRINT '(1A/)', 'K1 MATRIX IS IDENTICAL TO K0 MATRIX'
      GO TO 1872
      ENDIF
      PRINT '(/A/)', 'K1 MATRIX...'
      CALL MATPR (K1,M,P)
1827  PRINT*,'DC YOU WANT TO CHANGE K0, OR K1, OR BOTH?'
      PRINT*, 'ENTER 1 FOR K0, 2 FOR K1, 3 FOR BOTH, OR
              4 FOR NONE.>'
      READ*, CHECK
      IF (CHECK.EQ.4) GO TO 8015
      IFLAG(10) = 1
      IF (CHECK.EQ.2) GO TO 1828
      PRINT*, 'THIS IS TO CORRECT K0'
 25   CALL FIX (K0,M,P)
      PRINT*, ' NEW K0 MATRIX...'
      CALL MATPR (K0,M,P)
      CALL ANSWER (*25,*3015)
```

```
      IF (CHECK.EQ.1) GO TO 8015
1828  PRINT*,'THIS IS TO CORRECT K1'
 50   CALL FIX (K1,M,P)
      PRINT*,' NEW K1 MATRIX...'
      CALL MATPR (K1,M,))
      CALL ANSWER (*50,*8015)
      GO TO 8015
```

The IFLAG(10) = 1 statement is set when either or both of the $\underline{K}_0$ and $\underline{K}_1$ matrices are changed. This determines, if Option 114 is used again, (if alpha = 1) if both of the matrices should be printed out or if the statement "K1 MATRIX is IDENTICAL TO K0 MATRIX' should be used. Therefore, if one of them is changed both matrices are printed when Option 114 is used. The IFLAG(10) is reset to zero after otpion 14 recalculates the $\underline{K}_0$ and $\underline{K}_1$ matrices.

Bibliography

1. D'Azzo, John J., and Constantine H. Houpis. Linear Control System Analysis and Design (Second Edition). New York: McGraw-Hill Book Company, 1981.

2. Horowitz, Issac, "Quantitative Systhesis of Uncertain Multiple Input-Output Feedback System". International Journal of Control, 30 (1): 81-106 (1979)

3. Porter, B. Design of High Performance Tracking Systems. AFWAL-TR-82-3032, Air Force Flight Dynamics Laboratory, Wright-Patterson AFB, Ohio, July 1982.

4. Barfield, A. Finley. Multivariable Control Laws For The AFTI/F-16. MS Thesis, AFIT/GE/EE/83S-4, Air Force Institute of Technology, Wright-Patterson AFB, Ohio, September 1983.

5. Aerodynamic Data Package, AFTI F-16. AFWAL/FII. Wright-Patterson AFB, Ohio.

6. Locken, William J. Multivariable Digital Control Laws For the KC-135A. MS Thesis, AFIT/GE/EE/83D-40, Air Force Institute of Technology, Wright-Patterson AFB, Ohio, December 1983.

7. Ridgely, D. Brett, Siva S. Banda, and John J. D'Azzo. "Decoupling of High Gain Multivariable Tracking Systems." AIAA Paper No. 83-0280 presented at the AIAA 21st Aerospace Science Conference, Reno Nevada, 10-13 January 1983.

8. Neal, Peter J., and Roger E. Smith. An In-Flight Investagation to Develop Control System Design Criteria for Fighter Aircraft. AFFDL-TR-70-74, Volume 1. Air Force Flight Dynamics Laboratory, Wright-Patterson AFB, Ohio, December 1970

9. Masi, Michale A., and Daniel E. Russ, "MULTI User's Manual." Air Force Flight Dynamics Laboratory, Wright-Patterson AFB, Ohio, November 1983.

10. Porter, Douglas S., Design and Analysis of a Multivariable Digital Controller for the A-7D DIGITAC II Aircraft and the Development of an Interactive Computer Design Program. MS Thesis, AFIT/GE/EE/81D-48, Air Force Institute of Technology, Wright-Patterson AFB, Ohio, December 1981

VITA

Marc L. Hoffman was born on July 16, 1959, in Fort Pierce, Florida. His parents moved to Eau Gallie, Florida, where he graduated from Eau Gallie High School in 1977. He then attended the Citadel from September 1977 to May of 1981 where he received his Bachelor of Science Degree in Electrical Engineering. After graduating from The Citadel, he received his commission through the ROTC program in which he received a 3 year Air Force Scholarship.

He entered the Air Force Institute of Technology in June of 1982. His next assignment is with the Joint Cruise Missile SPO located in Arlington, Virginia.

SECURITY CLASSIFICATION OF THIS PAGE (When Data Entered)

REPORT DOCUMENTATION PAGE		READ INSTRUCTIONS BEFORE COMPLETING FORM
1. REPORT NUMBER AFIT/GE/EE/83D-30	2. GOVT ACCESSION NO. AD-A138269	3. RECIPIENT'S CATALOG NUMBER
4. TITLE (and Subtitle) Evaluation of a Digital Flight Controller for a Flexible-Fighter Aircraft		5. TYPE OF REPORT & PERIOD COVERED MS THESIS 6. PERFORMING ORG. REPORT NUMBER
7. AUTHOR(s) Marc L. Hoffman First Lieutenant USAF		8. CONTRACT OR GRANT NUMBER(s)
9. PERFORMING ORGANIZATION NAME AND ADDRESS Air Force Institute of Technology (AFIT/EN) Wright-Patterson AFB, Ohio 45433		10. PROGRAM ELEMENT, PROJECT, TASK AREA & WORK UNIT NUMBERS
11. CONTROLLING OFFICE NAME AND ADDRESS		12. REPORT DATE December 1983 13. NUMBER OF PAGES 156
14. MONITORING AGENCY NAME & ADDRESS(if different from Controlling Office) Flight Dynamics Laboratory Aeronautical Systems Division Wright-Patterson AFB, Ohio 45433		15. SECURITY CLASS. (of this report) 15a. DECLASSIFICATION/DOWNGRADING SCHEDULE

16. DISTRIBUTION STATEMENT (of this Report)

Approved for public release, distribution unlimited.

17. DISTRIBUTION STATEMENT (of the abstract entered in Block 20, if different from Report)

Approved for public release: IAW AFR 190-17.
LYNN E. WOLAVER 7 Feb 84
Dean for Research and Professional Development
Air Force Institute of Technology (AIC)
Wright-Patterson AFB OH 45433

18. SUPPLEMENTARY NOTES

Approved for public release; IAW AFR 190-17

19. KEY WORDS (Continue on reverse side if necessary and identify by block number)

Multivariable, Bending Mode, Neal-Smith Criteria

20. ABSTRACT (Continue on reverse side if necessary and identify by block number)

This thesis evaluates the effect of a digital flight controller on a flexible-fighter aircraft (FFA) at the flight condition of 0.8 Mach at 30,000 feet. The two maneuvers incorporated in this flight controller are the g-command pull-up maneuver and the pitch-pointing maneuver. Using a control law that is based on the control system theory developed by Professor Brian Porter at the University of Salford, England, a digital flight controller is first designed for a rigid body

DD FORM 1 JAN 73 1473 EDITION OF 1 NOV 65 IS OBSOLETE

SECURITY CLASSIFICATION OF THIS PAGE (When Data Entered)

20. aircraft. The same design is then used on a flexible-fighter aircraft. The effects of the controller for the rigid body design when used on the flexible-fighter are evaluated in this thesis. The results showed excellent performance by the flexible-fighter aircraft.

The flexible-fighter model is based on the rigid body dynamics of the AFTI/F-16 combined with the first bending mode of a flexible aircraft. The bending mode of the flexible aircraft was selected to correspond to the expected characteristics in a typical fighter aircraft.

Incorporating a time delay in the controller to represent the expected microprocessor computational time delay did not significantly affect the simulation time response of either the rigid body or the flexible-fighter aircraft.

To determine the acceptance of the design by a pilot, the Neal-Smith Criterion is used. The results of applying this criterion showed that the pilot would accept the design for both the rigid body and the flexible-fighter aircraft.